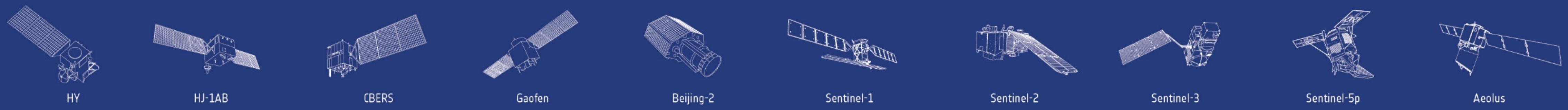

2023 DRAGON 5 SYMPOSIUM

3rd YEAR RESULTS REPORTING

11-15 SEPTEMBER 2023

ID 58815

IMPACTS OF FUTURE CLIMATE CHANGE ON WATER QUALITY AND ECOSYSTEM IN THE MIDDLE AND LOWER REACHES OF THE YANGTZE RIVER

THRUSDAY 14TH OF SEPTEMBER 2023

ID. 58815

IMPACTS OF FUTURE CLIMATE CHANGE ON WATER QUALITY AND ECOSYSTEM IN THE MIDDLE AND LOWER REACHES OF THE YANGTZE RIVER

CHEN XIAOLING & HERVE YESOU

HERVE YESOU, JIANZHONG LU , HONGTAO DUAN , JULIANE HUTH, SHIFENG HUANG LIANG ZHENG , XIJUN LAI, JUHUA LU , SABRINE AMZIL, TIANCI QI, JINGE MA, ZHAO LU, STEVEN LOISELLE AND XIAOLING CHEN

PRESENTED BY: HERVÉ YESOU & JIANZHONG LU

WATER QUALITY AND ECOSYSTEM IN THE MIDDLE AND LOWER REACHES OF THE YANGTZE RIVER

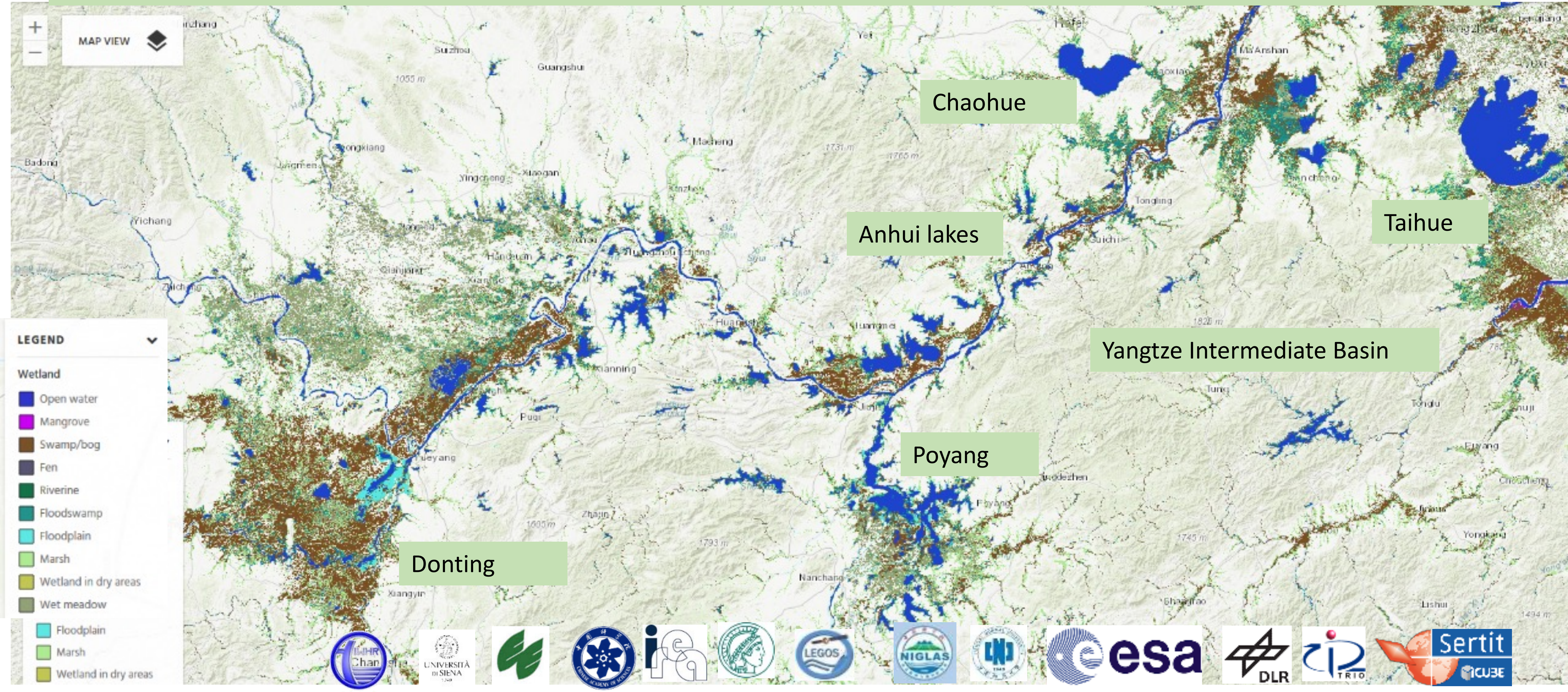

Dragon 5 Objectives

Provide indicators to answer the SDGs actions in a climate change context

5 work packages

WP1: Water extent LWE and height LWL monitoring

WP2: Water quality

WP3: Wetland mapping and biodiversity values analysis

WP4: Regional and global interactions

Keys words

- **Multiscale multi temporal => EO Times series**
- **Advanced algorithms**
- **In situ & validation**
- **Reproductivity**

EO Data Delivery

Data access (list all missions and issues if any). NB. in the tables please insert cumulative figures (since July 2020) for no. of scenes of high bit rate data (e.g. S1 100 scenes). If data delivery is low bit rate by ftp, insert "ftp"

ESA /Copernicus Missions	No. Scenes
1.Sentinel 1	3500
2. Sentinel 2 MSI	800
3.Sentienl 3 OCLI	250
4. ENVISAT MERIS	550
5. Sentinel 3 SRAL	150
6.	
Total:	

Issues: **Easier to access from AWS rather than EU DIAS!!!**

ESA Third Party Missions	No. Scenes
1.IcEye	5
2.Radarsat 2	3
3.	
4.	
5.	
6.	
Total:	

Issues: Initial Radarsat quota of 8 images reduced to 3due to a change of image mode

Others

1. Pleaides NEO (CNES)
2. DESIS (DLR)
3. ICeSAt

Chinese EO data	No. Scenes
1. GF-1 WFV	3000 + 200
2. GEF 2	20
3.	
4.	
5.	
6.	
Total:	

Issues:

ESA COPERNICUS: SENTINEL 2 MSI

Anhui lakes case

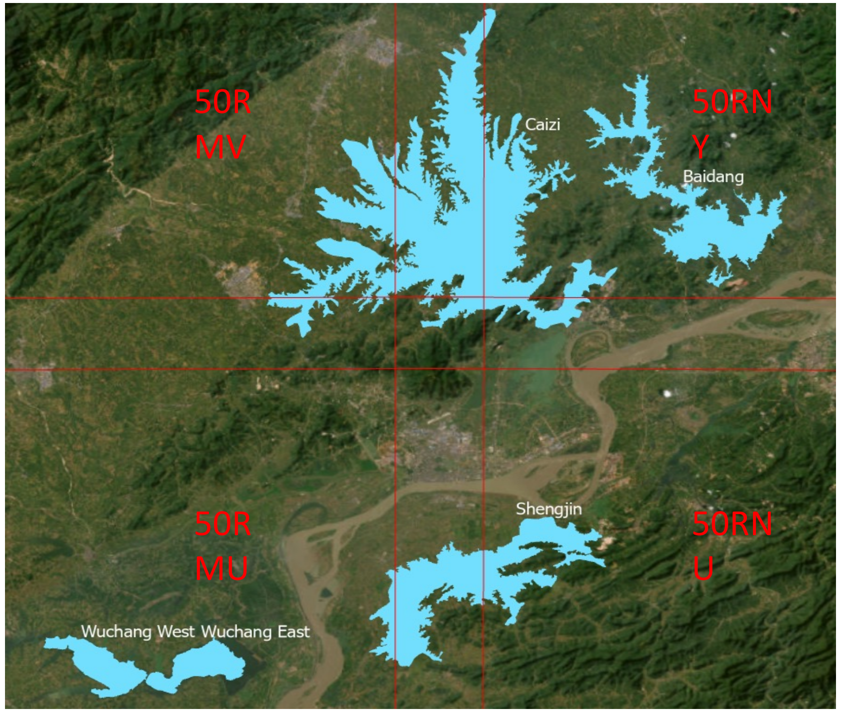

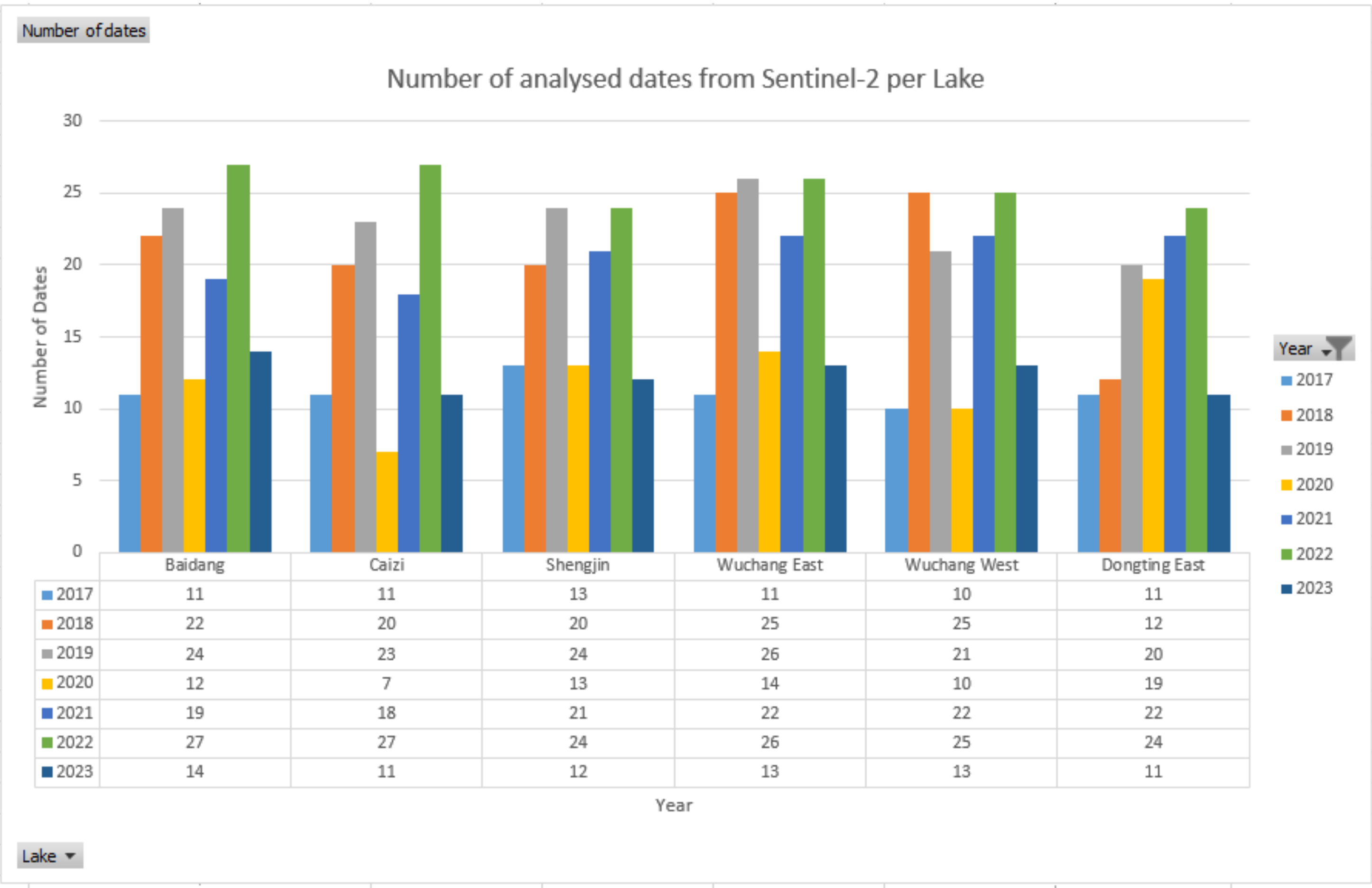

	Baidang	Caizi	Shengjin	Wuchang East	Wuchang West	Dongting East
2017	11	11	13	11	10	11
2018	22	20	20	25	25	12
2019	24	23	24	26	21	20
2020	12	7	13	14	10	19
2021	19	18	21	22	22	22
2022	27	27	24	26	25	24
2023	14	11	12	13	13	11

Lake	Number of dates
Baidang	129
Caizi	117
Shengjin	127
Wuchang East	137
Wuchang West	126
Dongting East	119

Third party mission: Radarsat 2

ExtraFine Mode images

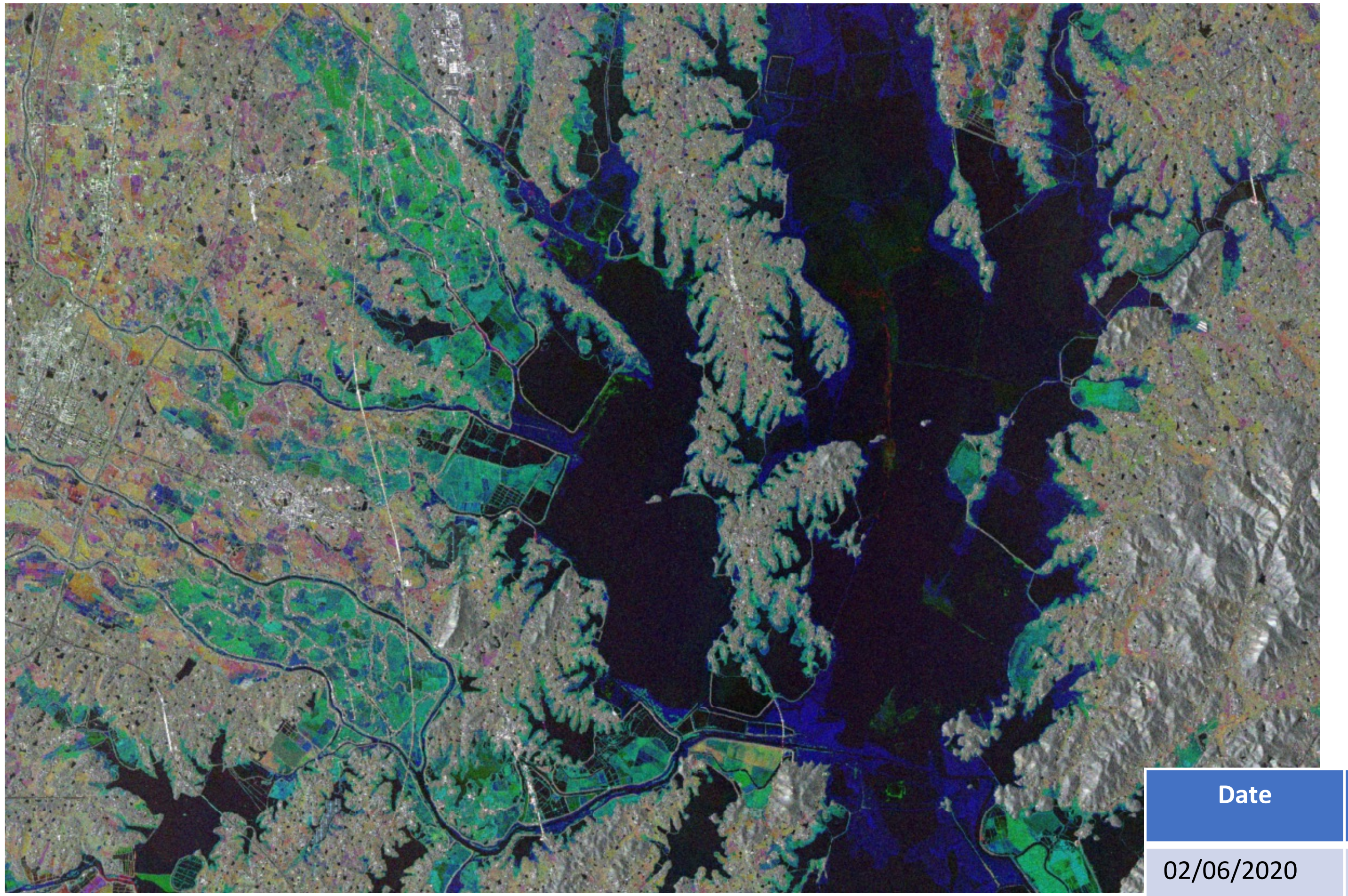

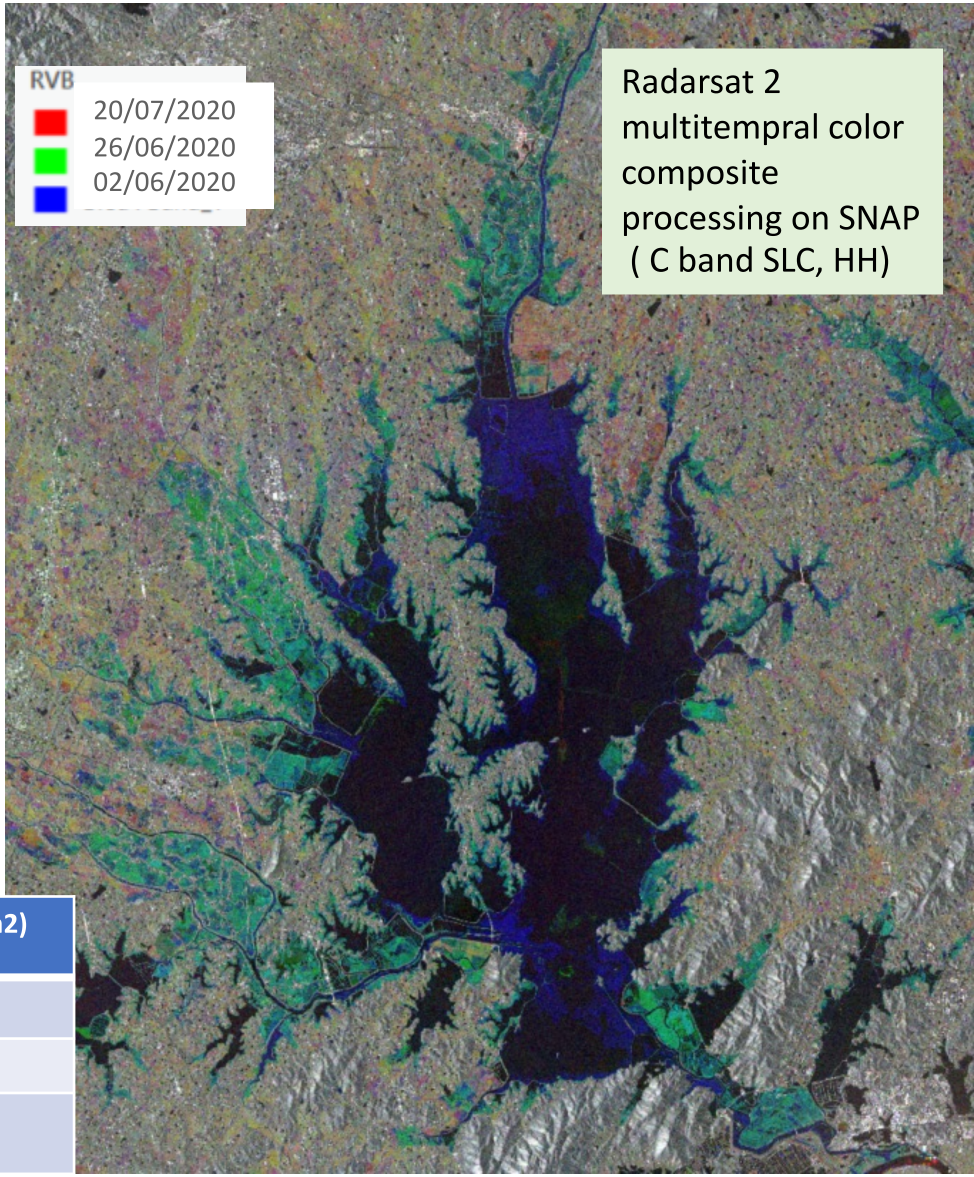

Radarsat 2 multitempral color composite processing on SNAP (C band SLC, HH)

Date	Area (km2)
02/06/2020	216.59
26/06/2020	263.48
20/07/2020	389.65

A few images but date selected carrfully to complete summer 2020 time series: more will be welcome

Third party mission: ICEYE

ICEYE_composite_bands.tif

RVB

- 25/03/2023 (red)
- 25/02/2023 (green)
- 25/12/2022 (blue)

Different crowns related to topography and done visible by, extent of water, wetness of the soils, sar attenuation by growing vegetation..

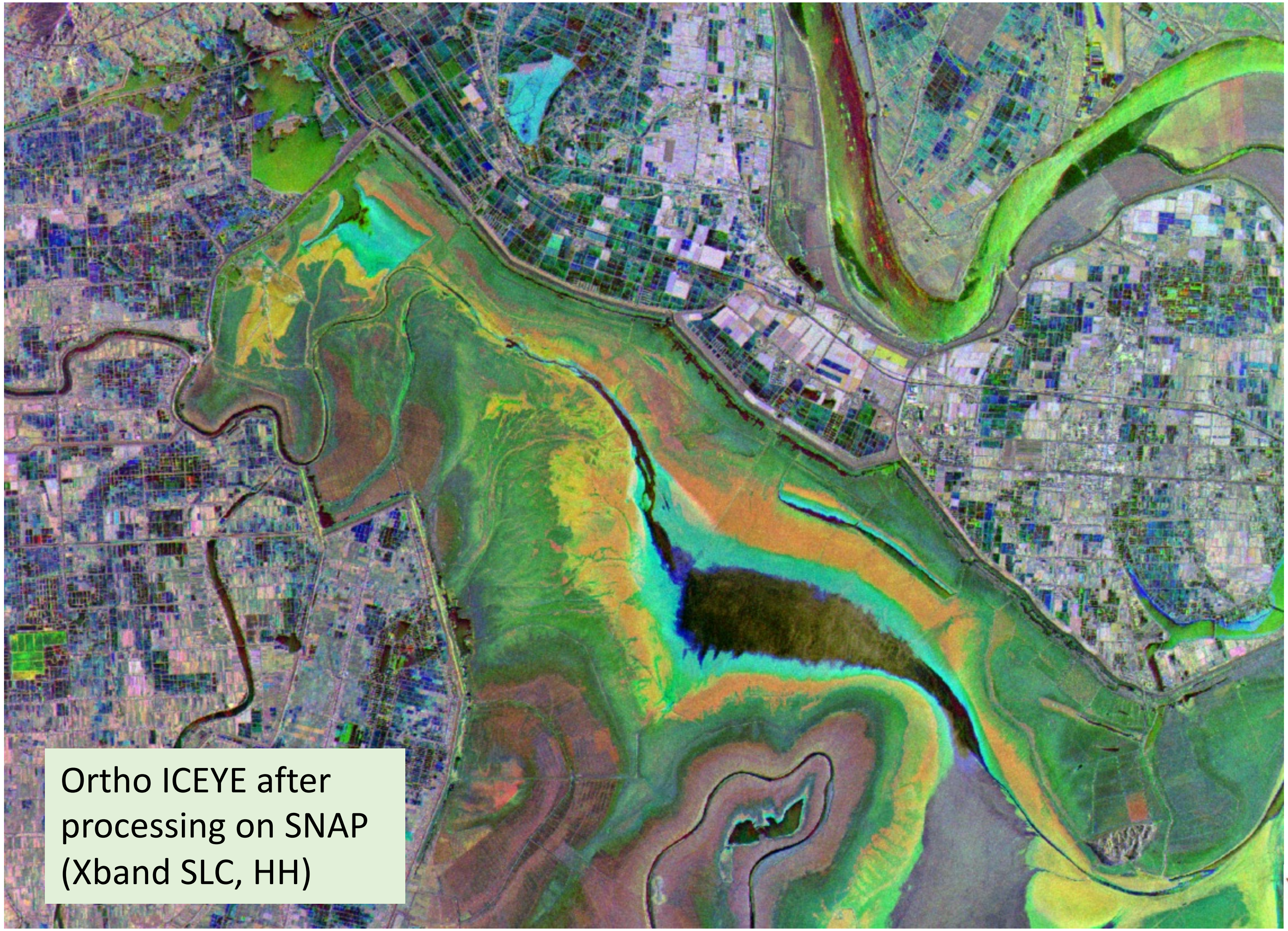

Ortho ICEYE after processing on SNAP (Xband SLC, HH)

Other missions

- **DESIS** = DLR Earth Sensing Imaging Spectrometer (DESIS) mounted on the International Space Station (ISS)

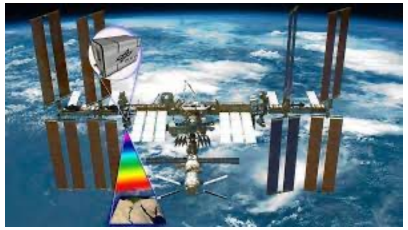

  - Hyperspectral imaging sensor - its “mechanical and optical characteristics qualify DESIS for applications like large-scale precision farming, forestry, land cover analysis and multitemporal environmental monitoring” (DLR).
  - Spectral range 400 – 1000nm VIS/NIR, spectral resolution 2,5 nm
  - 235 channels
  - 30m spatial resolution on the ground
  - Scientific Mission: an application for scientific use of the data can be submitted to DLR.

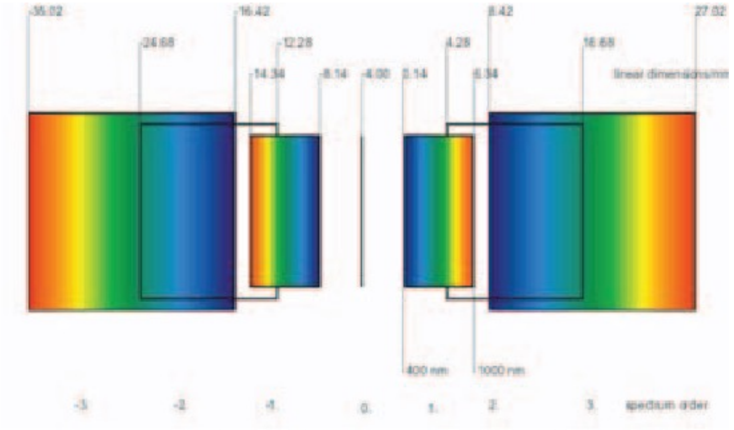

Figure 1 Spectra on the Detector

Andreas Eckardt and John Horack and Frank Lehmann and David Krutz and Jurgen Drescher and Mark S. Whorton and Mike Soutullo, 2015: DESIS (DLR Earth Sensing Imaging Spectrometer for the ISS-MUSES platform. IEEE International Geoscience and Remote Sensing Symposium (IGARSS, https://api.semanticscholar.org/CorpusID:20847431} }

In situ data/campaigns

CO2 flux in Poyang Lake using GASMET and spectrometers.

Hydrological Data of the Yangtze River Basin in the Hydrological Yearbook of the People's Republic of China (2018, 2019, 2020)

WP1: Water extent and level

Routine work flow : EEO

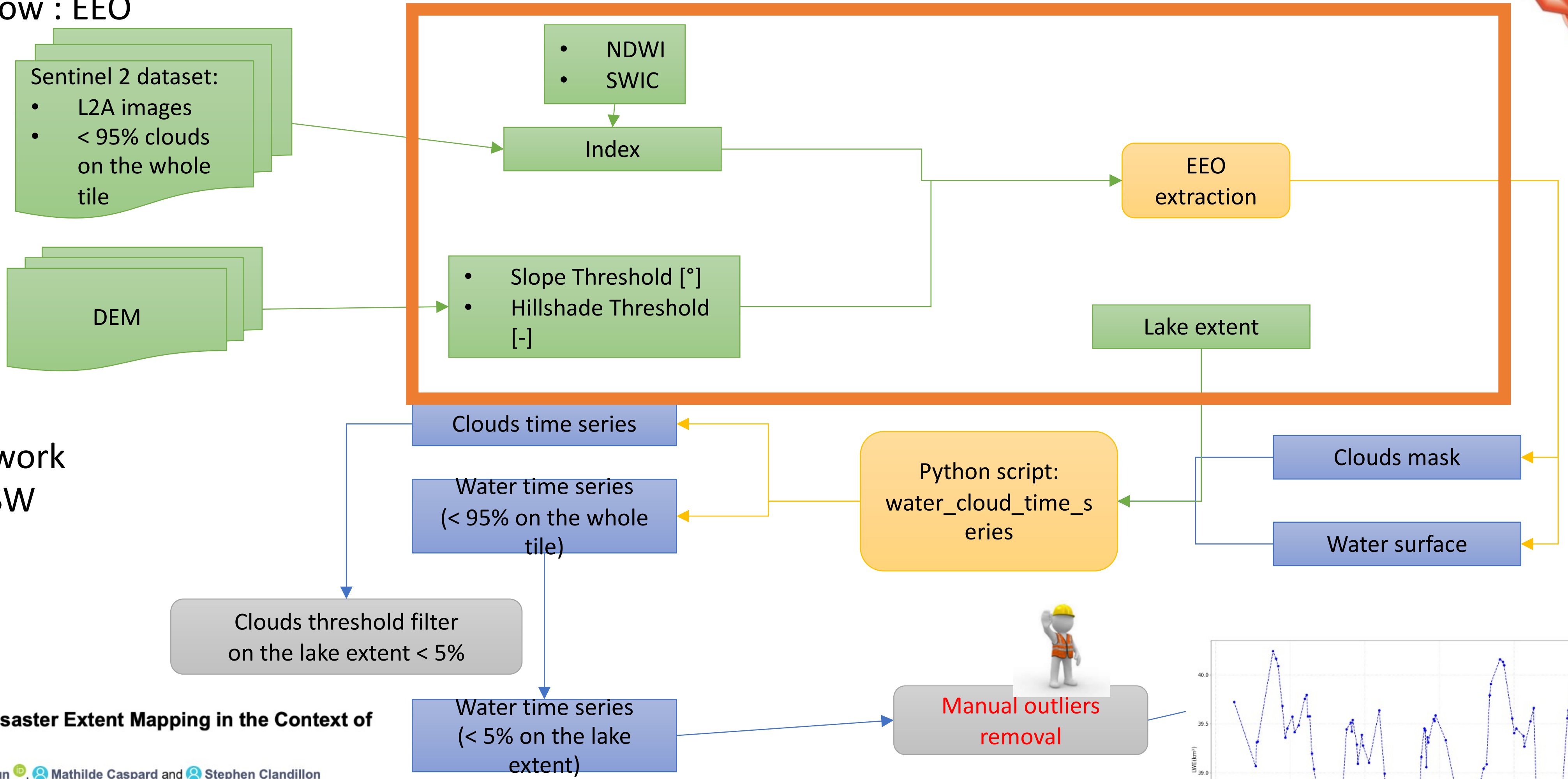

Indeces
DEM
Perception network
Sampling on GSW

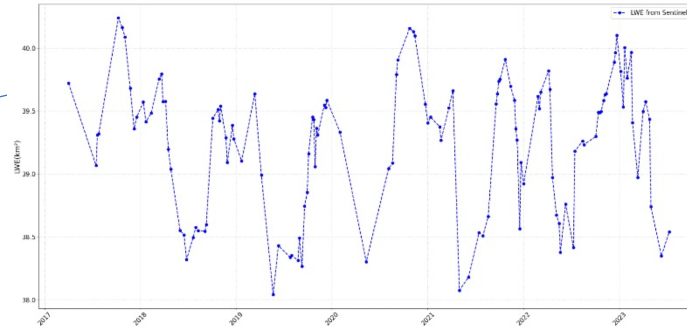

ExtractEO, a Pipeline for Disaster Extent Mapping in the Context of Emergency Management

by Jérôme Maxant *, Rémi Braun, Mathilde Caspard and Stephen Clandillon

ICUBE-SERTIT, Université de Strasbourg, 67412 Illkirch Graffenstaden, France

* Author to whom correspondence should be addressed.

Remote Sens. **2022**, *14*(20), 5253; **https://doi.org/10.3390/rs14205253**

WP1: Water extent and level

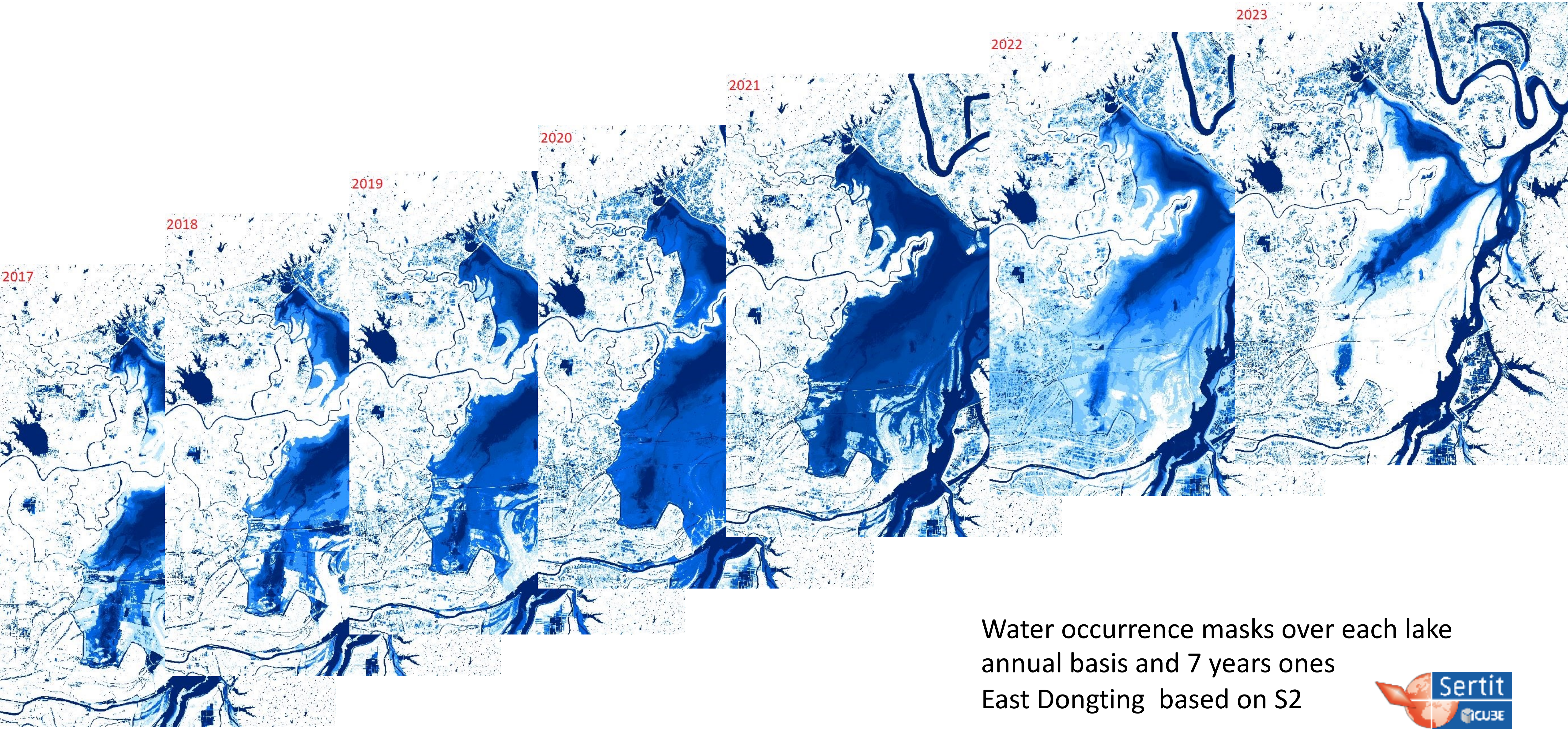

Water occurrence masks over each lake annual basis and 7 years ones
East Dongting based on S2

WP1: Water extent and level

Validation LWE by comparing water mask derived from HR and VHR EO data

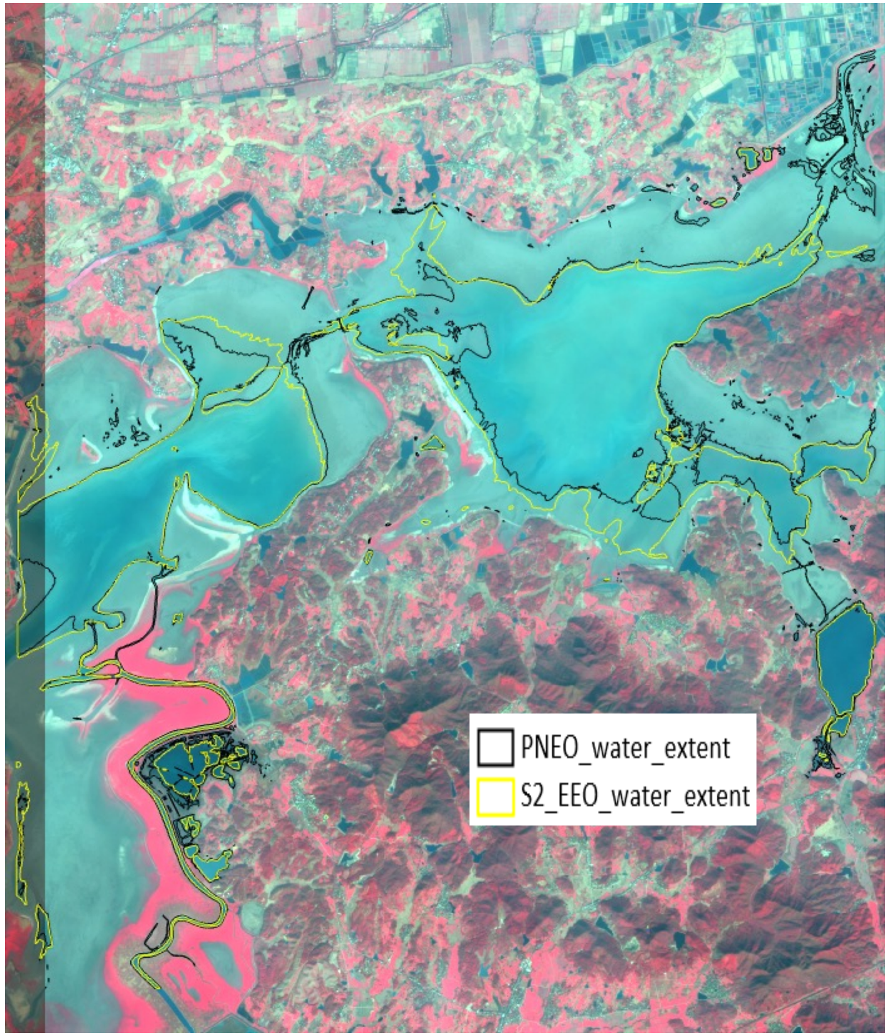

Sensor	Resol	Date	Surface (km2)	Extraction Method
Sentinel-2	10m	07/12/2021	33.7	SWIC [0.3,0.9]
Pleiades NEO	0,30	10/12/2021	32.7	SVM (100 samples)

Confusion Matix

type	FREQUENCY	SUM_area	pourcent
reference	513	32691145.8	100
database	41	33698468.7	103.08
omission	442	4099507.14	12.54
commission	30	5106830.03	15.15
taux_detection	36	28591638.7	87.46
taux_justesse	1	999999	84.85
BREAK	1	1	1.00
precision	1	1	0.85
recall	1	1	0.87
Fscore	1	1	0.86
CSI	1	1	0.76

WP1: Water extent and level

Water level from space- IceSAT-2 L3A

Few high precision tracks

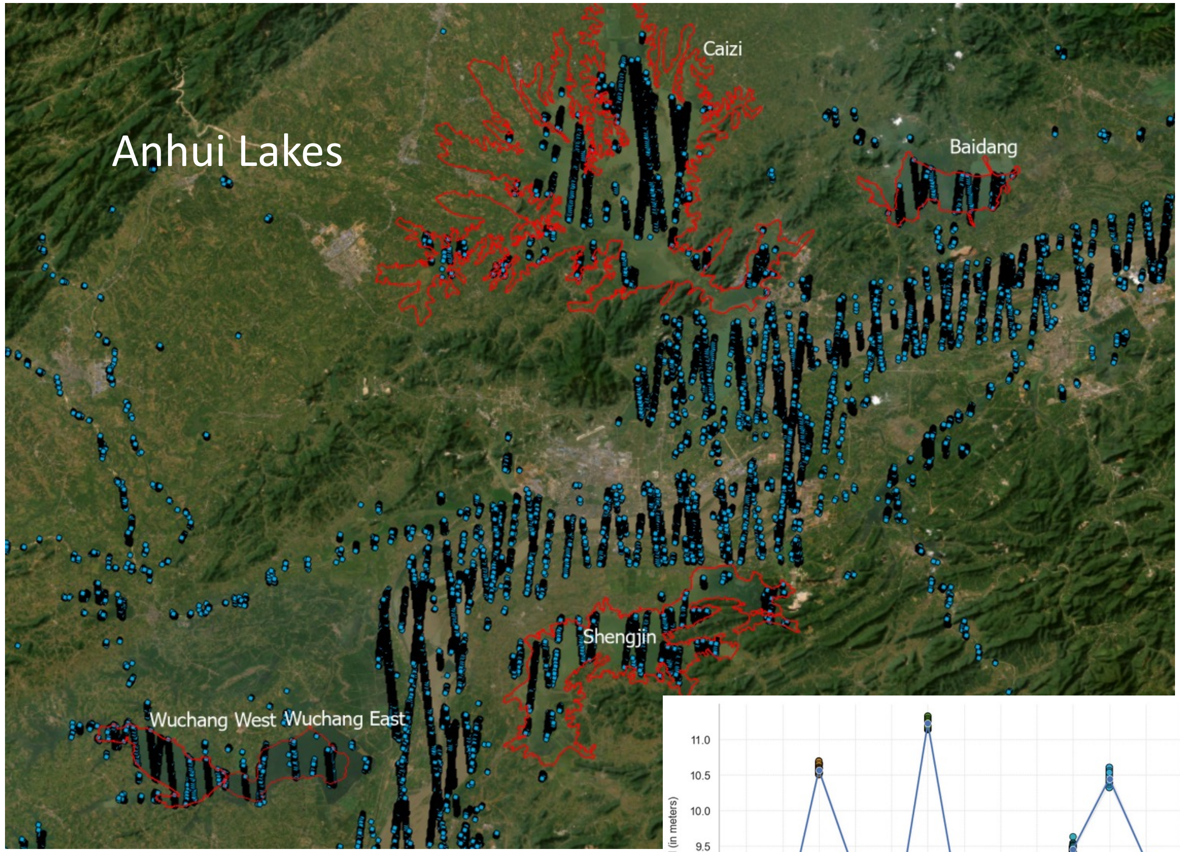

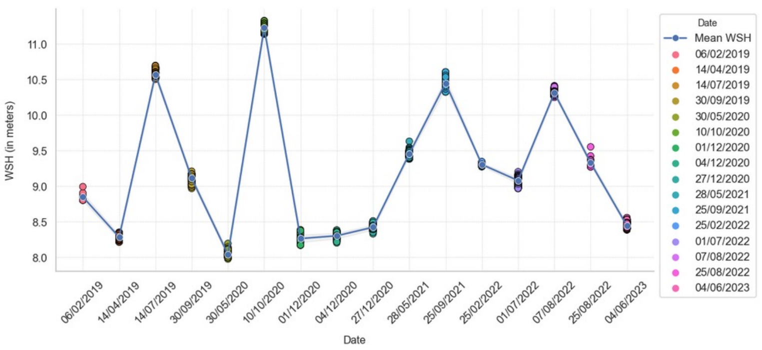

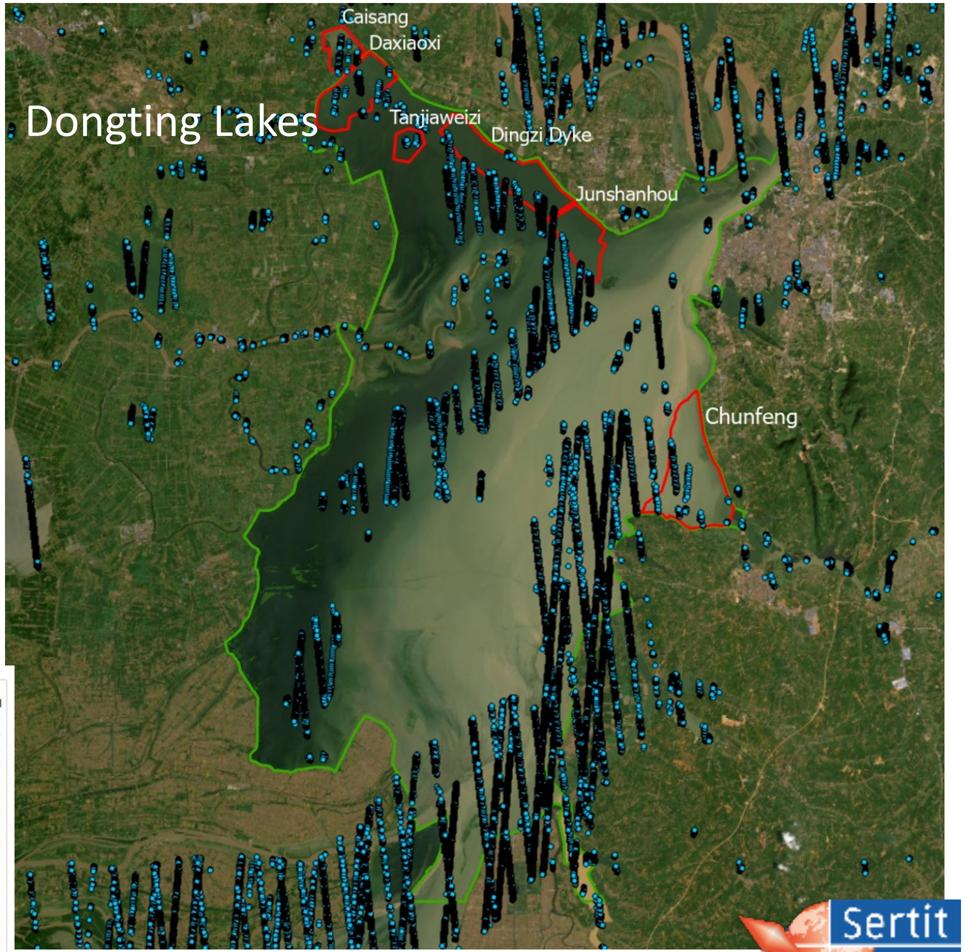

WP1: Water extent and level

Water level from space- Sentinel 3 SRAL

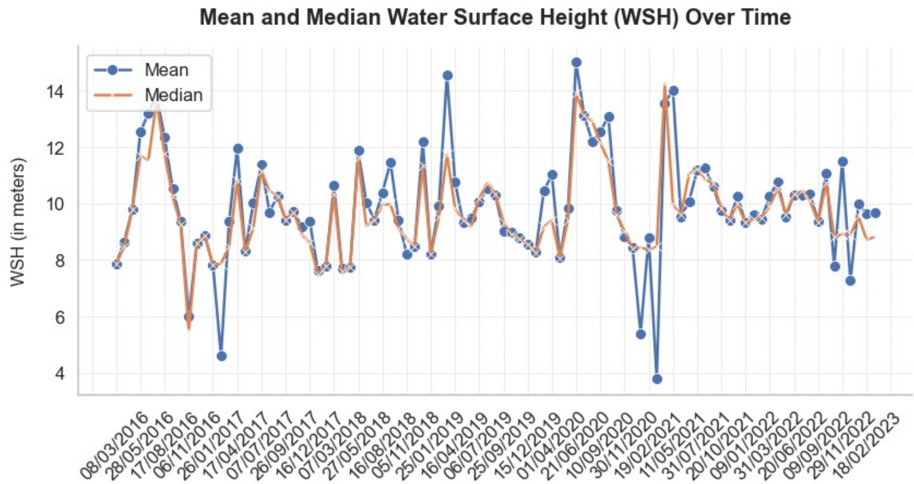

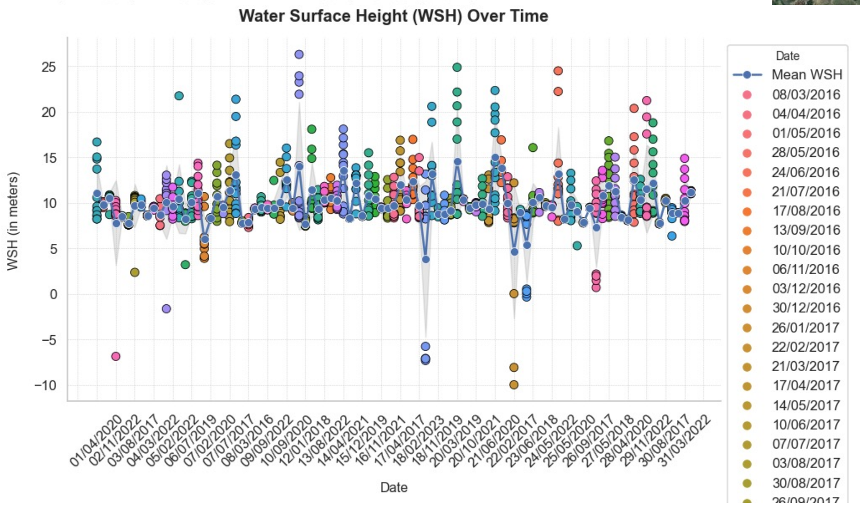

Only two lakes covered Wuchang and Baidang

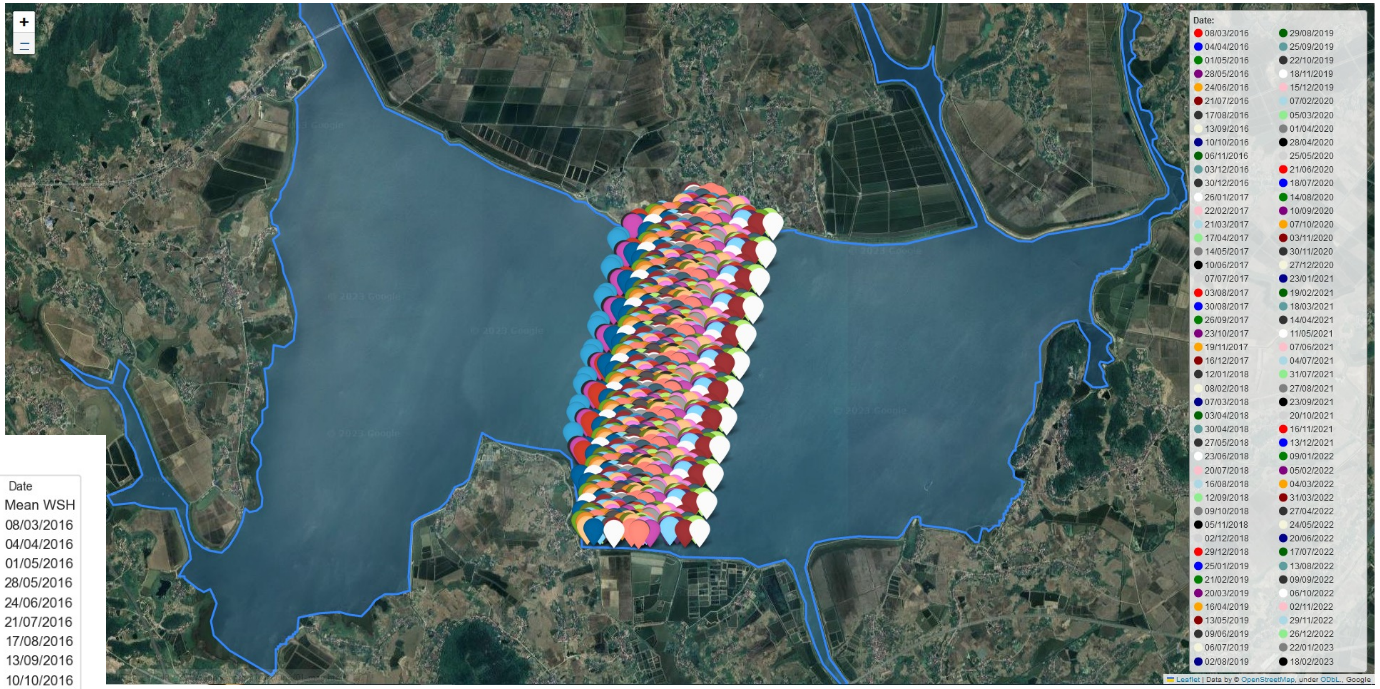

See Sabrine Amzil Poster

WP1: Water extent and level & volume variations

Water volume variations from space- LWE from IceSAt * LWE Sentinel2

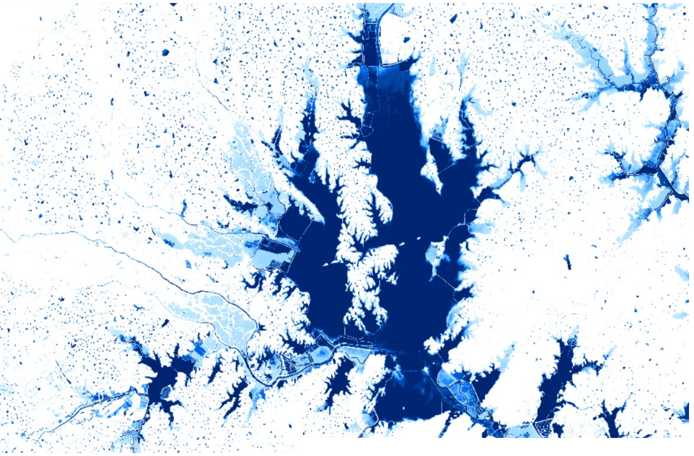

Caizi lake

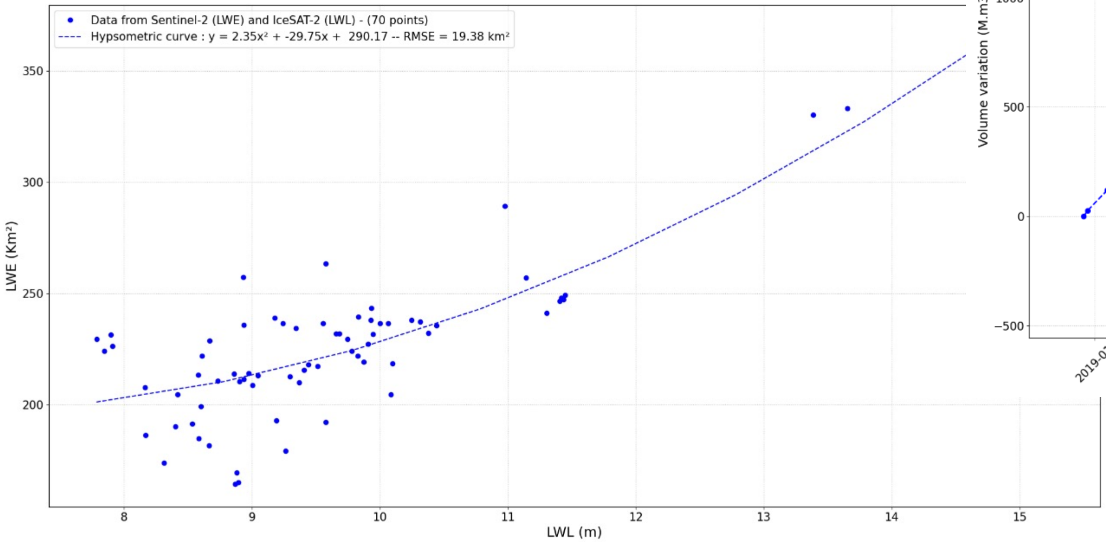

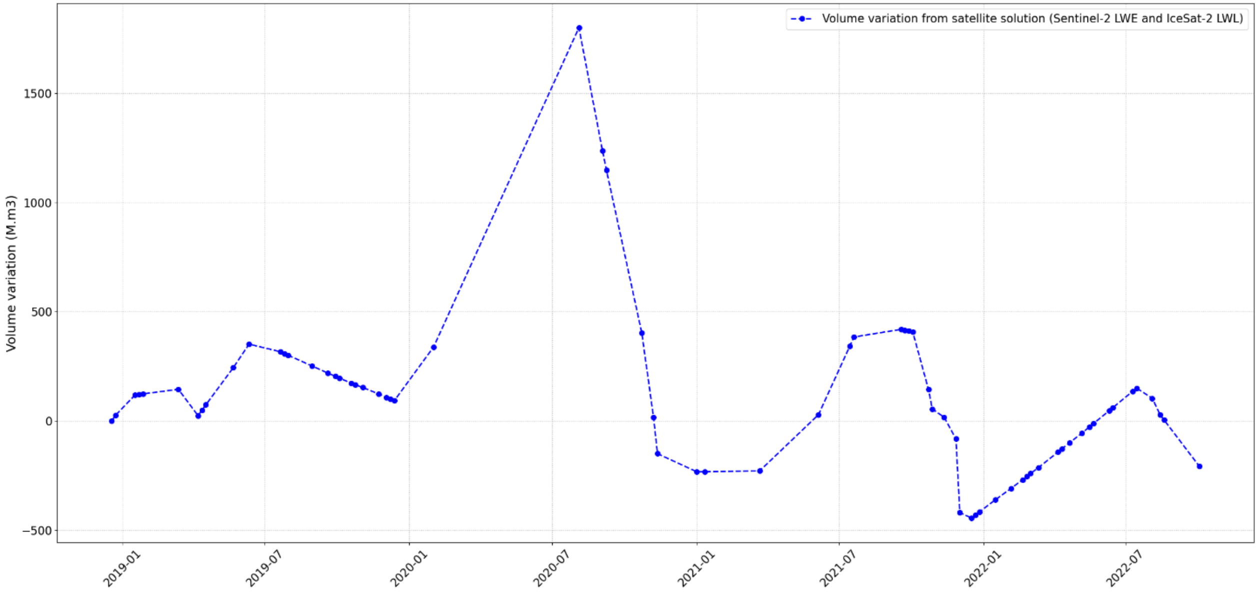

See Sabrine Amzil Poster

WP1: Water extent and level: algo development

To address the failure of spatiotemporal fusion algorithms in reconstructing flood areas that change abruptly, a multimodal spatiotemporal fusion framework is proposed to utilize the complementarity between synthetic aperture radar (SAR) and optical images.

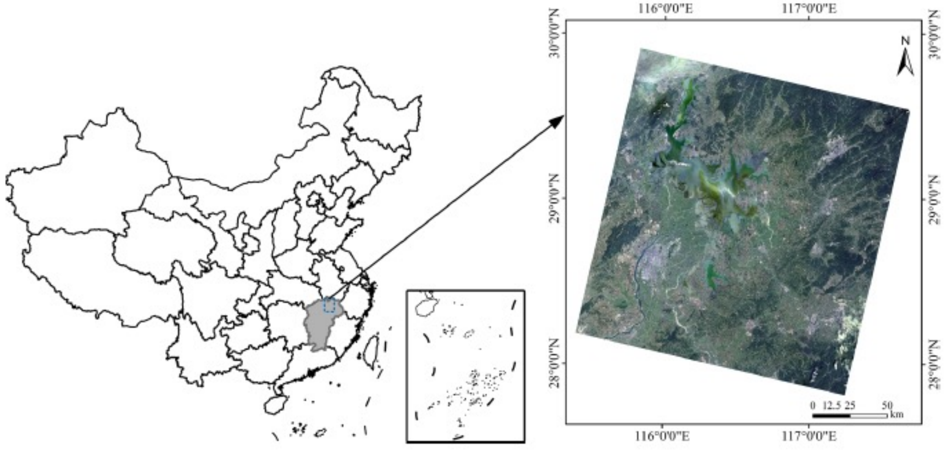

Figure 1 Study area

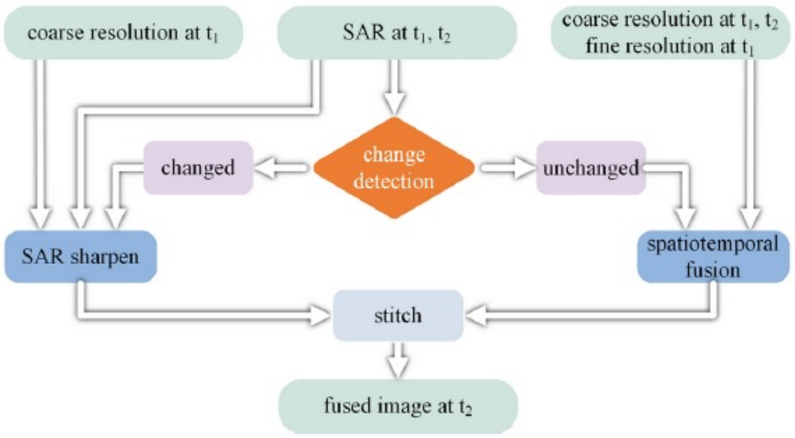

Figure 2 Proposed framework for SAR-aided spatiotemporal fusion

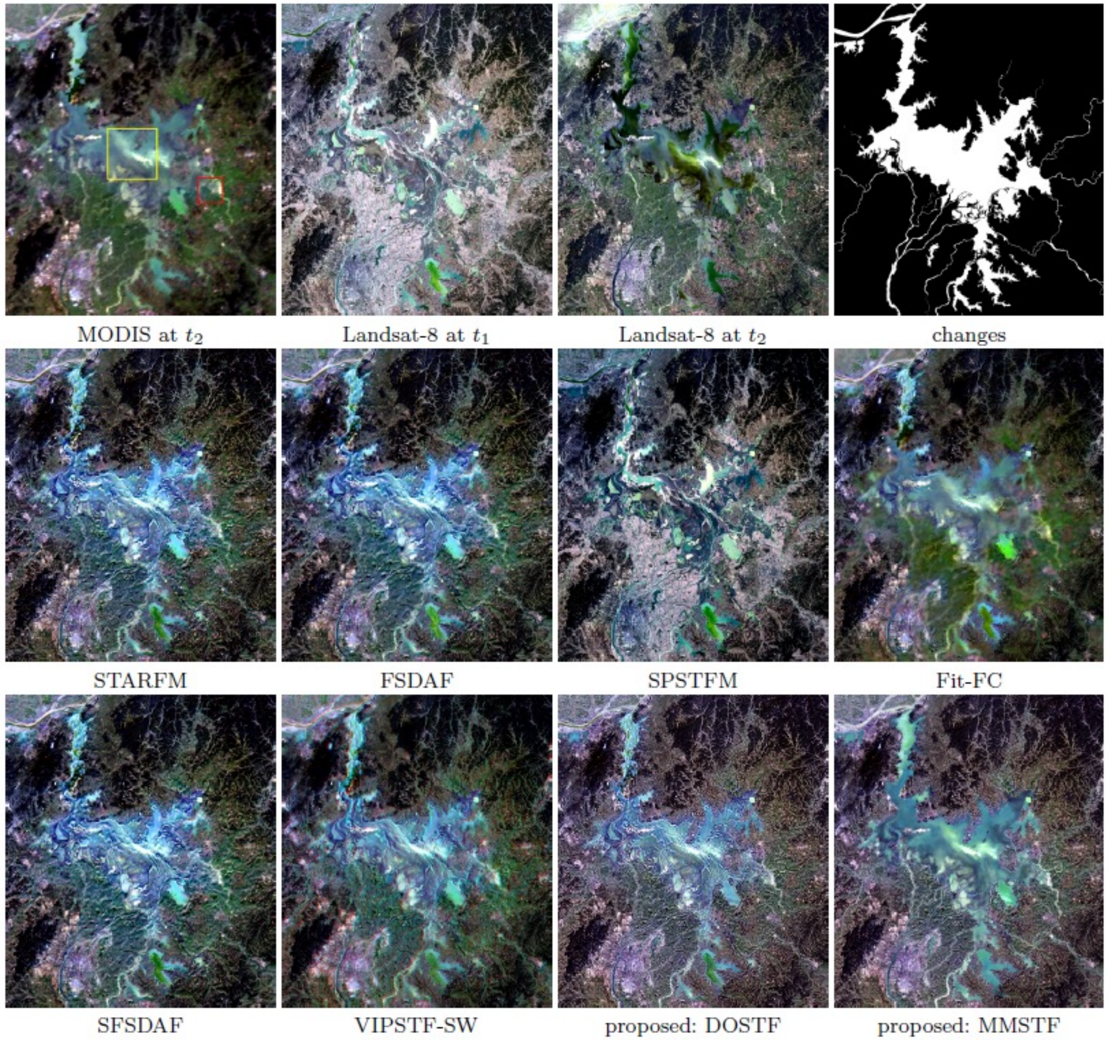

Figure 3 Spatiotemporal results at the moment t1 → t2

WP1: Water extent and level: algo development

1. A new one-pair fusion network is proposed and named deep learning-based one-pair SpatioTemporal Fusion (DOSTF).
2. The fusion network of SAR and MODIS is called GAN-based SAR sharpening and is abbreviated as GAN-SARSP.
3. A framework, together with the new fusion algorithms, is called MultiModal SpatioTemporal Fusion (MMSTF).

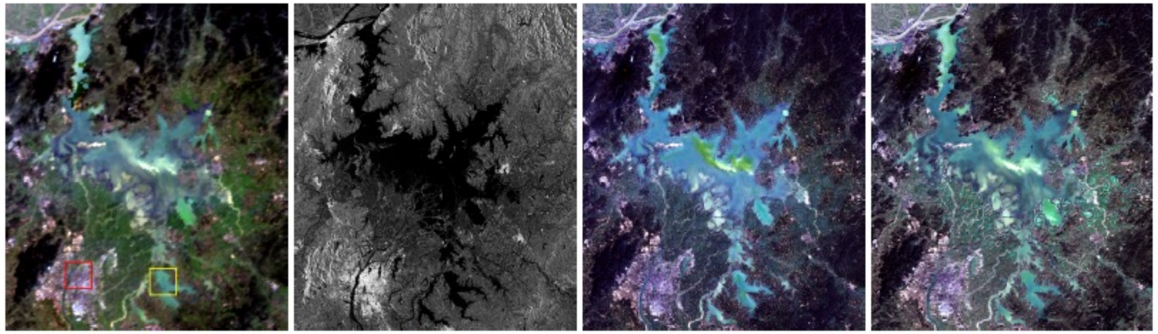

MODIS at t_2 SAR at t_2 DOSTF GAN-SARSP

Figure 4 SAR sharpening results at the moment t1 → t2

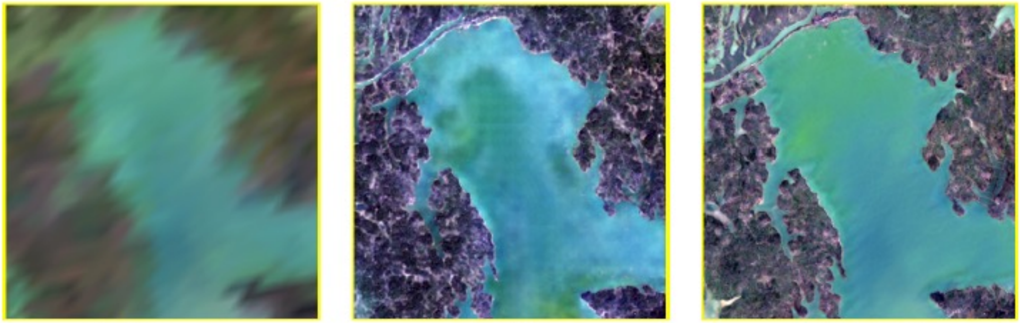

MODIS-water DOSTF GAN-SARSP

Figure 5 Local manifestation of the water in the t1 → t2

t1 → t2 EVALUATION

Model	RMSE	SAM	RASE	ERGAS	SSIM	Q4
STARFM	0.0441	0.1705	0.4161	0.4466	0.8208	0.5733
FSDAF	0.0437	0.1593	0.4127	0.4324	0.8317	0.5765
SPSTFM	0.0573	0.2424	0.5414	0.5085	0.7638	0.5038
Fit-FC	0.0417	0.1431	0.3938	0.3960	0.8535	0.5900
SFSDAF	0.0447	0.1620	0.4217	0.4403	0.8203	0.5631
VIPSTF-SW	0.0429	0.1494	0.4053	0.4028	0.8462	0.5833
DOSTF	0.0397	0.1329	0.3746	0.3895	0.8827	0.6285
MMSTF	**0.0372**	**0.1150**	**0.3513**	**0.3641**	**0.8996**	**0.6588**

The proposed method MMSTF is tested with the data consisting of Landat-8, MODIS, and Sentinel-1 images located in the Poyang Lake of China.

The experimental results confirm the effectiveness of incorporating SAR into spatiotemporal fusion. The quantitative evaluation on radiometric, structural, and spectral loss shows that images produced by our method can provide good reconstruction for flood areas.

WP1: Water extent and level: algo development

An **optimized Pyramid Convolutional Neural Networks and Bottleneck Residual Modules** for Classification SE MSI Images

Labeling

The categories were divided into Crop, Forest land, Artificial building, Bare soil, Wetland (Wet sand), Sediment (Bright water), NoRmal water, Dark water, Sands, 9 categories .

Figure 1 Sediment (bright water)

The parameters are optimized using the stochastic gradient descent algorithm. The training repeated 200 epoches. The learning rate is 0.0003 for the 1-100 epoches and 0.00015 for the 101-200 epoches.

8 input for Sentinel-2: Band 2 (492nm), Band 3 (559nm), Band 4 (664nm), Band 5 (704nm),
Band 8 (832nm), Band 11 (1613nm), Band 12 (2202nm), MNDWI

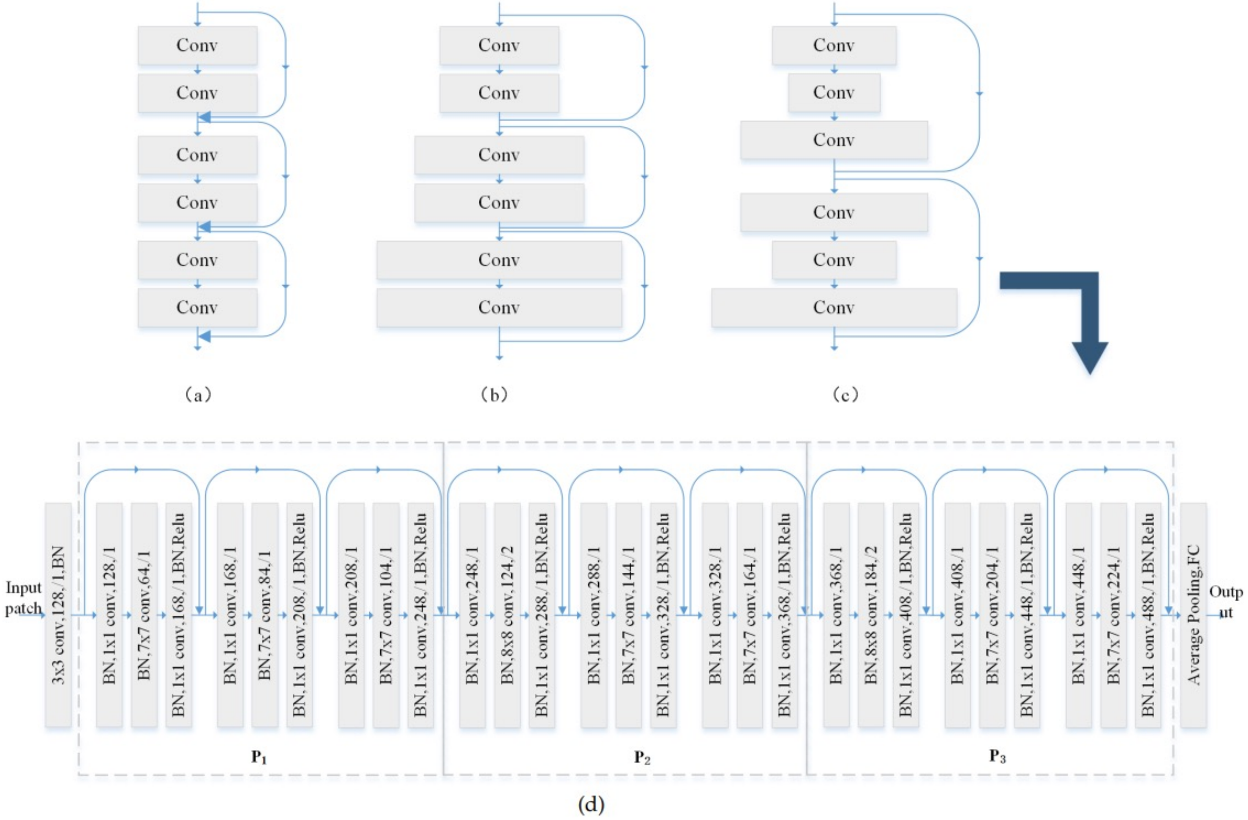

Figure 2 Different residual cells and deep network architectures used for pyramid residuals (a) Traditional residual unit (b) Bottleneck residual unit (c) Pyramid residual unit (d) Proposed pyramid residual network architecture

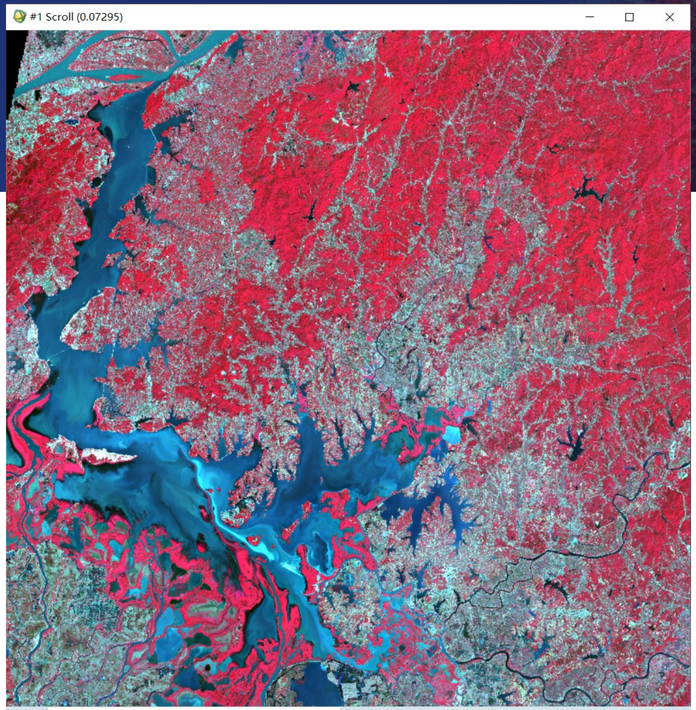

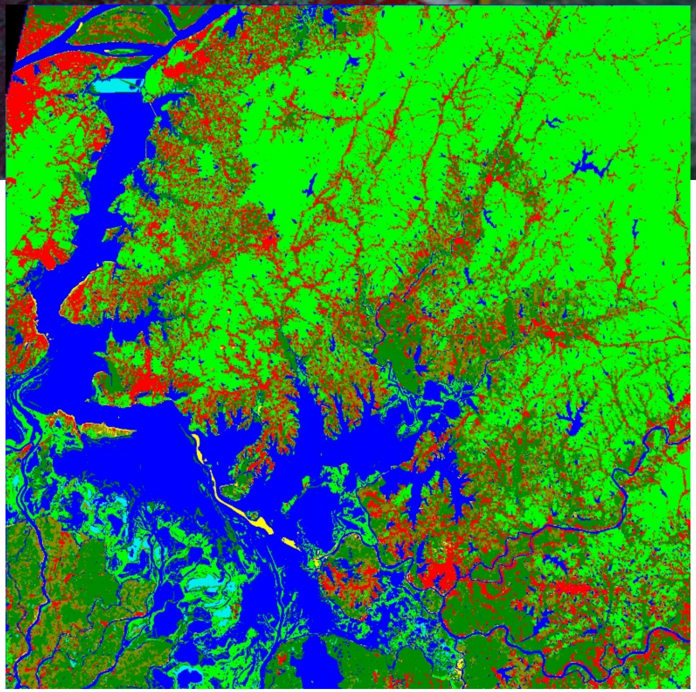

01/05/2021

Color bar

- Crop
- Forest
- Artificial building
- Bare soil
- Wetlands
- Sediment
- Nomal water
- Dark water
- Sands

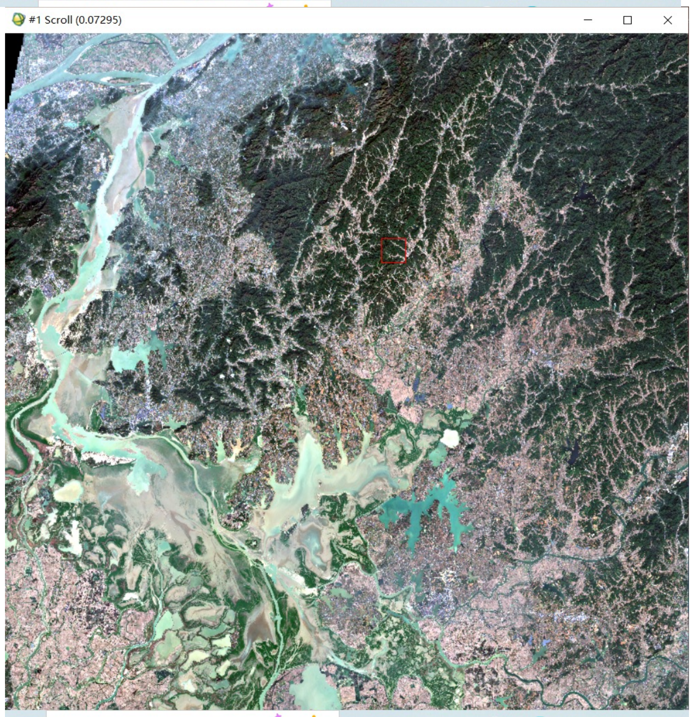

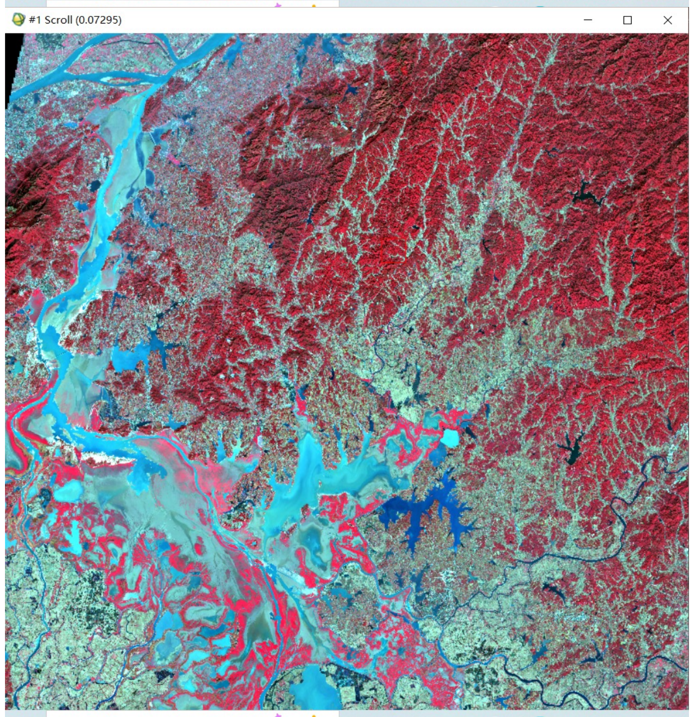

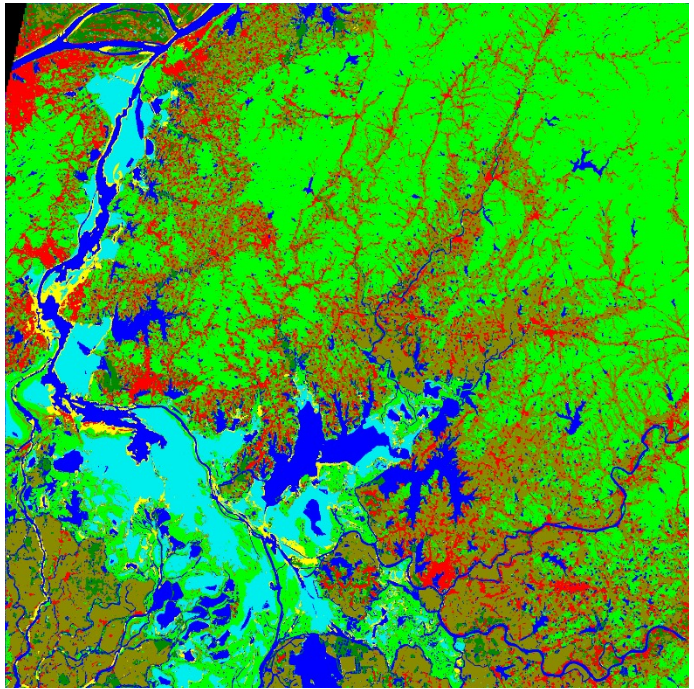

11/27/2021

WP1: Water extent and level & volume variations

Next steps for LWE and LWL :

- Continue in 2023-2024 the LWE/LWL monitoring, densify the derived times series, LWE with S1 for summer months, LWL with Jason and Jason CS/Sentinel6

- SWOT data analysis: challenging
  - Providing for all water bodies > 6ha LWE and LWL
  - Impact of floating vegetation on signal
  - Blackwater ?
  - Omision commision ? open water in lakes/cultures

- Data available soon : access end October?

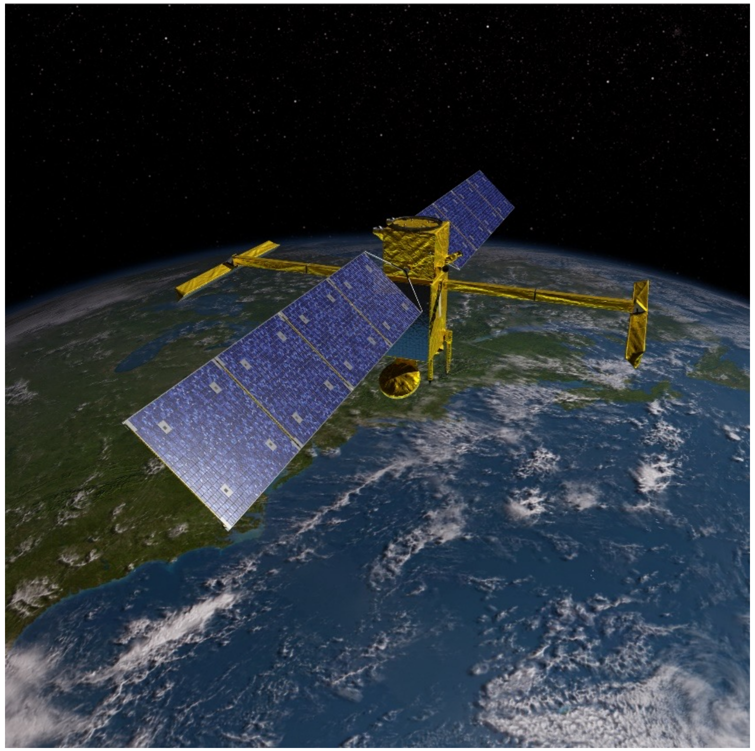

WP2: Water quality

Context

In shallow lakes problem of

- algal bloom, floating/emergent and submerged vegetation lakes
- dissolved CO2 concentrations
- Suspended sediments

With the increasing problem of eutrophication, lacustrine ecosystem shift from a clear macrophyte-dominated state to a turbid phytoplankton-dominated state.

However, it’s not clear how lake transitions occur at regional and global scales. This is due to a lack of long-term monitoring and difficultuy to separe floating/emergent aquatic vegetation (FEAV), submerged aquatic vegetation (SAV) and algal bloom (AB).

WP2: Water quality

Quantifying algal bloom, floating/emergent and submerged vegetation in eutrophic shallow lakes using Landsat imagery

26 large lakes
Exensive field data

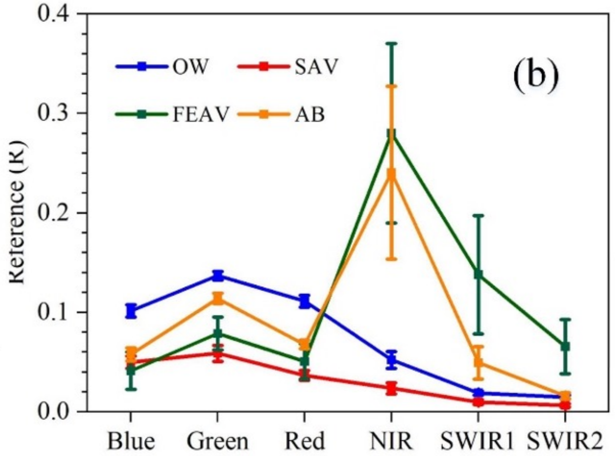

Landsat 8 OLI band reflectance of different groups

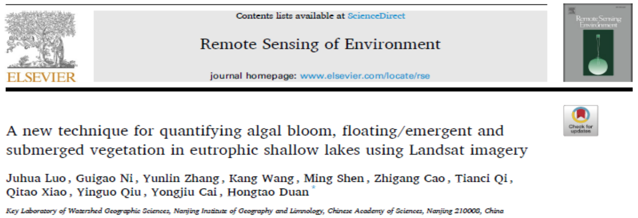
Contents lists available at ScienceDirect

Remote Sensing of Environment

journal homepage: www.elsevier.com/locate/rse

ELSEVIER

A new technique for quantifying algal bloom, floating/emergent and submerged vegetation in eutrophic shallow lakes using Landsat imagery

Juhua Luo, Guigao Ni, Yunlin Zhang, Kang Wang, Ming Shen, Zhigang Cao, Tianci Qi, Qitao Xiao, Yinguo Qiu, Yongjiu Cai, Hongtao Duan

Key Laboratory of Watershed Geographic Sciences, Nanjing Institute of Geography and Limnology, Chinese Academy of Sciences, Nanjing 210008, China

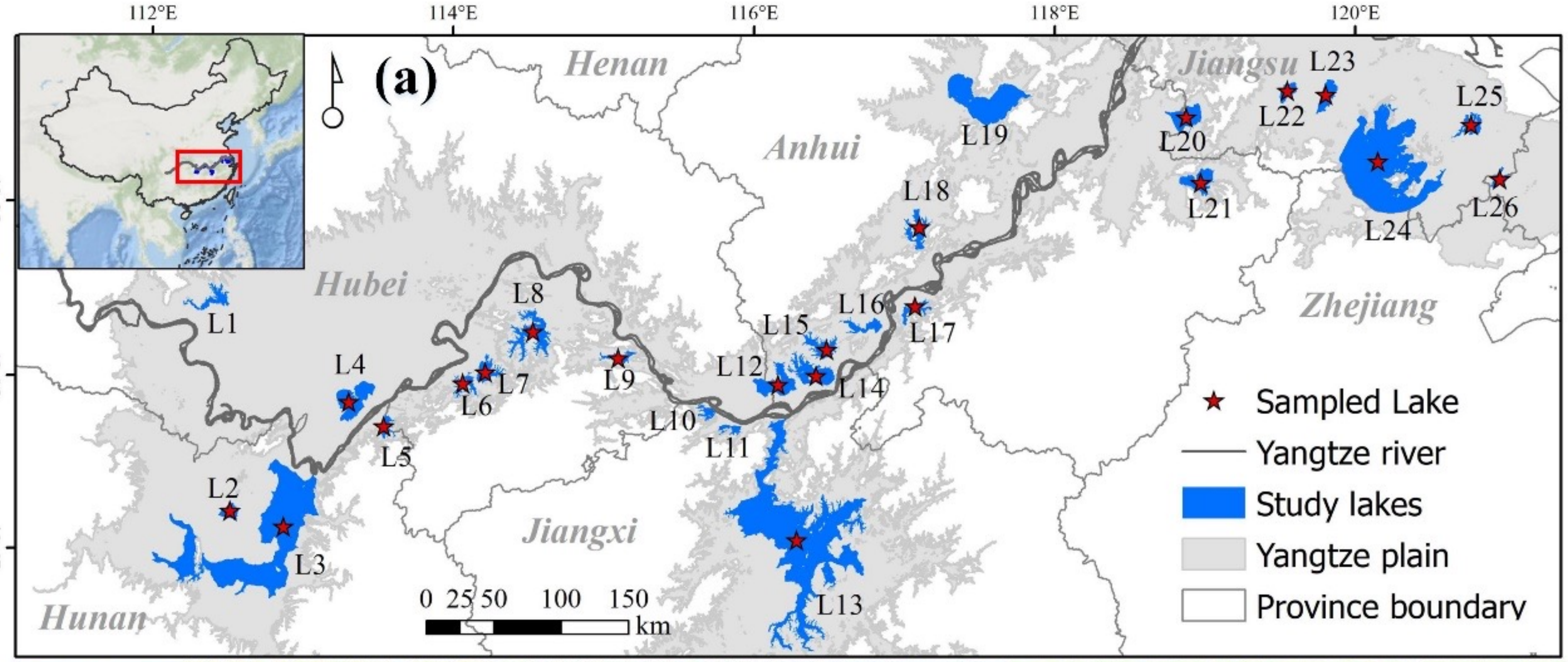

Floating-leaved and emergent aquatic vegetation (FEAV) (b1 – b3), submerged aquatic vegetation (SAV) (c1 – c3) and algal bloom (AB) (d1 – d3).

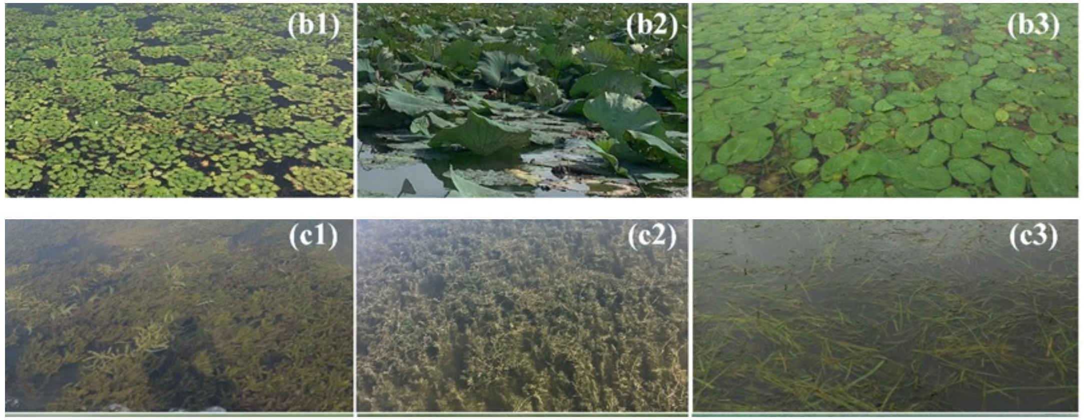

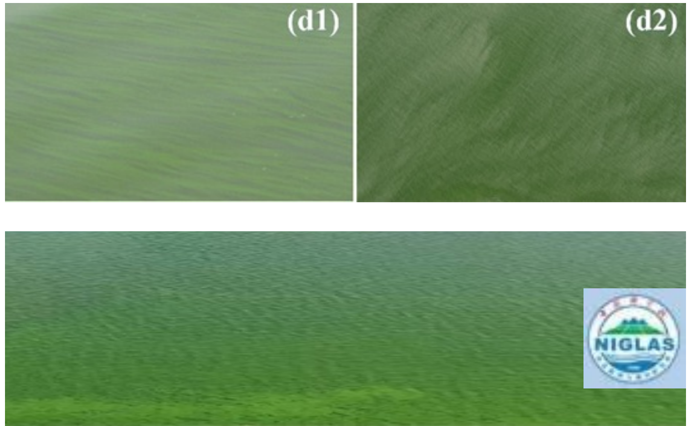

WP2: Water quality

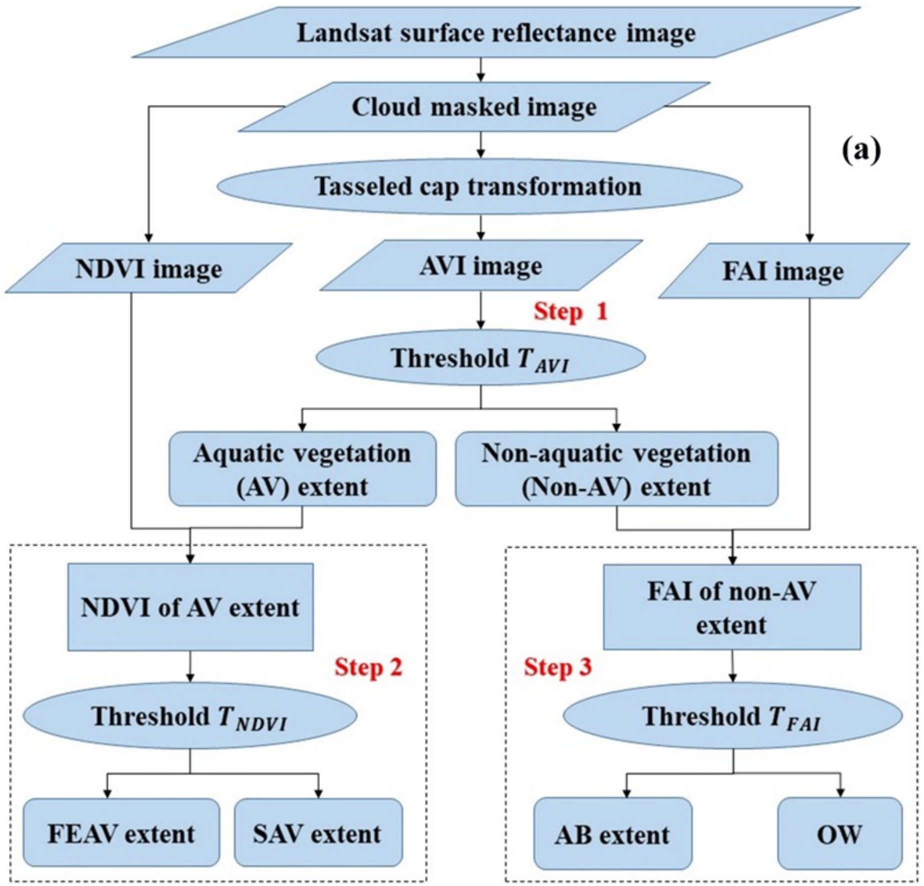

Workflow of the vegetation and bloom indices (VBI) algorithm proposed for mapping FEAV, SAV and AB

Novel three-step classification algorithm based, vegetation and bloom indices (VBI) algorithm):

(1) to distinguish between aquatic vegetation (AV) and non-aquatic vegetation (non-AV) extents by an aquatic vegetation index (AVI) derived from tasseled cap transformation;

(2) to identify Emerged and floating AV and Submergerd AV within AV extent by using the normalized difference vegetation index (NDVI),

(3) to extract AB from non-AV extent with floating algae index (FAI).

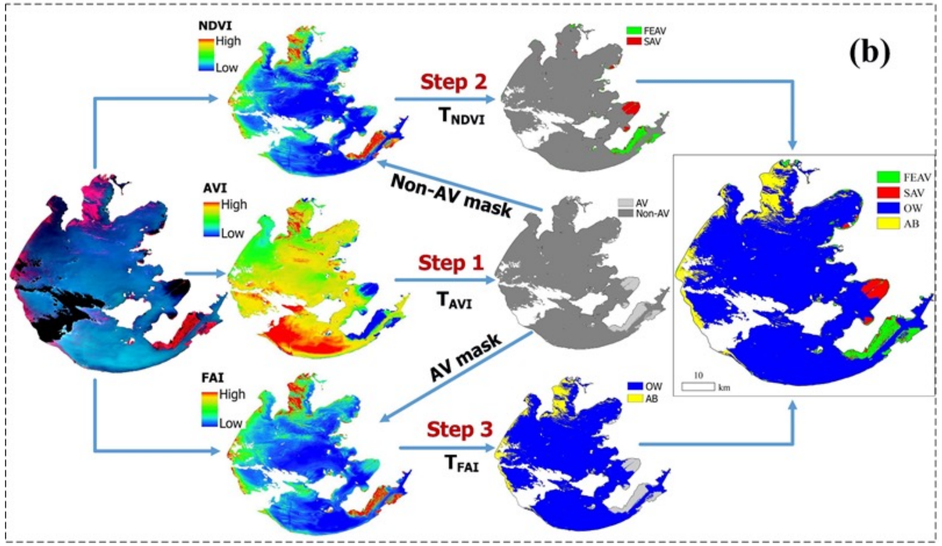

Tai Hu
2019/8/21

WP2: Water quality

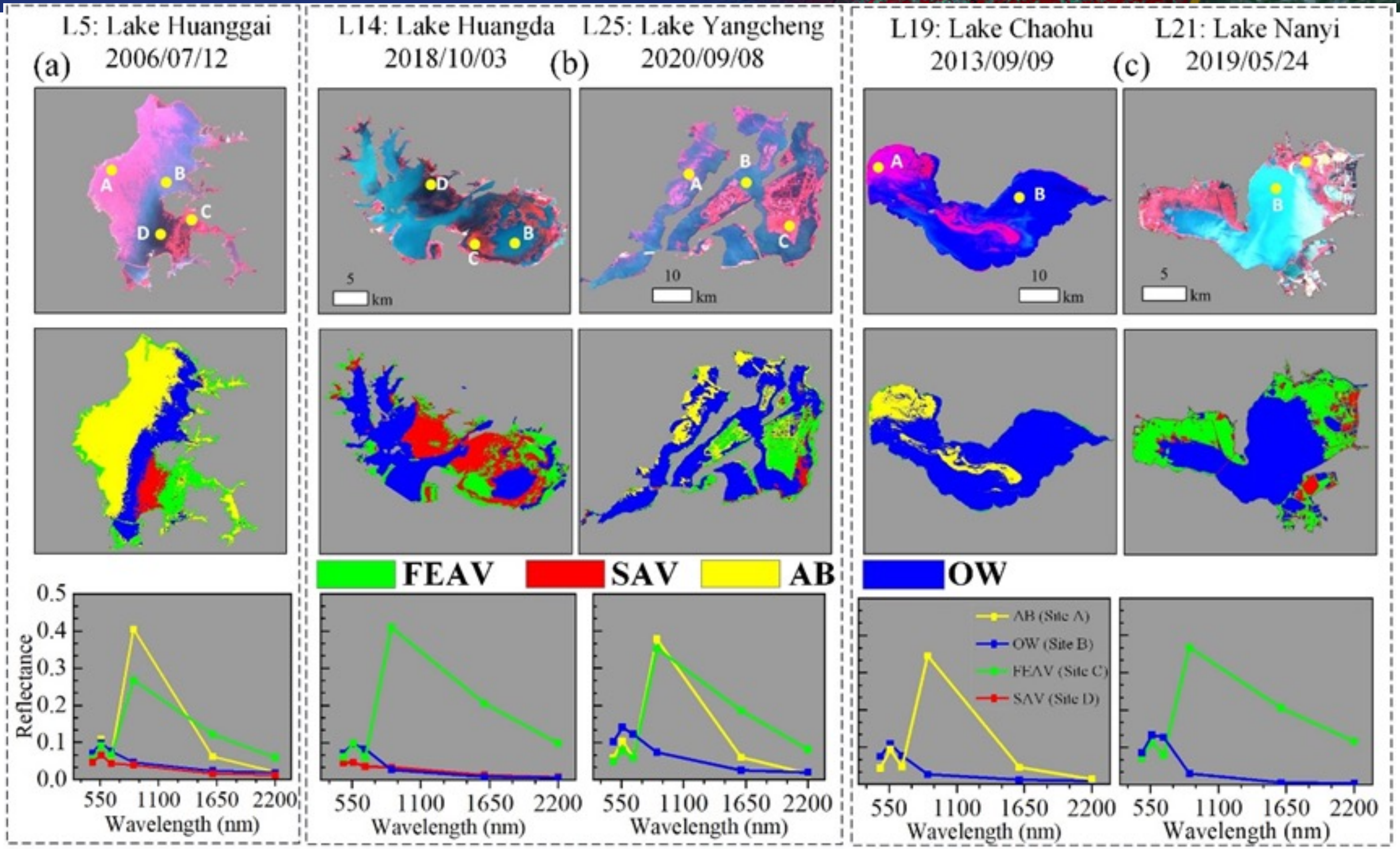

Landsat RGB false images and corresponding classification maps derived from our VBI algorithm in five lakes with different dominant communities and Landsat bands reflectance of typical classes. (a) Lake Huanggai with three types such as FEAV, AB and SAV; (b) lake with two main types (i. e. SAV and FEAV in L14, AB and FEAV in L25); (c) lake with single dominant type (i.e., AB in L19 or FEAV in L21).

WP2: Water quality

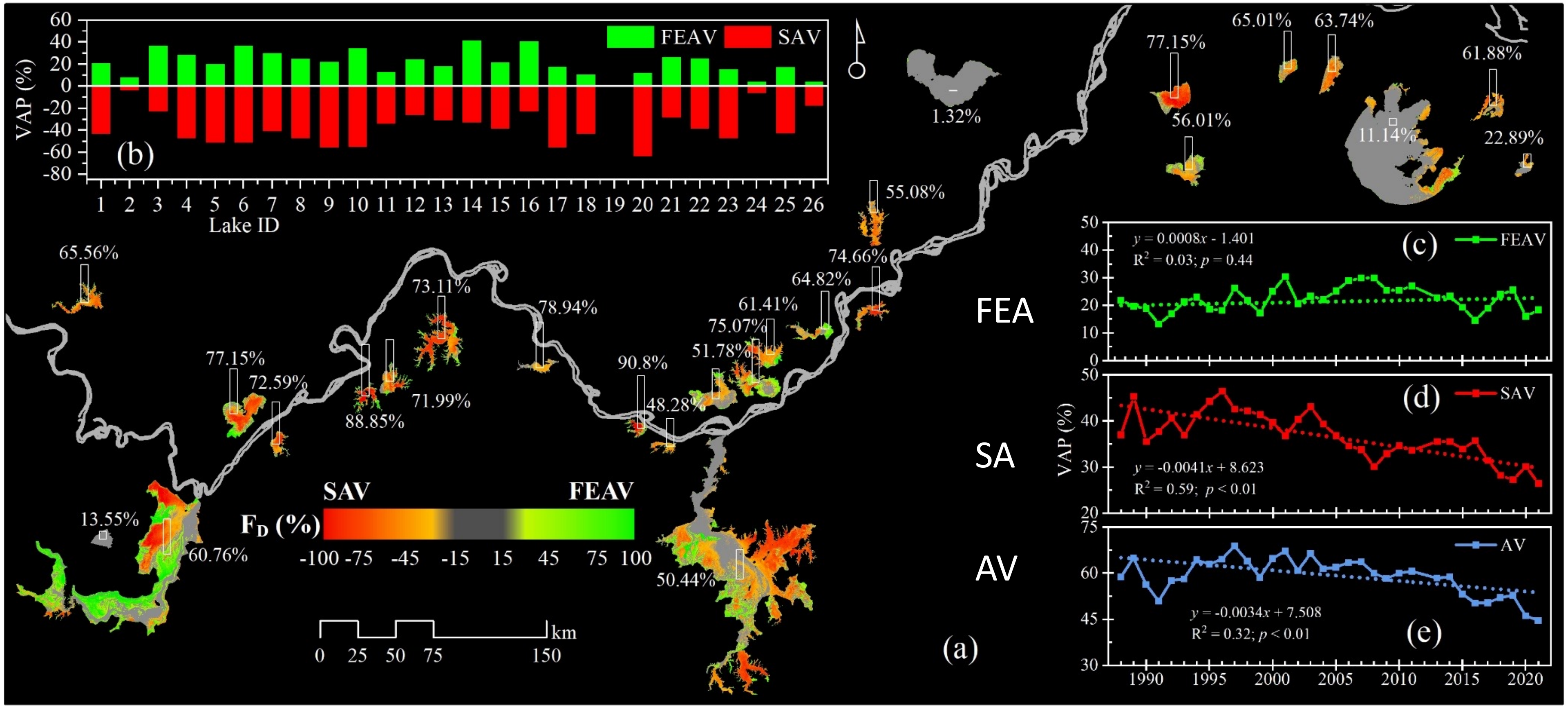

Aquatic Vegetation

Submerged versus Floating & emerged vegetation

Spatial-temporal distribution of AV in the lakes (> 50km2) of the middle and lower reaches of the Yangtze River from 1985 to 2021. (a) Frequency distribution of dominant AV types and average aquatic vegetation percentage (AVP); (b) VAP of FEAV and SAV in 26 lakes; (c – e) change trends of VAP for FEAV, SAV and AV

WP2: Water quality

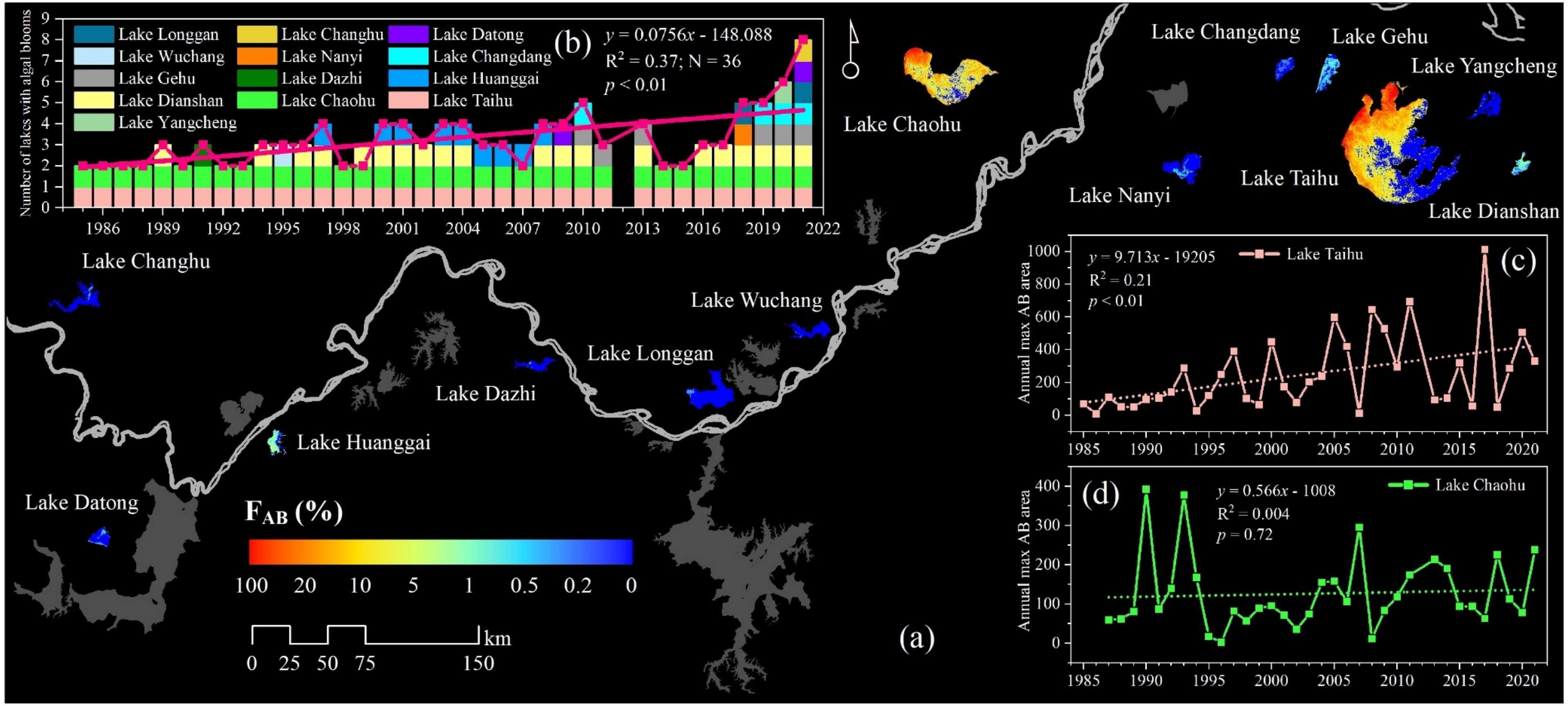

Alga Bloom

Spatial-temporal distribution of FAB in the lakes (> 50km2) of the middle and lower reaches of the Yangtze River from 1985 to 2021. (a) Frequency distribution of AB; (b) number of lakes with AB; (c – d) change trends of AB in Lake Taihu and Lake Chaohu, respectively.

WP2: Water quality

in the past 30 years, the aquatic vegetation, especially SAV, in the lakes in MLY, has decreased significantly, while the number of lakes and occurrences of AB has increased significantly

This phenomenon may be a warning: the lakes in MLY may be gradually shifting from macrophyte-dominated lakes to phytoplankton-dominated lakes.

New validated method exploiting SWIR Band

Landsat limitations both in term of spatial resolution and frequency of revisit

=> Next steps exploitation of Sentinel2

WP2: Water quality

Remote sensing of dissolved CO2 concentrations in meso-eutrophic lakes using Sentinel-3 imagery

16 lakes in the middle and lower reaches of the Yangtze and Huai River (ML_YHR) basins in Eastern China (N = 248).

Stepwise quadratic polynomial regressions of several combinations of chlorophyll-a (Chl-a), water temperature (Tw), Secchi disk depth (ZSD), and photosynthetic active radiation (PAR)-related variables were tested and validated to select the best approach.

Contents lists available at ScienceDirect
Remote Sensing of Environment
journal homepage: www.elsevier.com/locate/rse
ELSEVIER

Remote sensing of dissolved CO_2 concentrations in meso-eutrophic lakes using Sentinel-3 imagery

Tianci Qi[a,b], Ming Shen[a], Tiit Kutser[c], Qitao Xiao[a], Zhigang Cao[a], Jinge Ma[a,b], Juhua Luo[a], Dong Liu[a], Hongtao Duan[a,d,*]

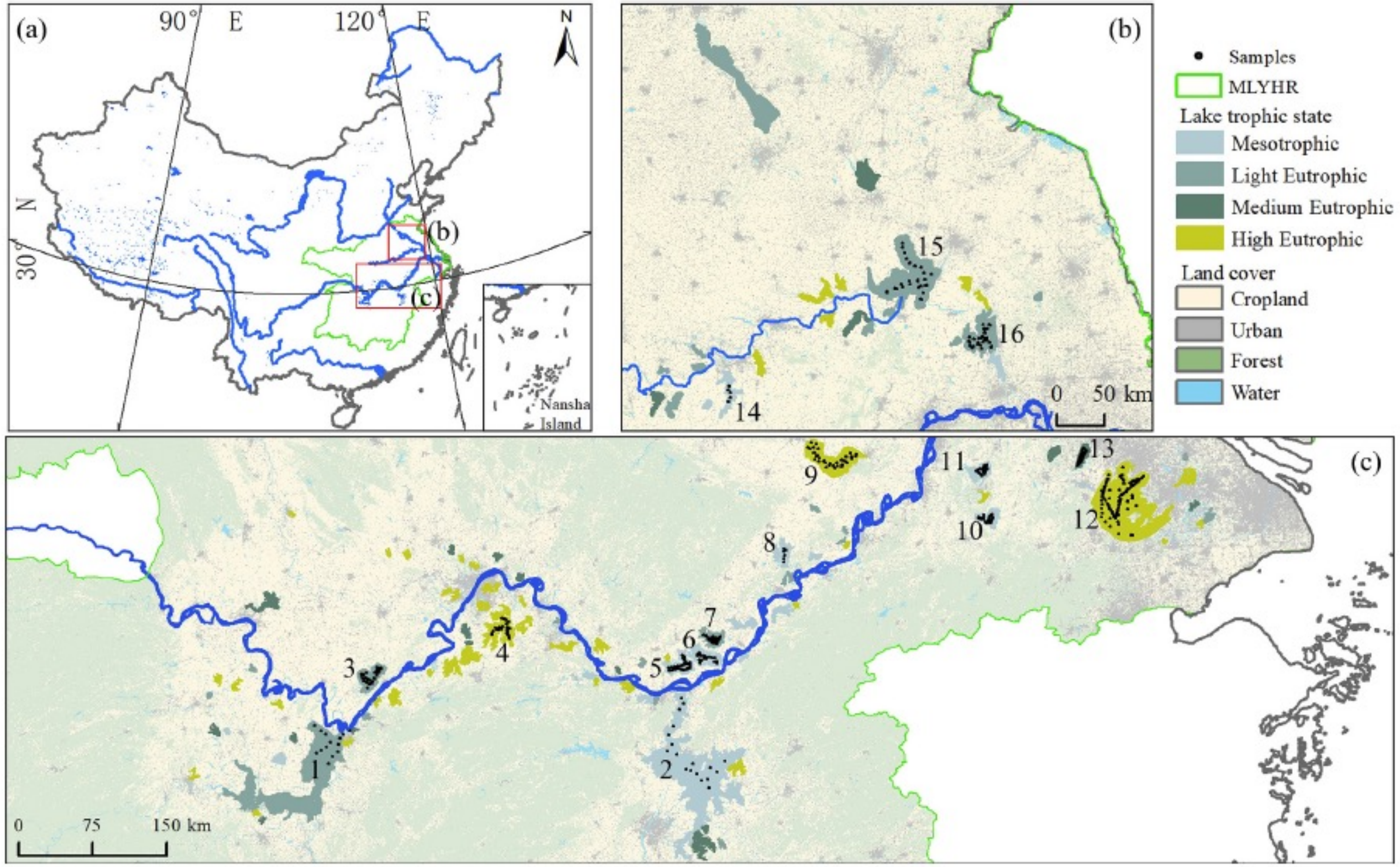

Map of lakes larger than 10 km2 in the Huai River basin and the middle and lower reaches of the Yangtze River basin.
16 sampled lakes as black dots.

WP2: Water quality

Remote sensing of dissolved CO_2 concentrations in meso-eutrophic lakes using **Sentinel-3 imagery**

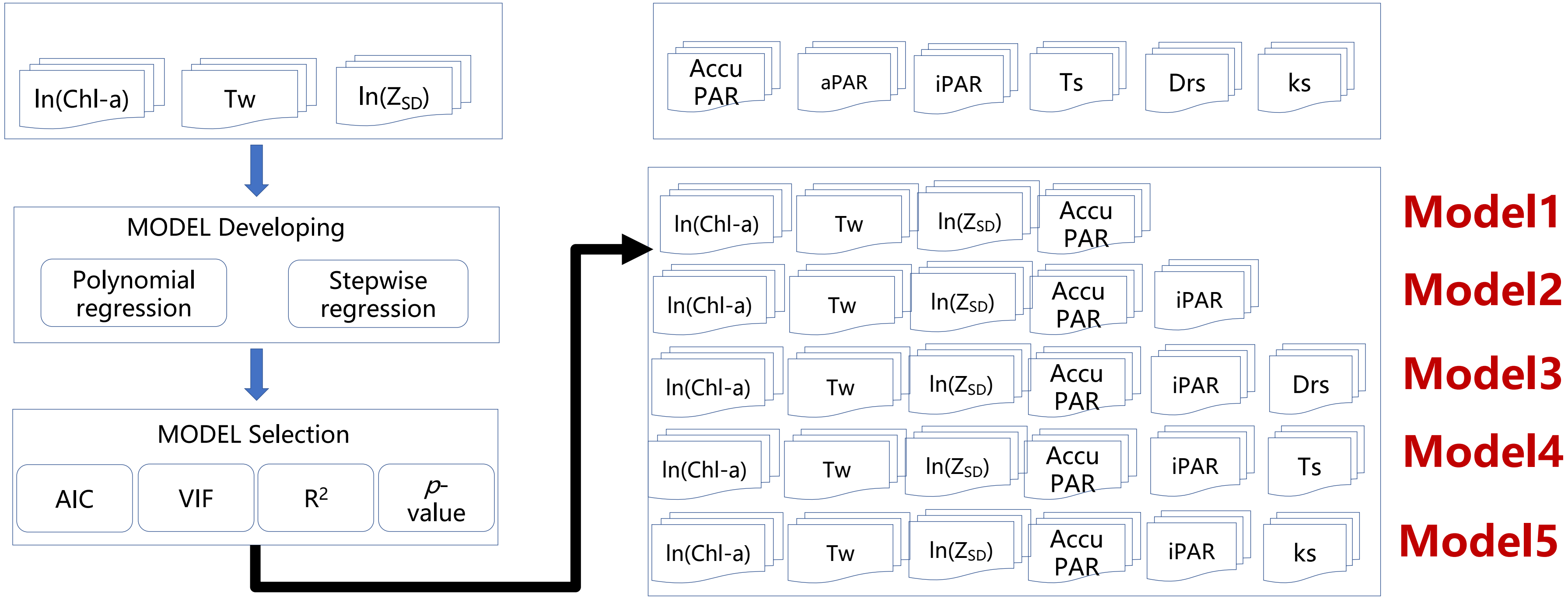

Schematic block diagram illustrating the primary process of satellite data processing and model development.

WP2: Water quality

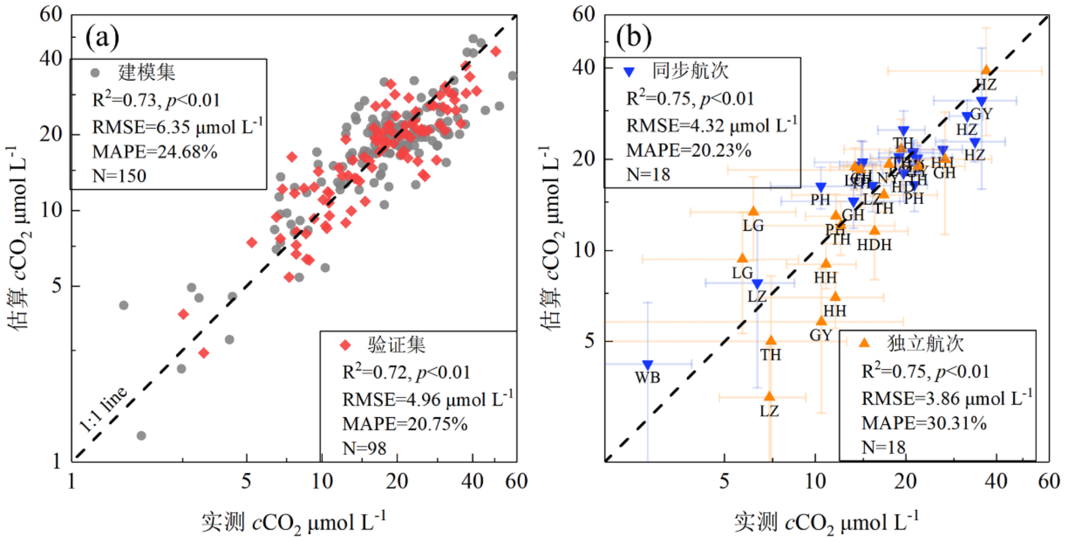

Precision comparison using the *c*CO2 estimation model

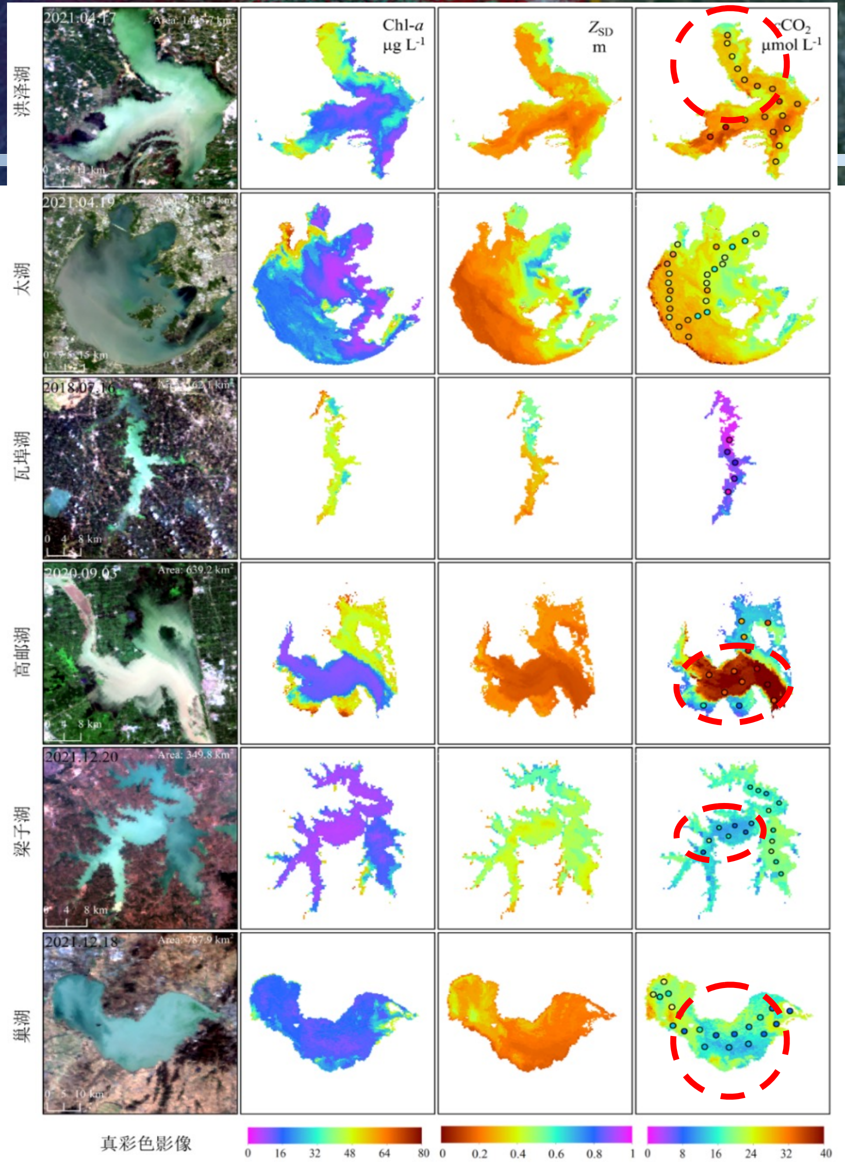

Models' comparison

Spatial pattern comparison of *c*CO2 estimation models. The first column shows RGB images obtained from Sentinel-3 OLCI. The second and third columns show satellite-derived Chl-*a* and *ZSD*, respectively. The fourth colums show satellite-estimated images of *c*CO2 based on our model

WP2: Water quality

S3 : 10:30

Aqua 13:00

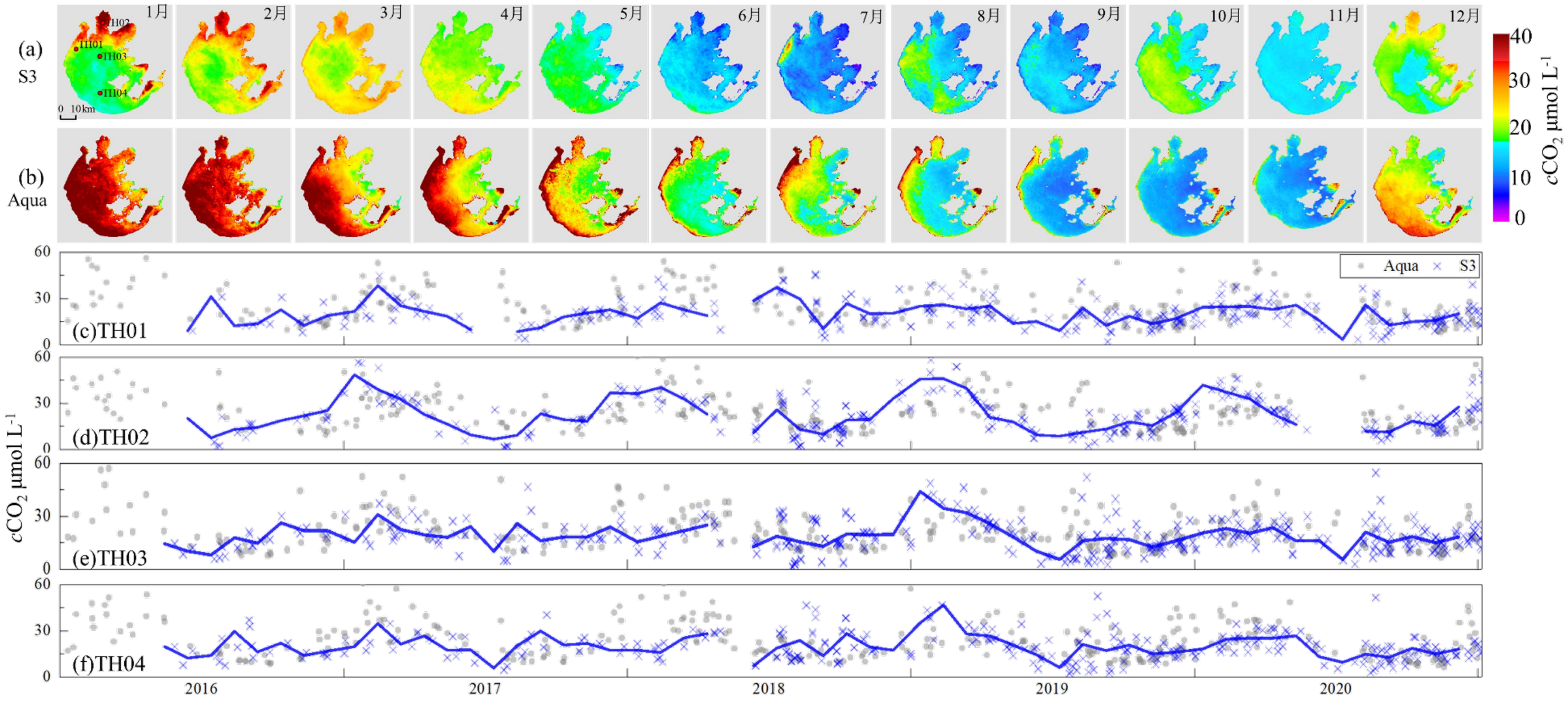

Models' comparison

Monthly spatial variation of cCO2 estimated by (a) our model using Sentinel-3 data and by (b) Qi et al. (2020) model using Aqua data from 2016 to 2020 in Lake Taihu. (c-f) time series of daily cCO2 in Lake Taihu represented by Aqua-estimated (gray dots) and Sentinel-3-estimated (blue Xs).

Blue lines are Sentinel-3-estimated variations in the monthly mean estimates for cCO2 from 2016 to 2020

WP2: Water quality

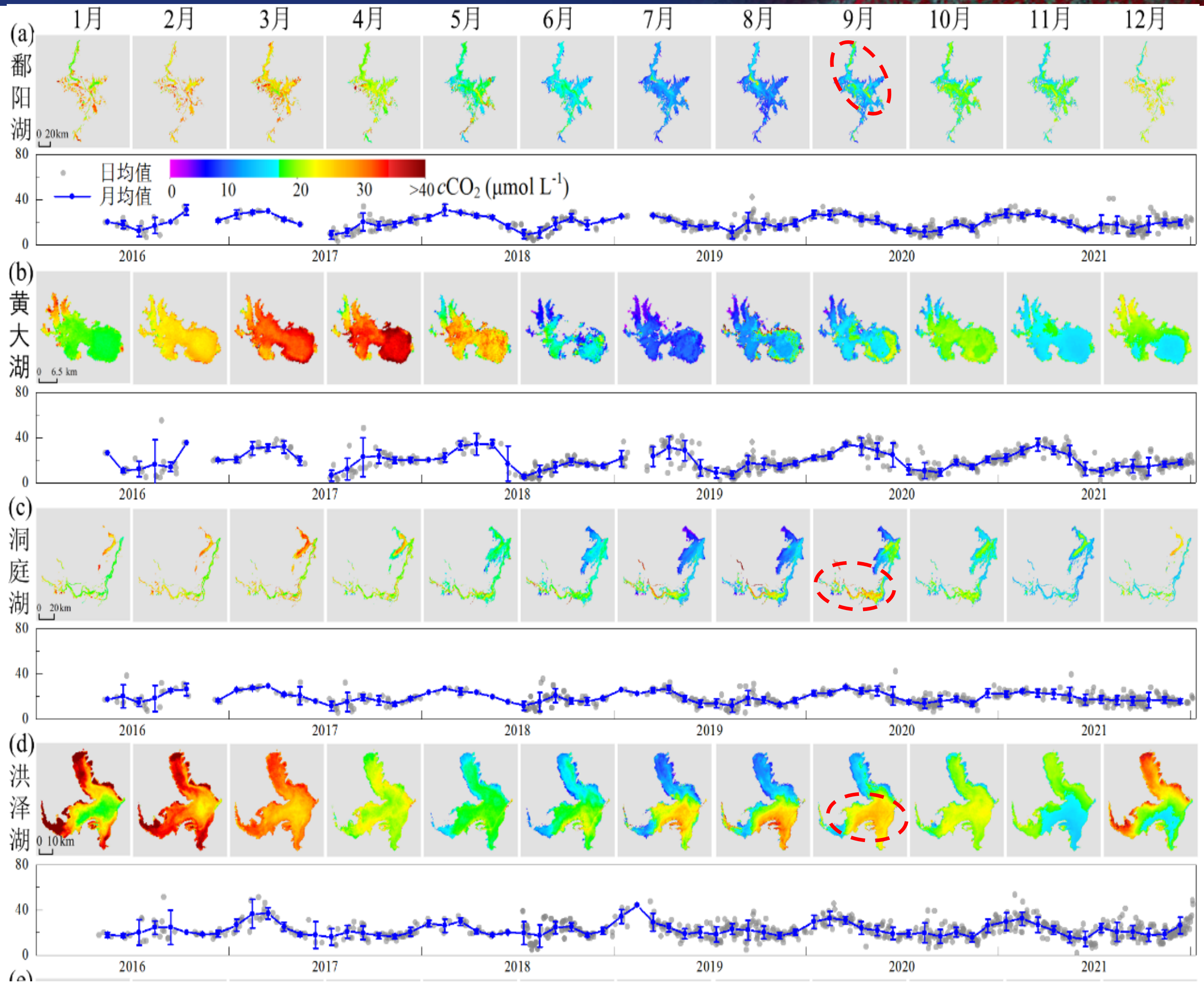

Mesotrophic lakes

(a) Lake Poyang

(b) Huangda

Light eutrophic lakes:

(c) Lake Dongting

(d) Hongze;

Monthly spatial variation of satellite-estimated cCO2 from 2016 to 2021

WP2: Water quality

Model Sensitivity: Monte Carlo

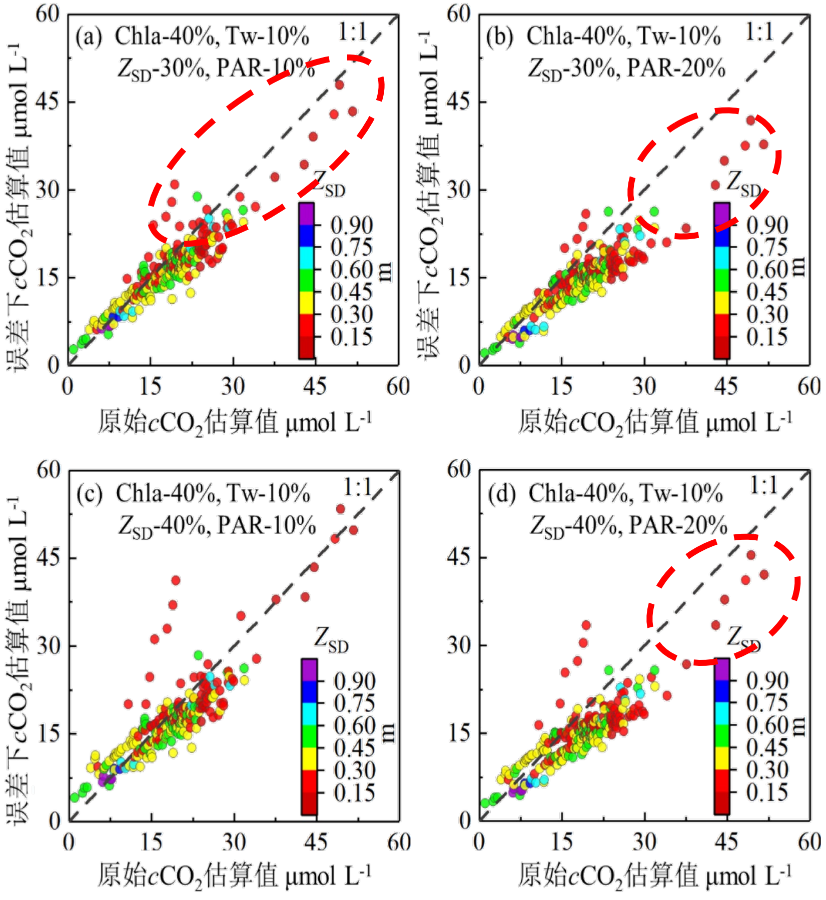

Model sensitivity to changes in Chl-*a*, Tw, *ZSD*, and PAR based on Monte Carlo simulation.

包含误差的输入变量	*RMSE* μmol L^{-1}	*MAPE* %	*MRD* %	*MB* μmol L^{-1}	*MR*
Chla, 40%; Tw, 10%	3.03	11.86	-3.25	-1.20	0.97
Chla, 40%; Zsd, 40%	4.53	21.90	9.16	0.19	1.09
Chla, 40%; PAR, 20%	5.18	21.17	-20.33	-4.08	0.80
Tw, 10%; Zsd, 40%	4.42	20.76	14.08	1.33	1.14
Tw, 10%; PAR, 20%	4.03	15.84	-14.04	-2.76	0.86
Zsd, 40%; PAR, 20%	3.91	18.10	-6.66	-1.94	0.93
Chla, 40%; Tw, 10%; Zsd, 40%;	4.30	21.85	7.91	-0.09	1.08
Chla, 40%; Tw, 10%; PAR, 20%	5.37	21.59	-20.72	-4.20	0.79
Chla, 40%; Zsd, 40%; PAR, 20%	5.17	24.62	-12.39	-3.30	0.88
Tw, 10%; Zsd, 40%; PAR, 20%	3.96	18.56	-6.56	-1.98	0.93
Chla, 40%; Tw, 10%; Zsd, 30%; PAR, 10%	**3.54**	**15.98**	**-4.81**	**-1.75**	**0.95**
Chla, 40%; Tw, 10%; Zsd, 30%; PAR, 20%	5.14	21.68	-17.31	-3.84	0.83
Chla, 40%; Tw, 10%; Zsd, 40%; PAR, 10%	4.14	20.88	1.53	-1.06	1.02
Chla, 40%; Tw, 10%; Zsd, 40%; PAR, 20%	**5.18**	**24.53**	**-12.89**	**-3.40**	**0.87**

WP2: Water quality

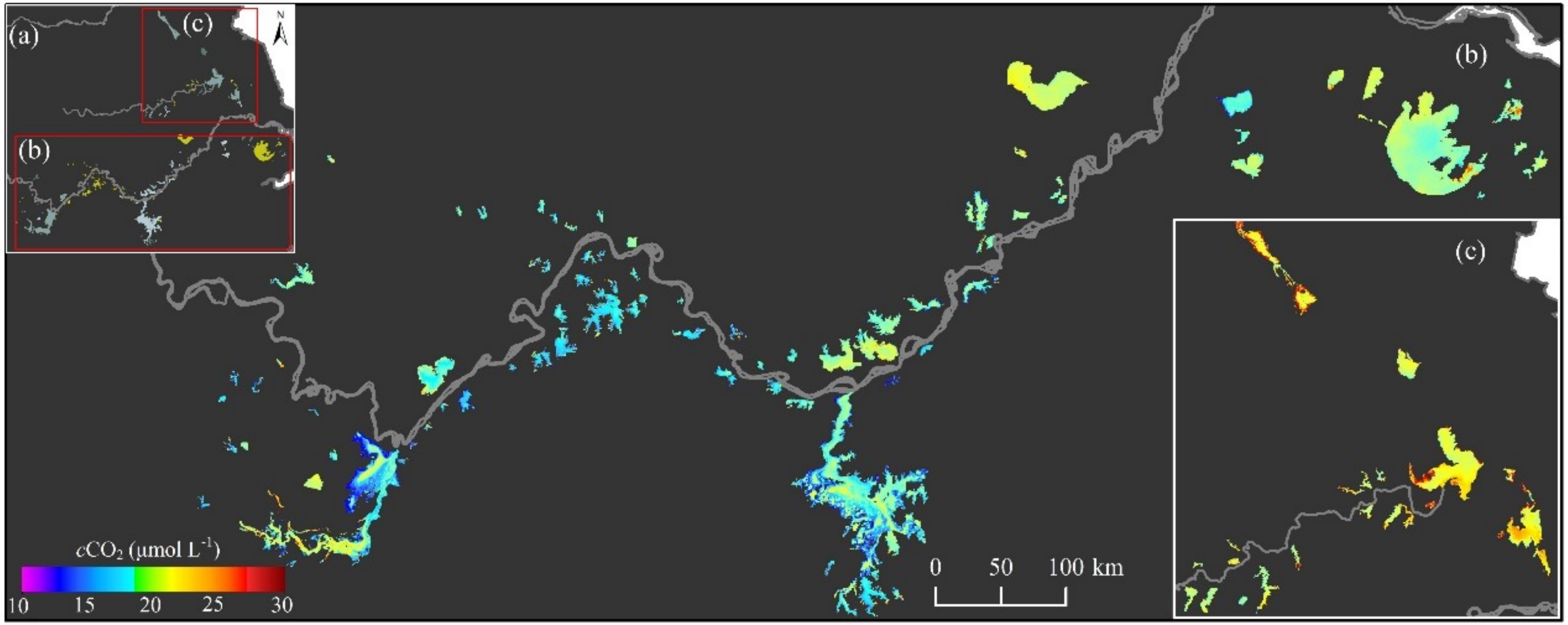

Extension of the model to 113 lakes

Spatiotemporal variations of satellite-estimated *c*CO2 from 2016 to 2021 for lakes larger than 10 km2 in the study area. (a): location and trophic state of lakes in the middle and lower reaches of the Yangtze River and the Huai River (ML_YHR) basins in China

WP2: Water quality

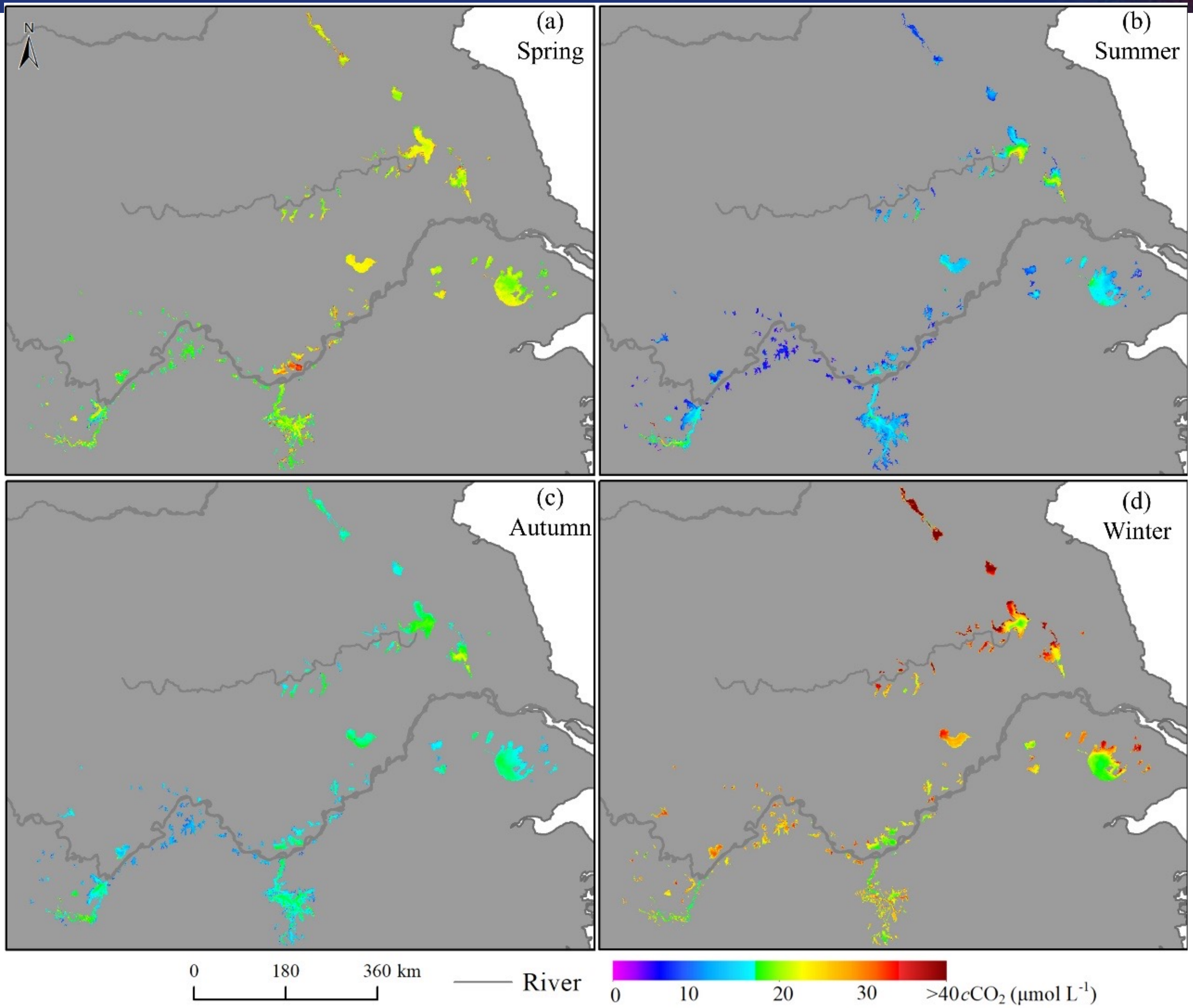

Satellite-estimated seasonal variation of *c*CO2 for lakes larger than 10 km2 in the middle and lower reaches of the Yangtze River and the Huai River basins,

Overall, the satellite-estimated cCO2 of lakes in the ML_YHR basins also showed dramatic seasonal variations with a mean variation coefficient of the monthly mean cCO2 as high as 52.59%.

The cCO2 of eutrophic lakes was higher than that of the mesotrophic lakes in the winter months but lower than that of mesotrophic lakes during other seasons.
At the same time, this difference would increase with the degree of eutrophication. Specifically, in the summer and autumn months, the estuary areas of lakes showed extremely high values of the cCO2, while the more eutrophic areas showed extremely low values of cCO2 (b, c).

Conversely, the more eutrophic areas of lakes in spring and winter showed relatively high cCO2 values, while the estuary areas had relatively low cCO2 values

WP2: Water quality

Satellite-estimated spatial cCO2 variations for large lakes (>100 km2) with different trophic states showed dramatic but reasonable heterogeneity

Satellite estimates showed high cCO2 near the channel or estuary of rivers in lakes with a high river–lake connectivity, such as Lake Poyang, Lake Dongting, and Lake Hongze

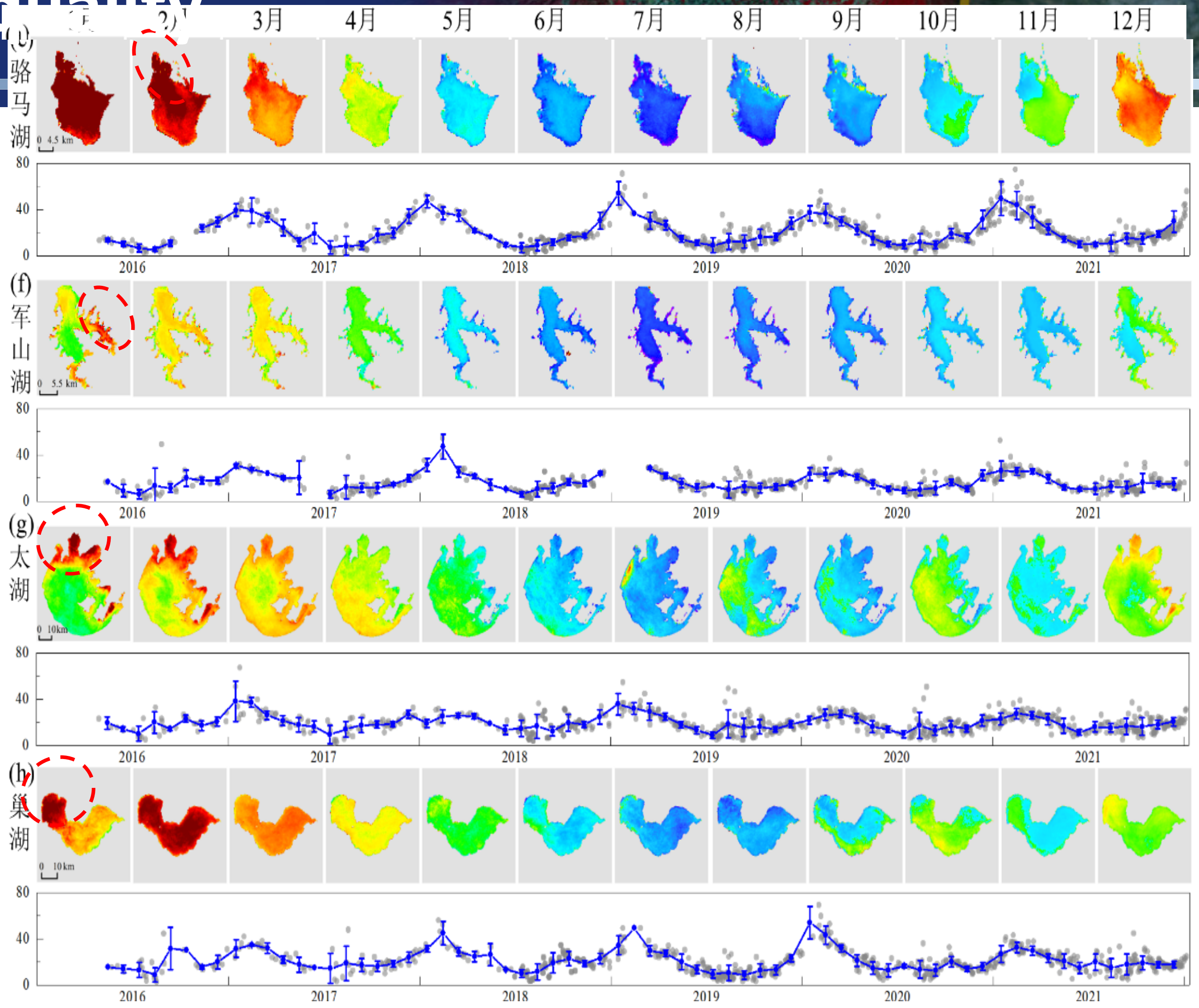

Medium eutroph
Lake Luoma

Junshan;.

High eutrophic:
Lake Taihu

Chaohu

Monthly spatial variation of satellite-estimated *c*CO2 from 2016 to 2021 for the largest two lakes in each trophic state among the 113 studied lakes. :

WP2: Water quality

Satellite-derived Chl-a, ZSD, Tw, and PAR products are good cCO2 predictors for lakes in the ML_YHR basins with conditions ranging from mesotrophic to highly eutrophic.

The reconstructed multi-year cCO2 spatiotemporal dynamics of lakes in the ML_YHR basins showed dramatic seasonal variations, which were low in the summer and autumn but high in the winter and spring.

This study is the first estimate and the reconstruction of multi-year cCO2 covering regional lakes using satellite data, which proves the application potential of the remote sensing approach in large-scale lake CO2 emission estimations.

Remote sensing approach will contribute to further reducing uncertainty in global lake CO2 emission estimates.

WP3: Wetland Mapping and Biodiversity

Land Cover/Land Use Classification

Overview Map of Inner Dongting Lake and Ramsar No. 551 in Hunan Province, China

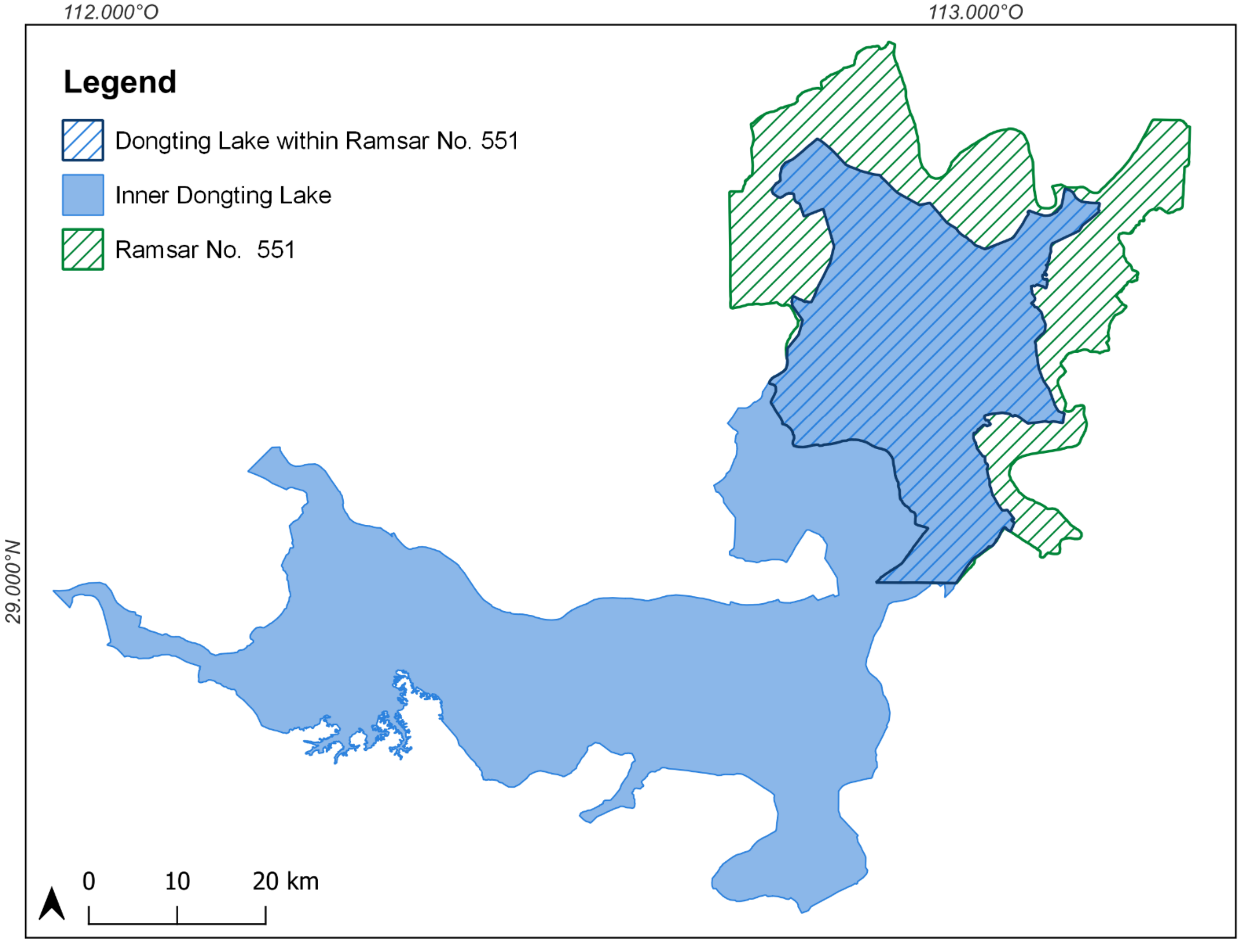

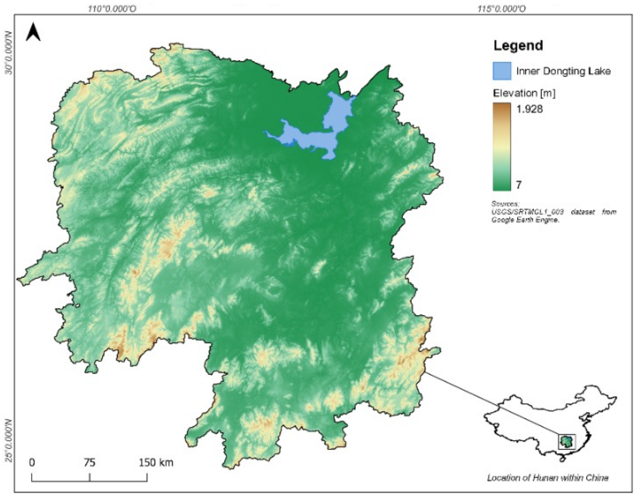

WP3: Wetland Mapping and Biodiversity

Copernicus Global Landcover Layer 100m of Dongting Lake, China

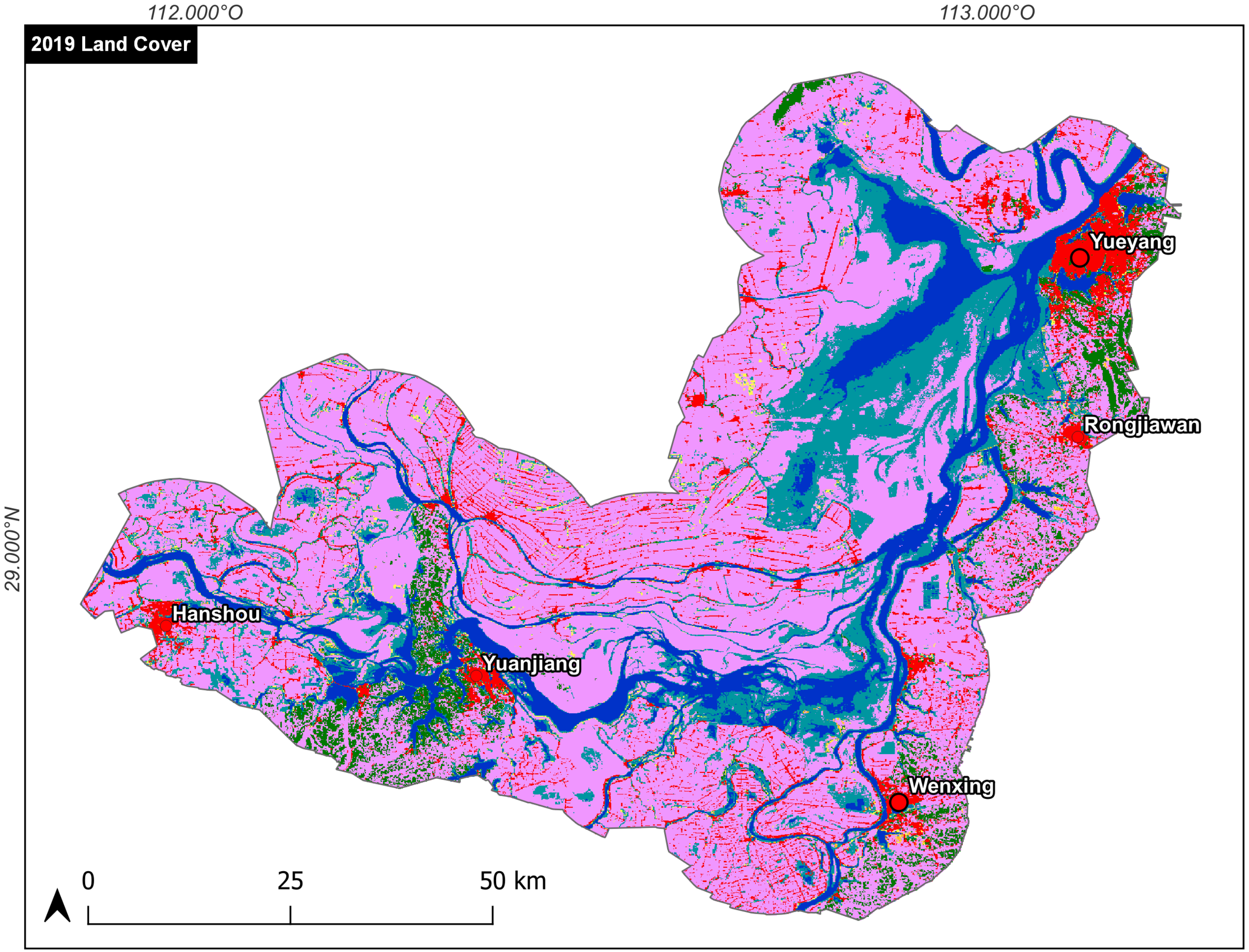

Legend

Kanal 1: discrete_classification (Palette)

- Shrubs
- Herbaceous Vegetation
- Cultivated and Managed Vegetation / Agriculture
- Urban / Built up
- Permanent Water Bodies
- Herbaceous Wetland
- Moss and Lichen
- Treecover

WP3: Wetland Mapping and Biodiversity

Comparison of Copernicus Global Landcover Product and DLR Sentinel 2 Land Cover Classification

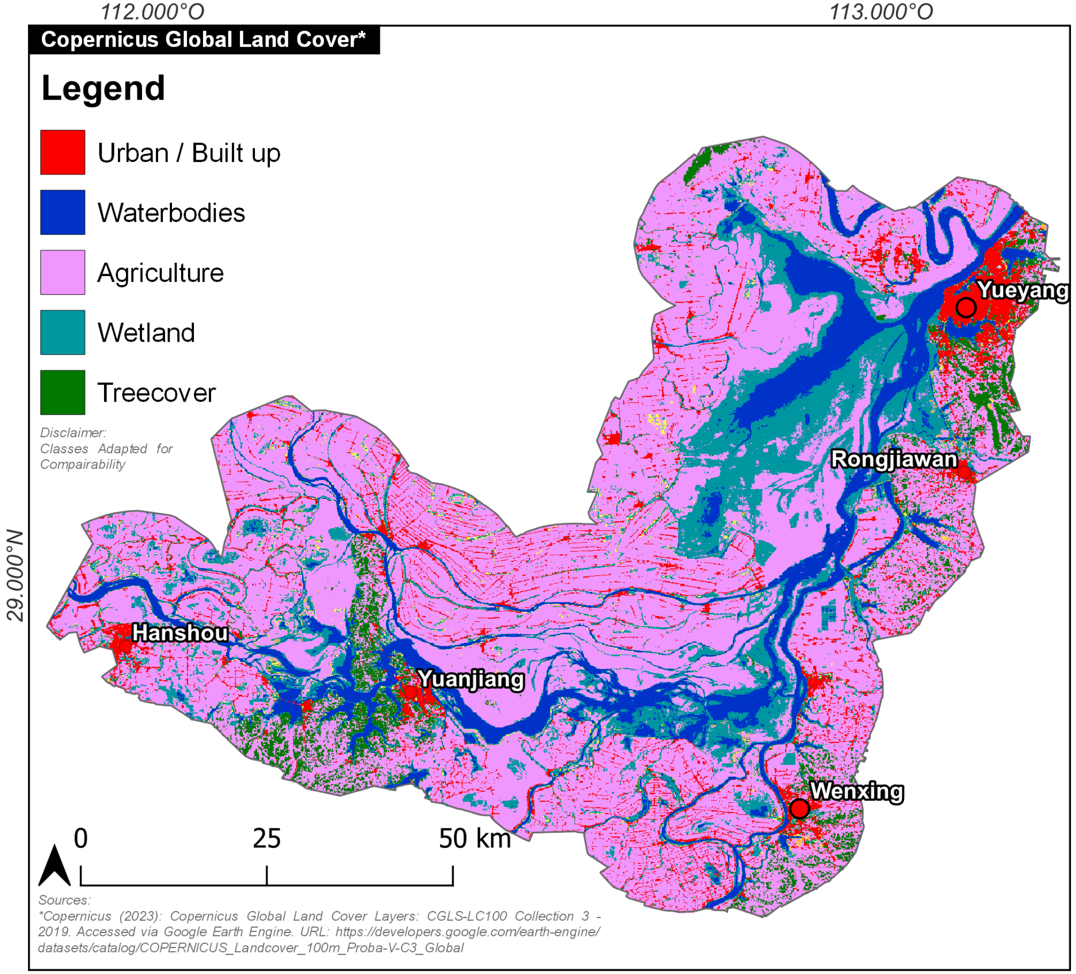

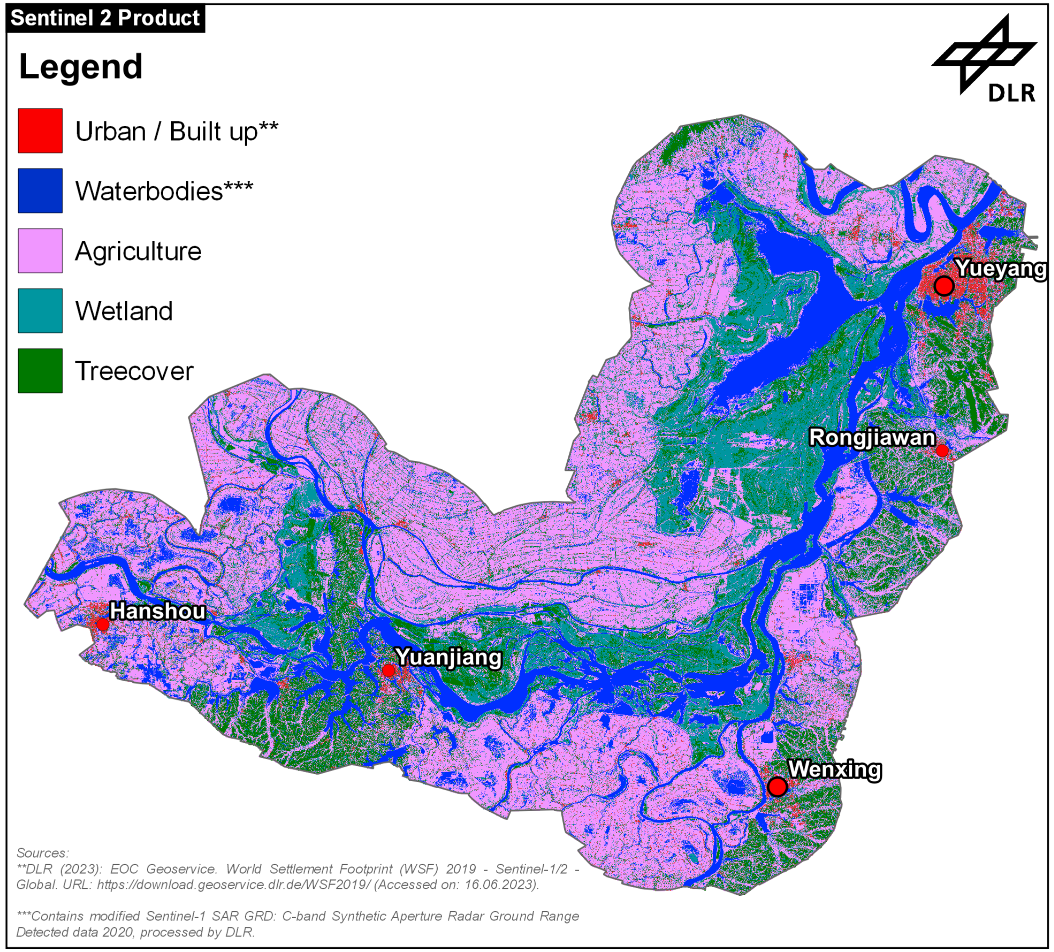

WP3: Wetland Mapping and Biodiversity

Comparison of Copernicus Global Landcover Product and DLR Sentinel 2 Land Cover Classification

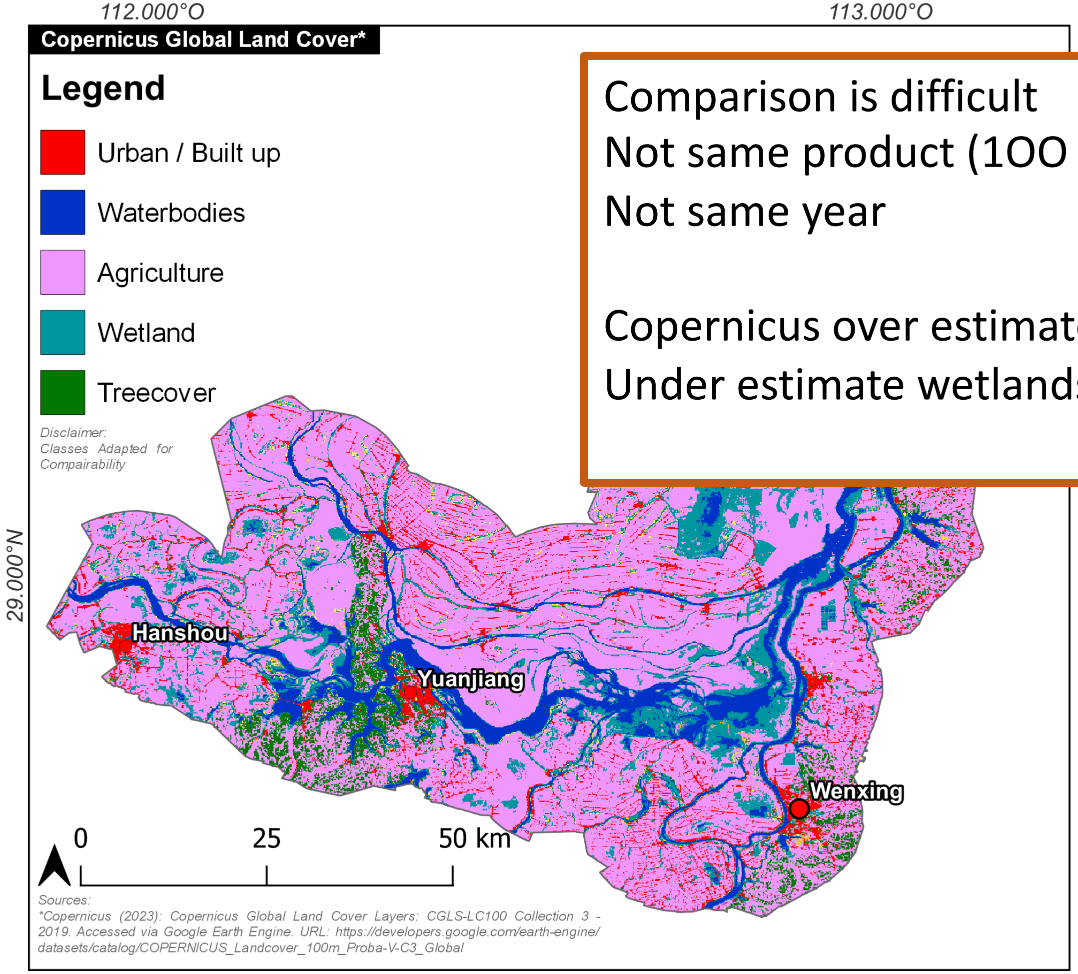

Comparison is difficult

Not same product (1OO m global 10 m local)

Not same year

Copernicus over estimate urban area

Under estimate wetlands

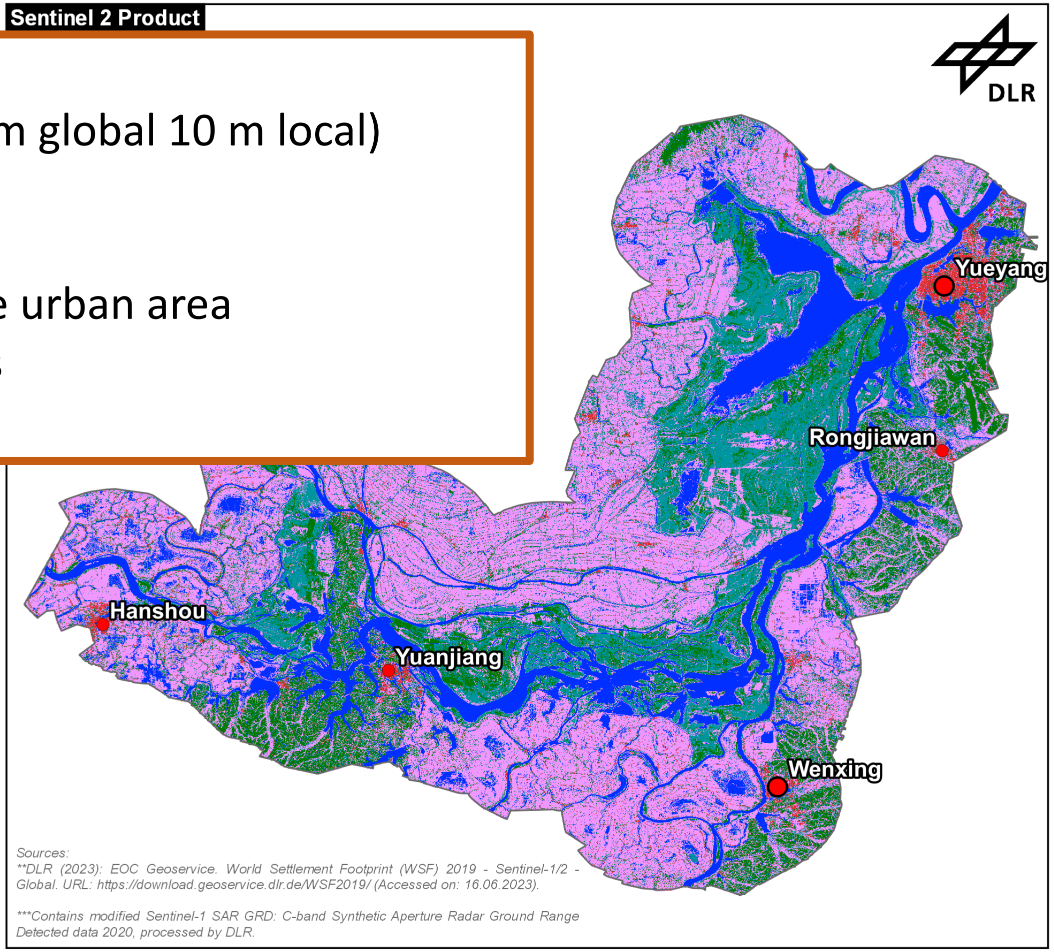

WP3: Wetland Mapping and Biodiversity

DLR Sentinel 2 Land Use Classification of Dongting Lake, China (2020)

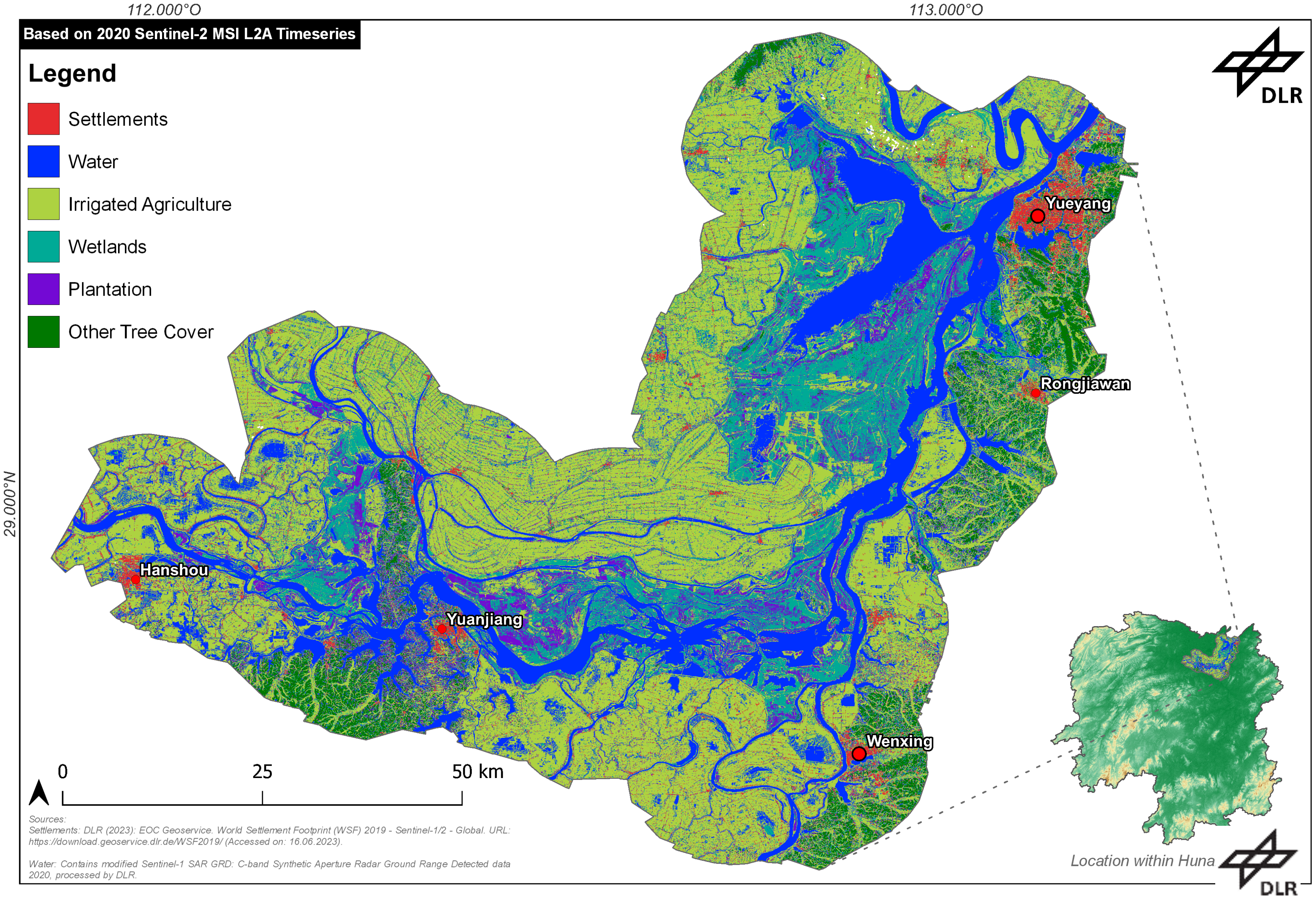

RF + times series classification tools on GEE

1 Sentinel2 by month over one year
11 bands, 5 indices

Urban coming from WSF mask

Distinguishing between plantation and other tree cover

WP3: Wetland Mapping and Biodiversity

Vegetation Mapping

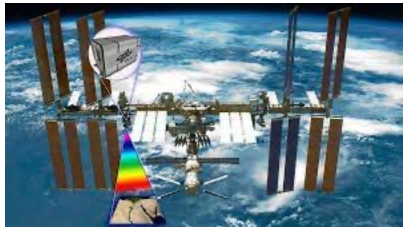

- **DESIS** = DLR Earth Sensing Imaging Spectrometer (DESIS) mounted on the International Space Station (ISS)

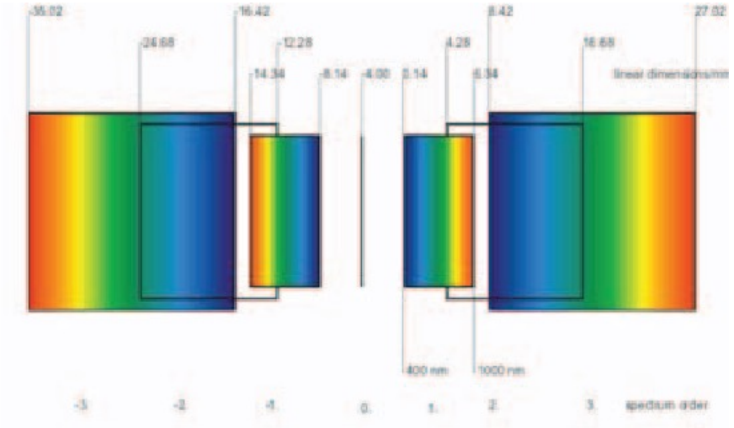

Figure 1 Spectra on the Detector

  - Hyperspectral imaging sensor - its “mechanical and optical characteristics qualify DESIS for applications like large-scale precision farming, forestry, land cover analysis and multitemporal environmental monitoring” (DLR).
  - Spectral range 400 – 1000nm VIS/NIR, spectral resolution 2,5 nm
  - 235 channels
  - 30m spatial resolution on the ground
  - Scientific Mission: an application for scientific use of the data can be submitted to DLR.

Andreas Eckardt and John Horack and Frank Lehmann and David Krutz and Jurgen Drescher and Mark S. Whorton and Mike Soutullo, 2015: DESIS (DLR Earth Sensing Imaging Spectrometer for the ISS-MUSES platform. IEEE International Geoscience and Remote Sensing Symposium (IGARSS, https://api.semanticscholar.org/CorpusID:20847431} }

True Color and Color Infrared Analysis of Dongting Lake, China

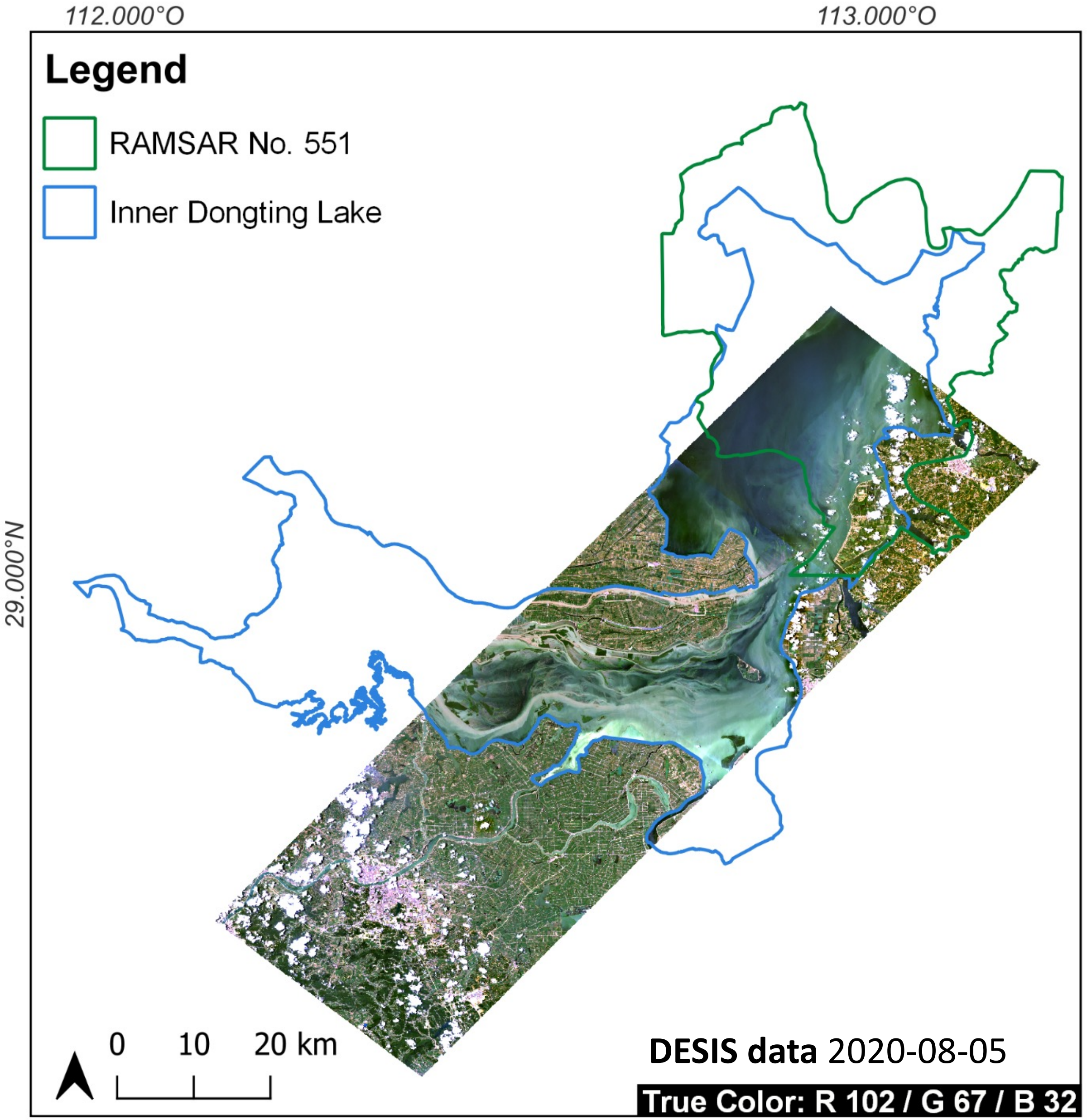

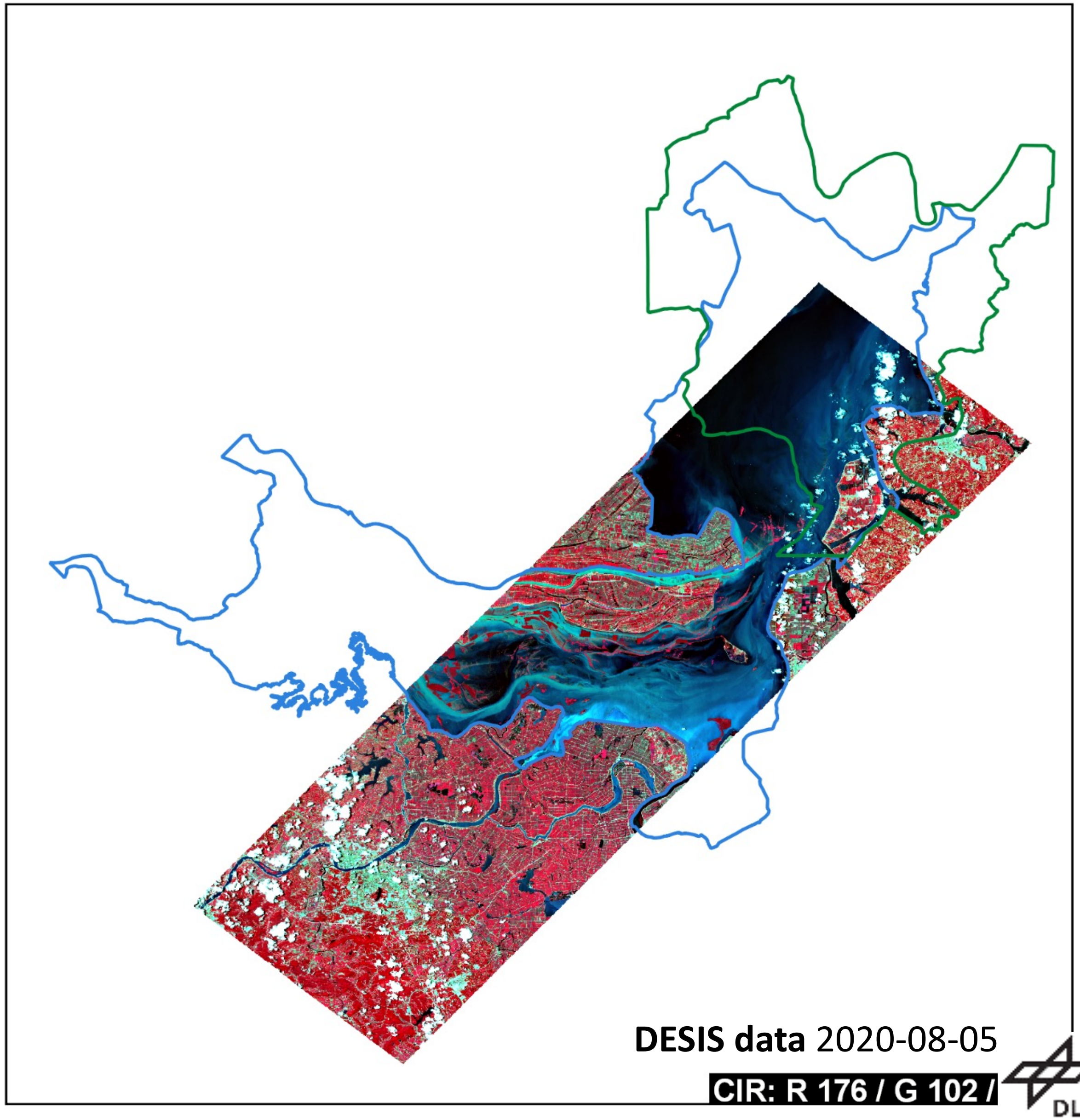

Spectral Analysis of Vegetation POIs in Dongting Lake, China

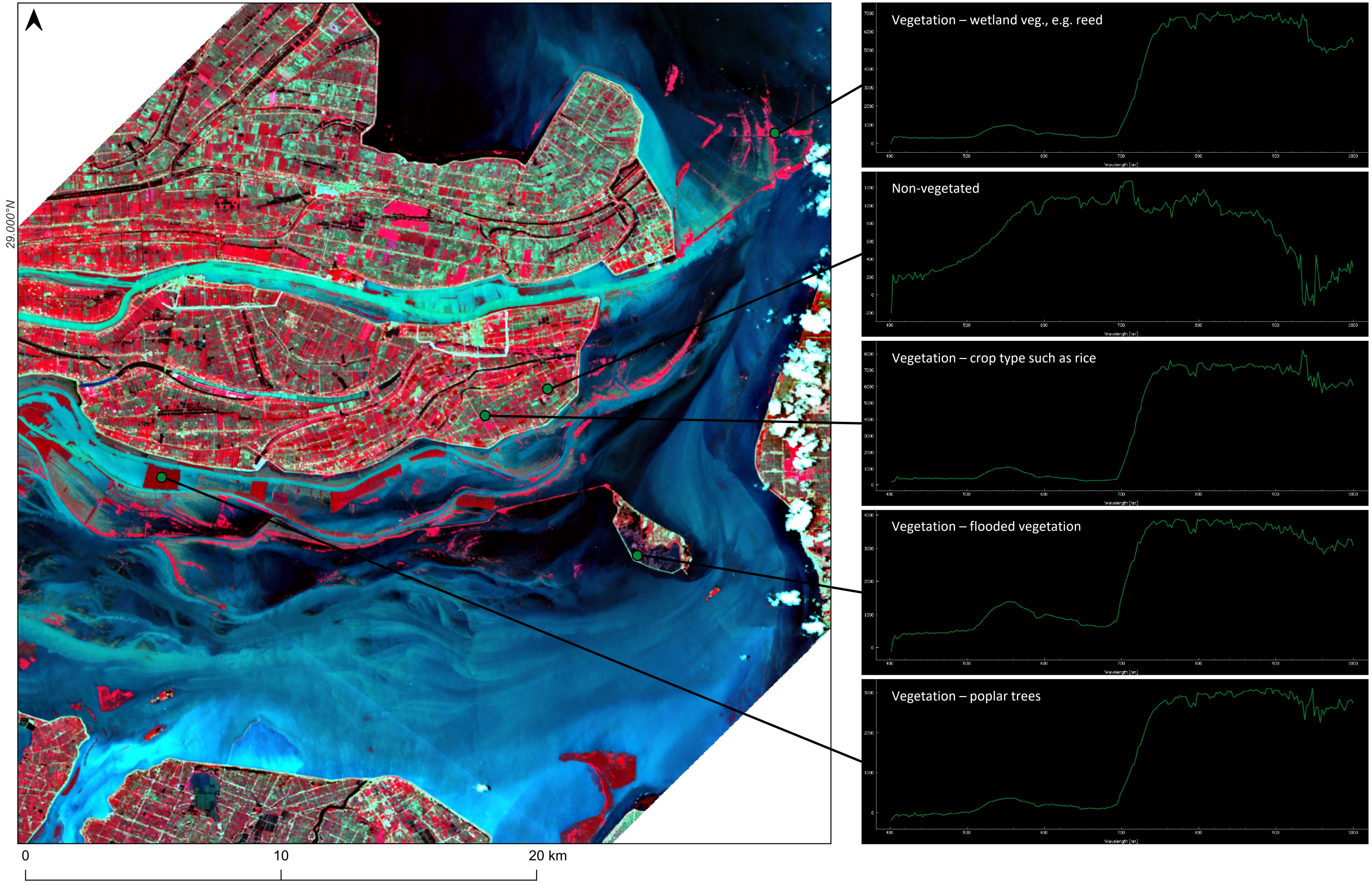

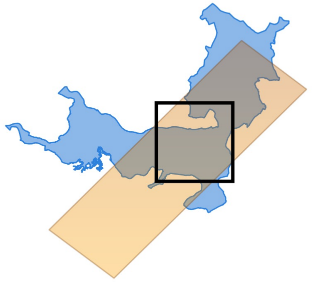

Location within the Study Area

DLR

Spectral Analysis of Water POIs in Dongting Lake, China

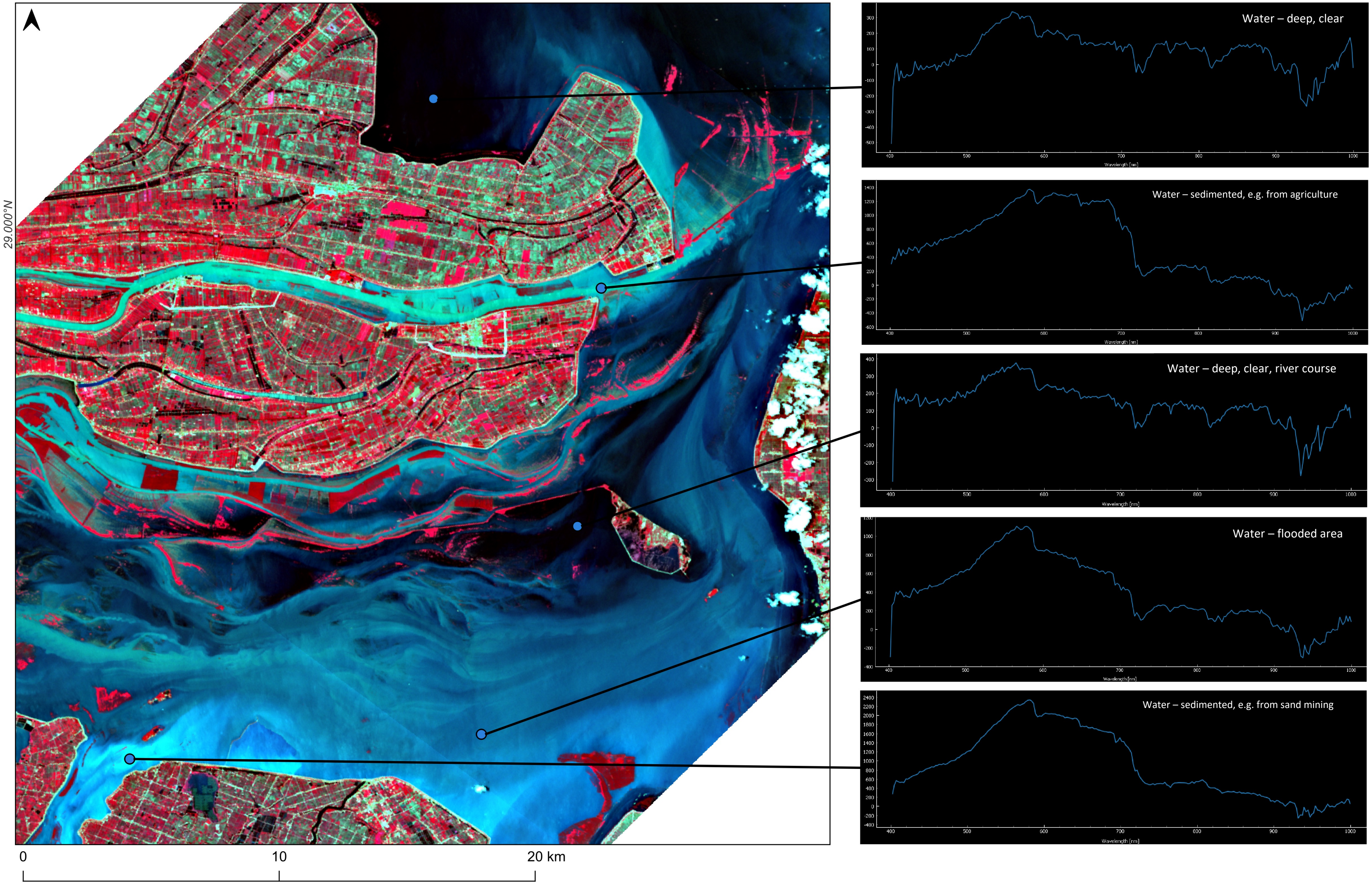

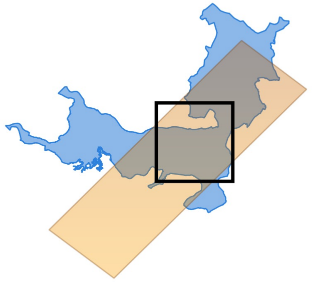

Location within the Study Area

WP4: Regional and global interactions

Evolution of Poyang Lake wetland using remote sensing and modeling methods.

Pr LAI Xijun and PhD student, LU Zhao

Overall Evolution of the Poyang Lake Marshland

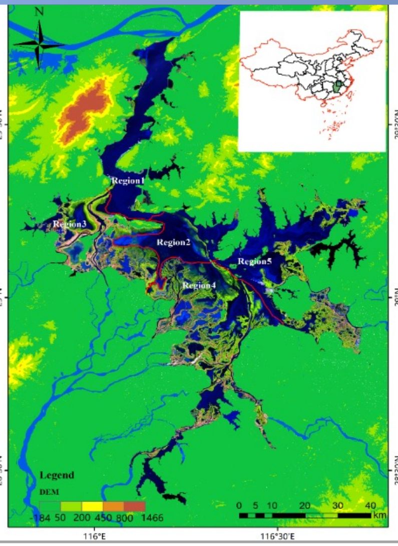

Date	Water level		Satellite
	Hukou	Xingzi	
24 Dec 1973	8.13	8.75	Landsat 1
31 Jan 1987	7.1	7.96	Landsat 5
31 Jan 1993	7.53	8.67	Landsat 5
10 Jan 1997	7.68	8.68	Landsat 5
08 Jan 2002	7.69	8.73	Landsat 5
15 Feb 2004	6.87	7.31	Landsat 5
15 Dec 2004	8.76	9.03	Landsat 5
21 Nov 2006	8.16	8.66	Landsat 5
01 Jan 2008	7.29	7.54	Landsat 7(SLC-off)
18 Dec 2008	8.80	9.04	Landsat 7(SLC-off)
14 Jan 2010	7.71	7.96	Landsat 5
11 Dec 2011	8.49	8.67	Landsat 7(SLC-off)
22 Nov 2013	8.83	8.98	Landsat 8
17 Jan 2014	7.72	7.84	Landsat 7(SLC-off)
05 Feb 2015	7.77	7.88	Landsat 7(SLC-off)
10 Feb 2017	8.30	8.47	Landsat 7(SLC-off)
15 Nov 2019	9.29	9.32	Landsat 7(SLC-off)
09 Dec 2019	7.29	7.33	Landsat 8
12 Sep 2022	7.58	7.68	Landsat 8
14 Oct 2022	8.1	8.17	Landsat 8

Figure on the distribution and change in the size of the marshland

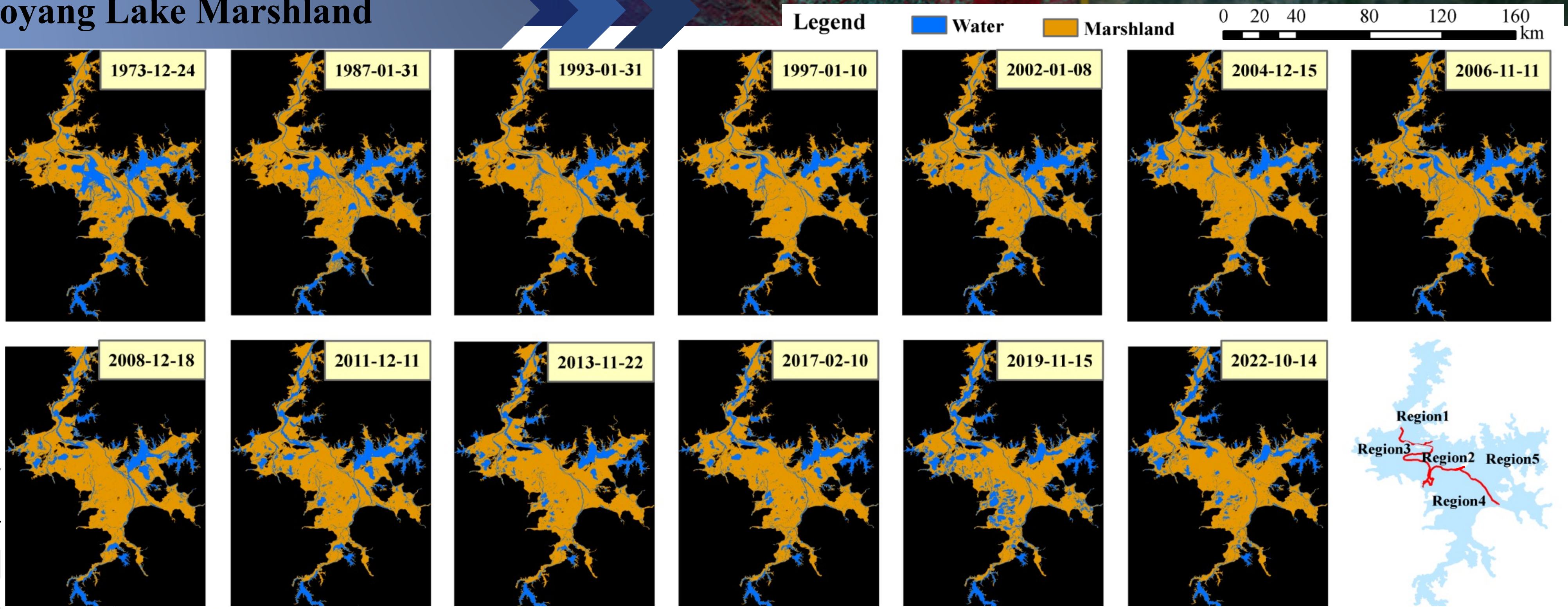

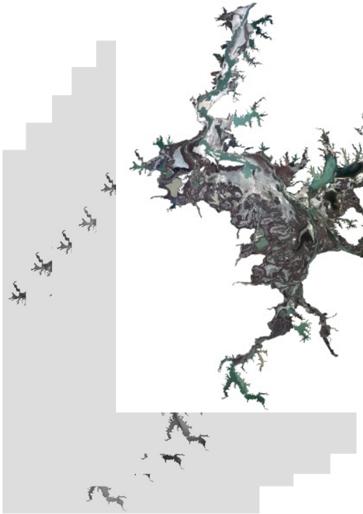

Remote Sensing Data

Date in red color indicates extreme water levels used to extract the sand mining range.

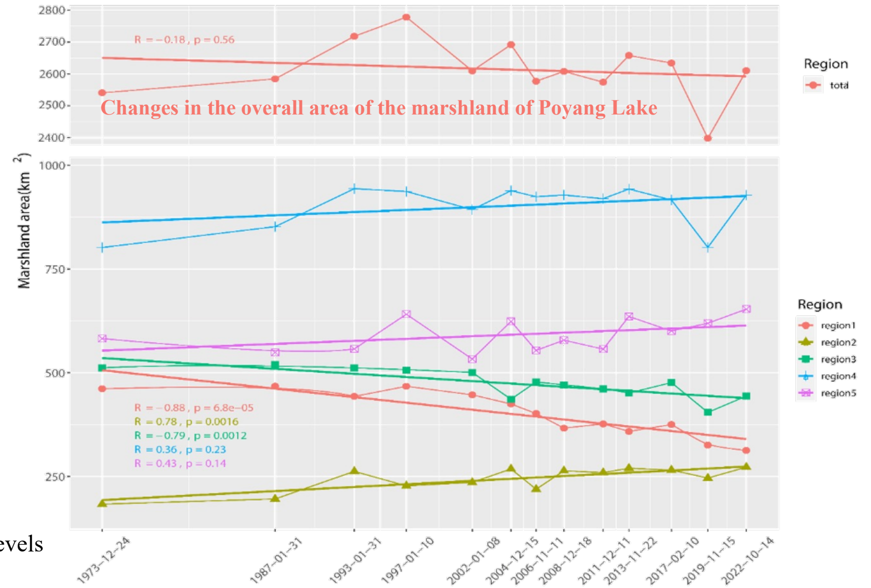

Changes in the marshland area show a trend of increasing and then decreasing:

Phase 1: the marshland area has continued to rise of 2,450 km² in 1973 to 2,778 km² in 1997;

Phase 2: after 1997, the marshland area of Poyang Lake as a whole showed a fluctuating and balanced situation.

Poyang Lake marshland growth areas are concentrated in **Region 2, 4and 5**; While growth areas are concentrated in **Region 1, 3.**

Overall Evolution of the Poyang Lake Marshland

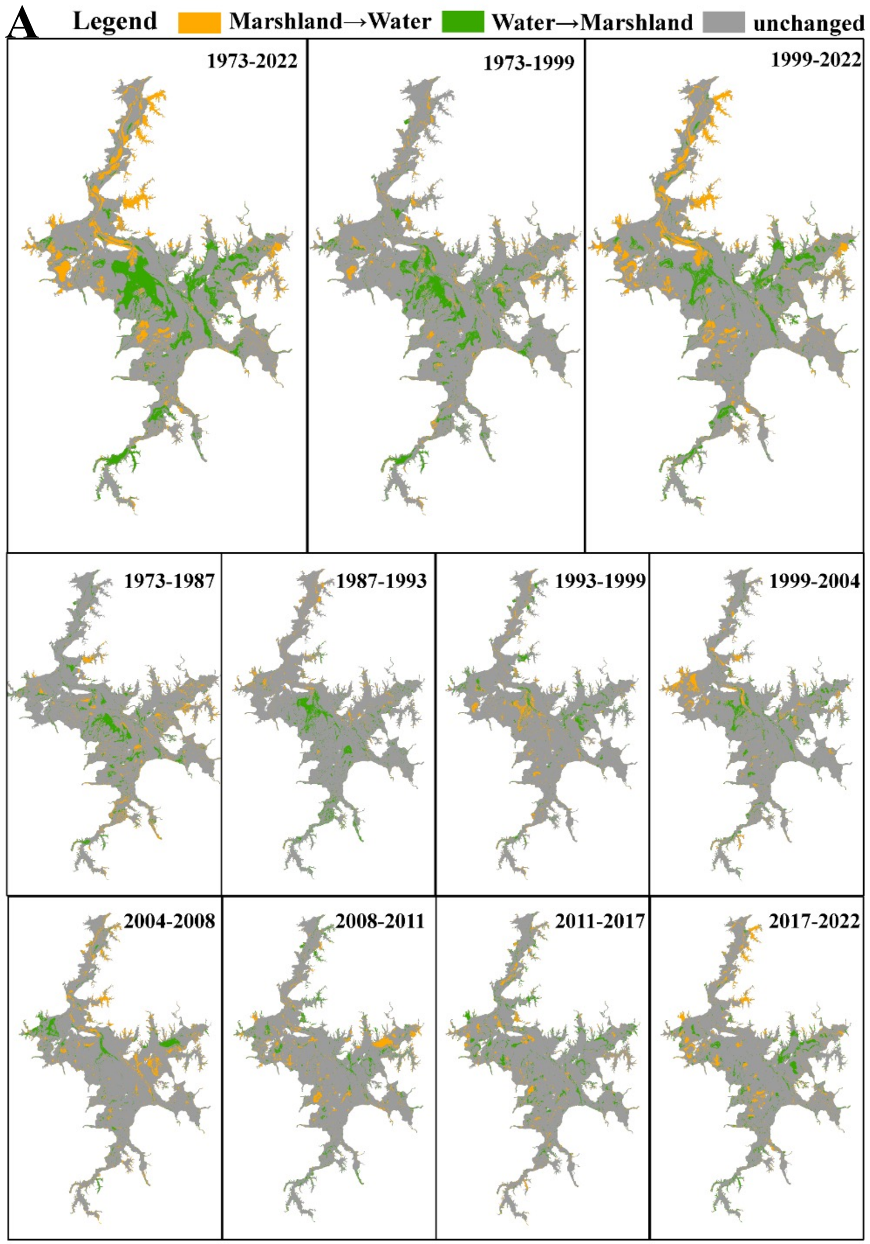

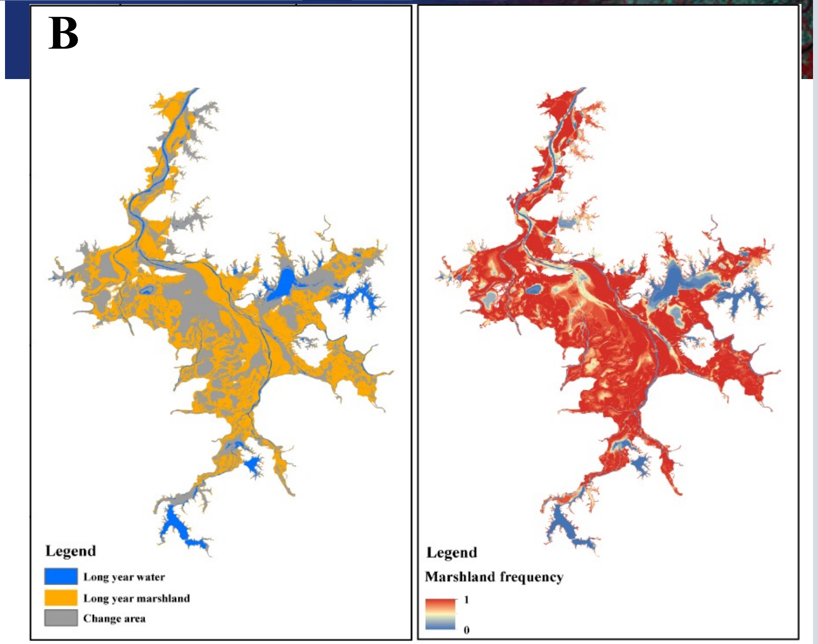

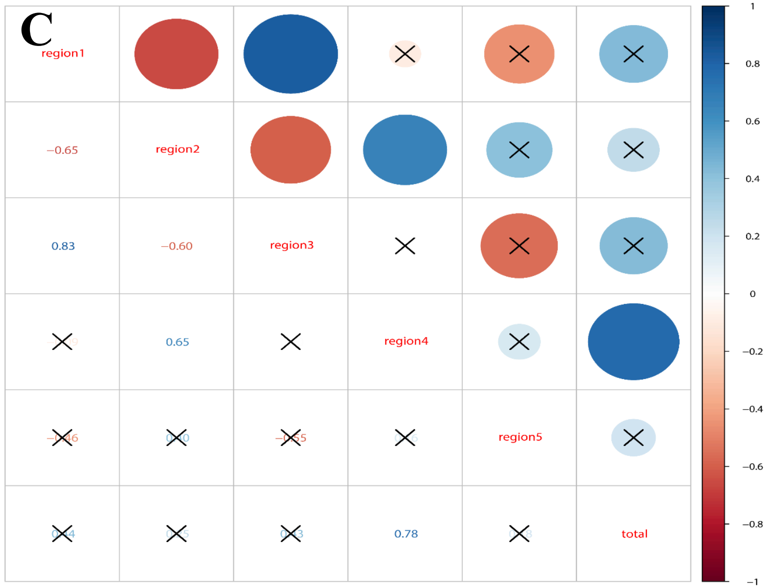

- In **1973-1999**, main transformation concentrated in the central lake area and the major transformation trend is from water to marshland .In **1999-2022**, evolution trend changes from a single shift (water to marshland) to a mutual shift between water and marshland.
- Areas of marshland change are mainly distribute in the center of the lake, with most of the peripheral areas of the lake being permanent marshland or water areas.
- The overall marshland change is highly positively correlated with **Region 4**, and **Region 1 and 2** are negatively correlated among subregions.

Fig.A Transformation of marshland and water in Poyang Lake between different years

Fig.B Distribution of permanent marshlands and permanent water bodies in Poyang Lake and frequency of marshland occurrence.

Fig.C Correlation of marshland changes in different regions.

Poyang Lake Marshland Reduction and Drivers

Sand Mining

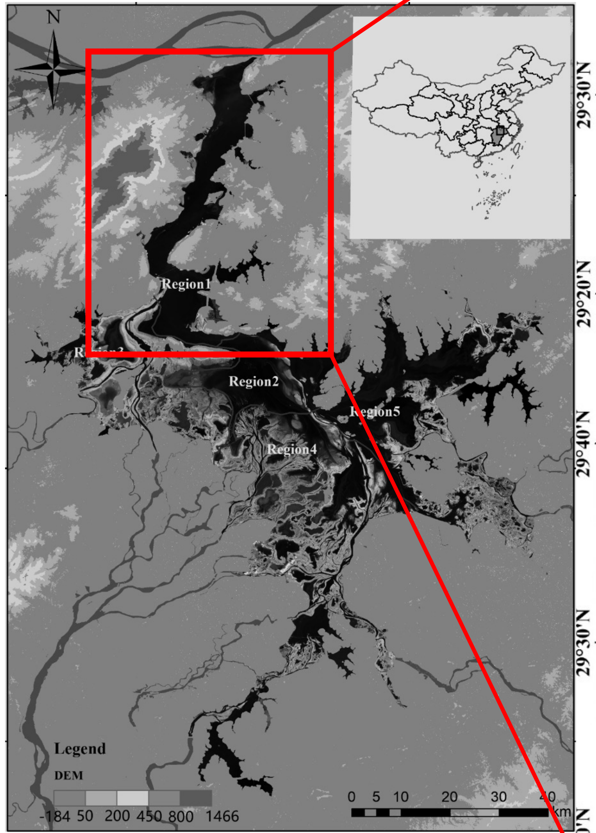

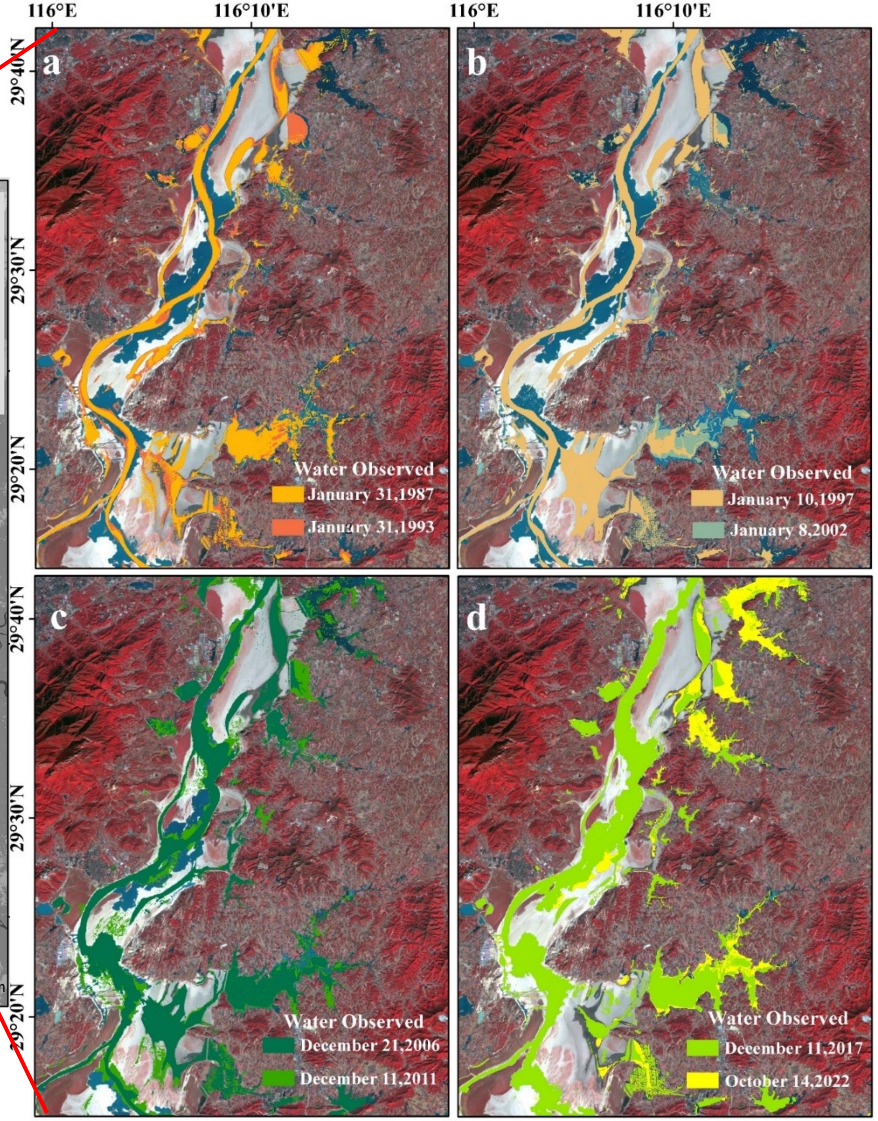

Changes in water surface in the northern lakes over years

The loss of marshland in Poyang Lake is mainly concentrated in the northern part of the lake, and the large reduction of marshland can be visualized by the change of the water surface area.

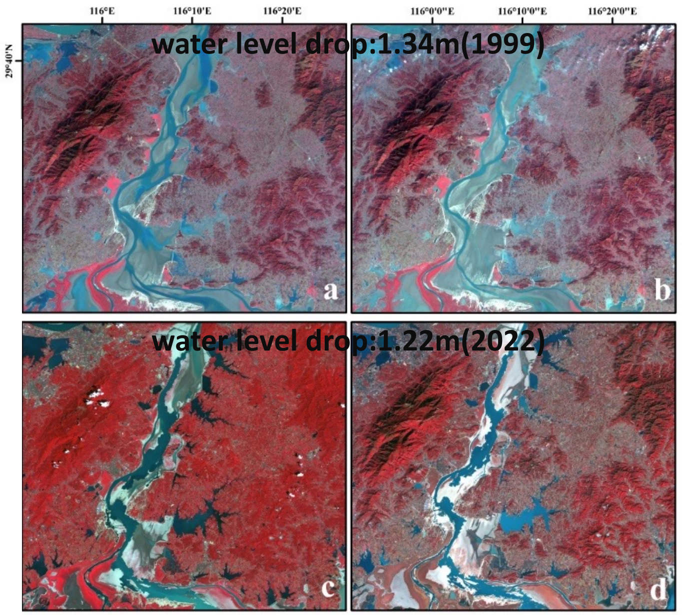

Differences in marshland outcrop area under similar water level changes

The sensitivity of the marshland to changes in water level decreases significantly, with the exposed area of the marshland decreasing from **53.27km²** in 1999 to **6.02 km²** in 2022 for similar water level.

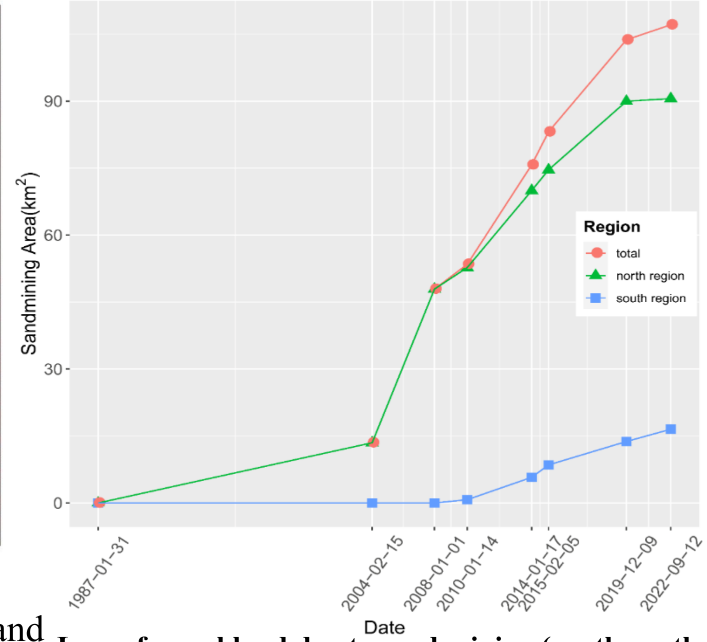

Loss of marshland due to sand mining (north-south region bounded by Songmen mountain)

In the northern part of Poyang Lake, the loss of marshland due to **sand mining** increased significantly after 2004. In 2010, the sand mining area was expanded to the south of Songmen Mountain.

Poyang Lake Marshland Increase and Drivers

Localized Water Level Drop

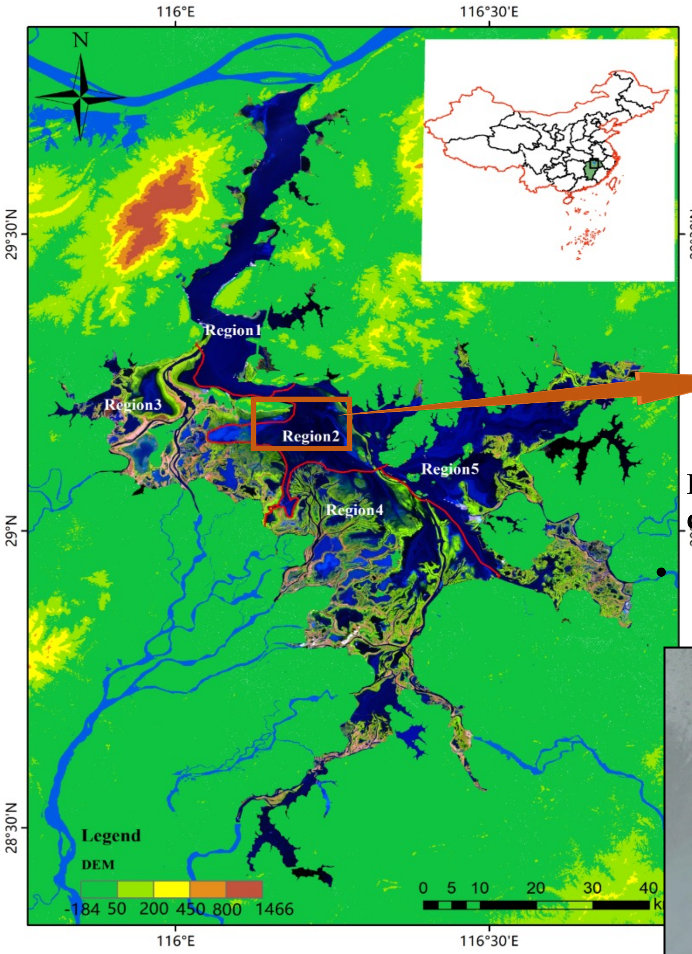

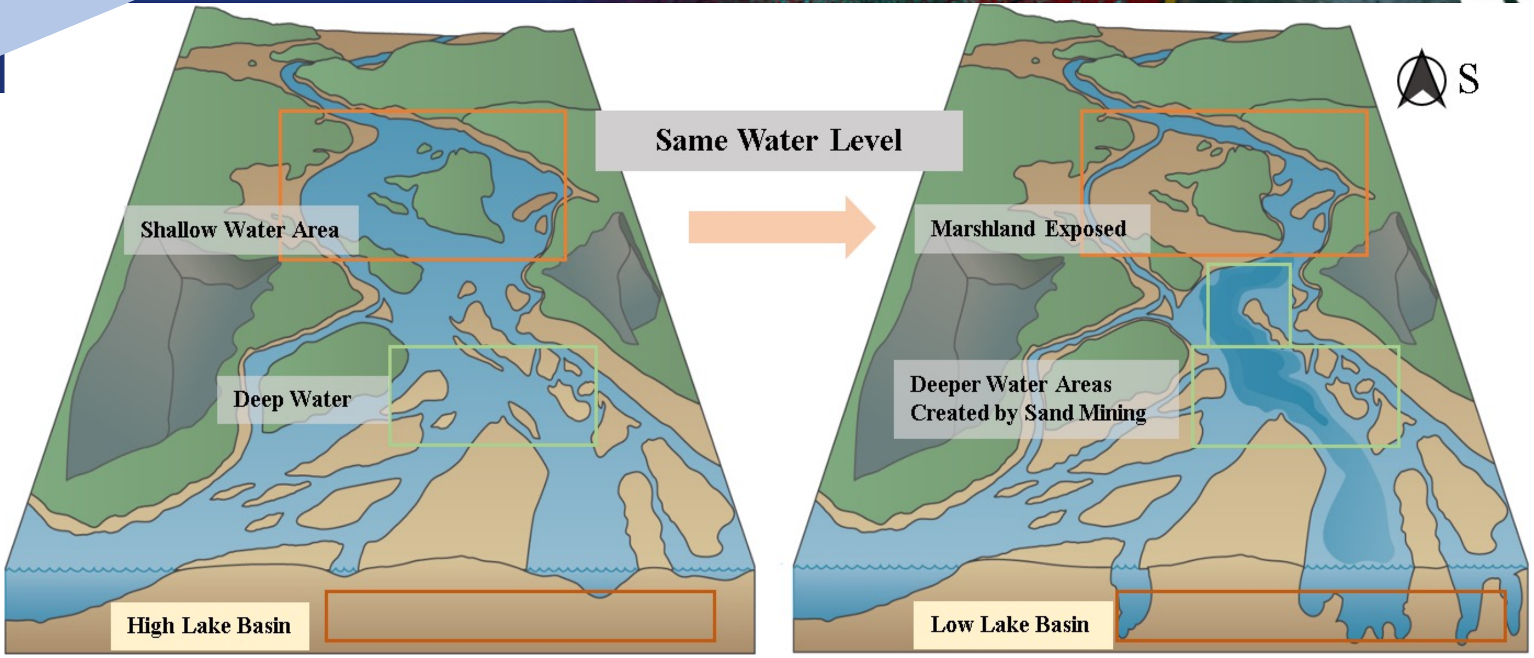

Pictures of marshland outcropping due to localized drop in water level. The large hydraulic drop between the submerged marshland and the deep water created by sand mining leads to an increase in flow

- Deeper water created by sand mining has resulted in more exposed marshland in shallower areas under similar water level conditions.

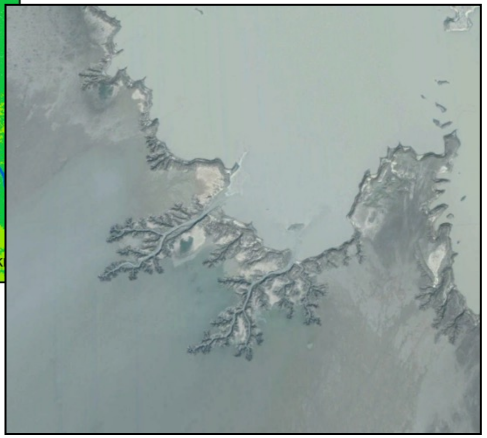

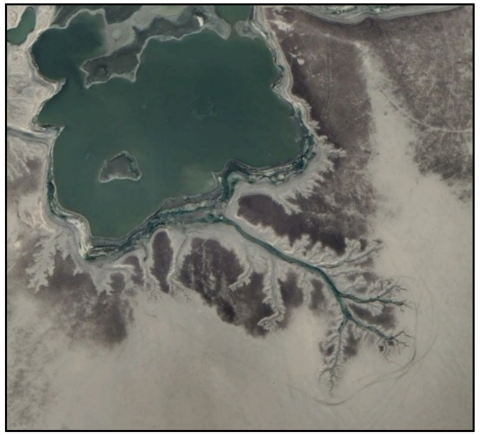

- The disc-shaped sub-lakes, under the action of retrospective erosion of the water flow, formed many drains, which destroyed the original natural dykes, objectively increasing the hydrological connectivity between the disc-shaped lakes and the main lake area, and **the decline in water level is more significant**.

Poyang Lake Marshland Increase and Drivers

Sediment Deposition

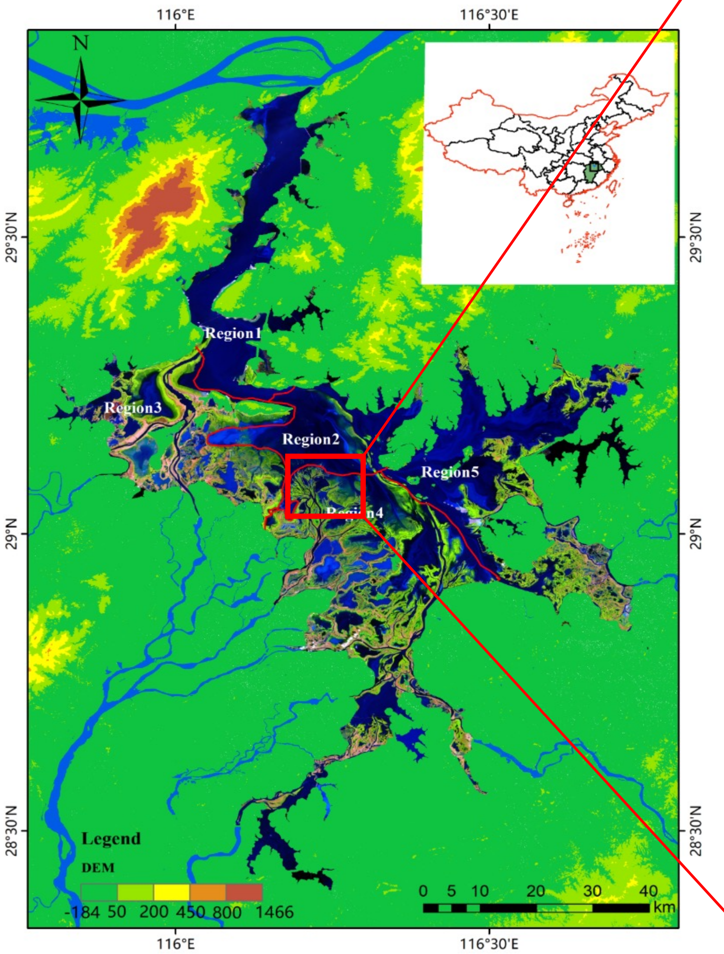

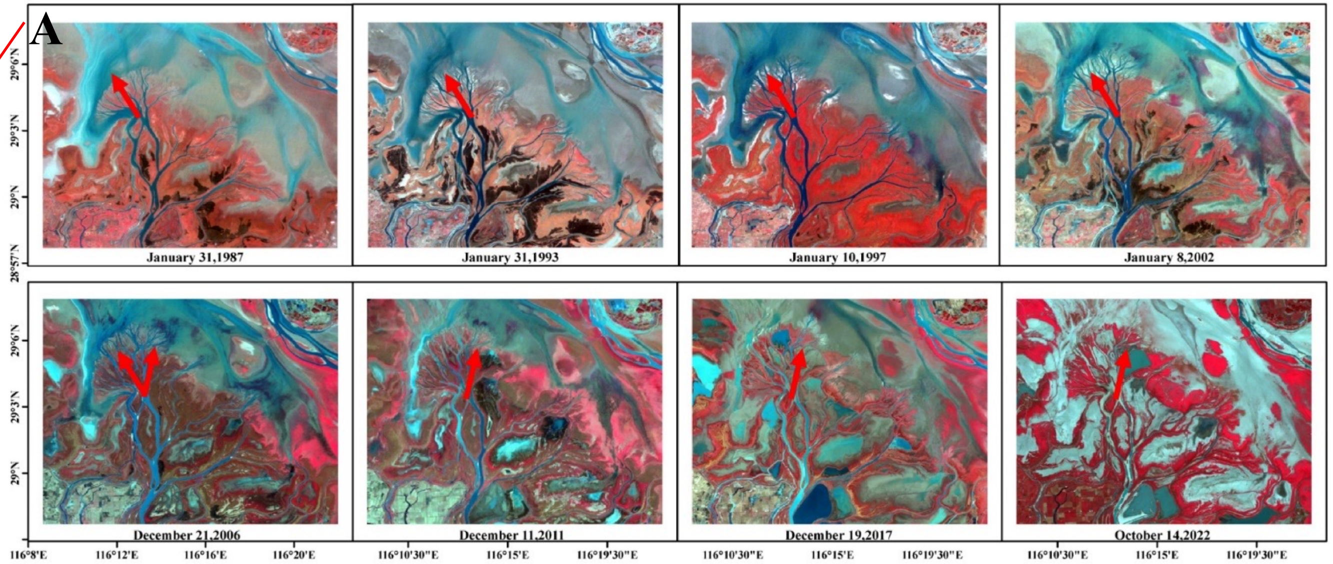

- Delta extension is an important pathway for increasing marshland area, but the direction and rate of delta siltation is affected by changes in upstream water and sand control.

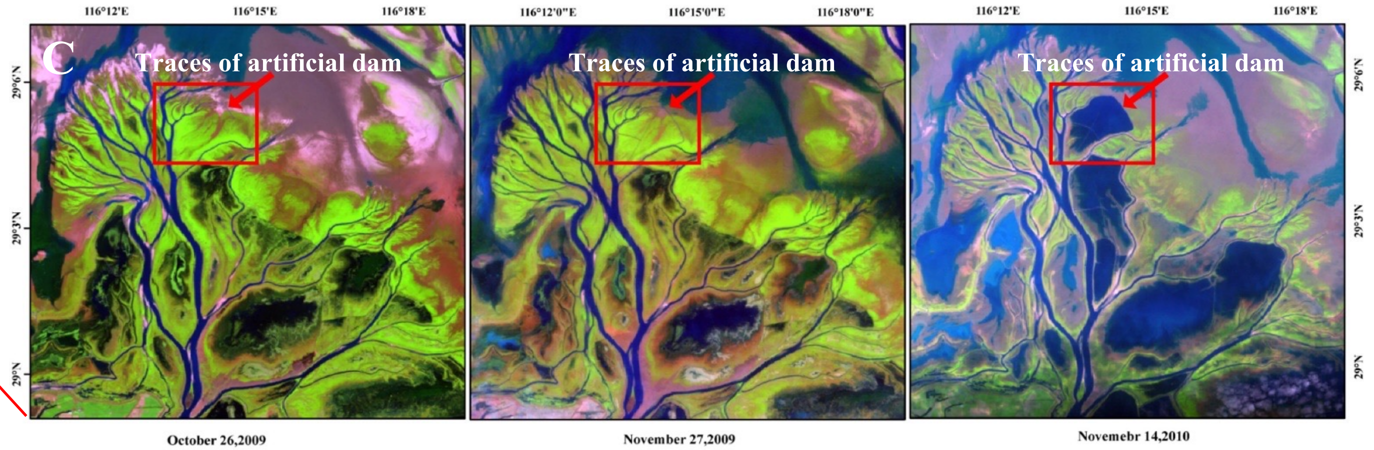

Fig.A Extension of the Gangjiang Delta of Poyang Lake and its direction of extension

- The formation of disc-shaped lakes within the delta due to **artificial reclamation and natural siltation** has increased the uncertainty of marshland outcrops.

WP4: Regional and global interactions

Climate Change and Hydrology Response

Jianzhong Lu, Xiaoling Chen, Liang Zheng, and Liqiong Chen

Wuhan University

WP4: Regional and global interactions

- Machine learning methods optimized global ensemble CMIP6 GCM dataset for climate change projection and its application

➢ **17 CMIP6 GCMs were selected.**

➢ **Machine learning (OLS-DT-DNN) and their ensemble methods help to improve the projection of climate change.**

➢ **An optimal climate change dataset was published: https://zenodo.org/record/6565574**

Model Name	Modeling group	Original resolution (lon x lat)
BCC-CSM2-MR	Beijing Climate Center, China / Meteorological Administration, China	1.125°×1.125°
CanESM5	Canadian Centre for Climate Modelling and Analysis, Canada	2.8125°×2.8125°
CESM2-WACCM	National Center for Atmospheric Research, Climate and Global Dynamics Laboratory, USA	1.25°×0.9375°
CMCC-CM2-SR5	Fondazione Centro Euro-Mediterraneo sui Cambiamenti Climatici Italy	1.25°×0.9375°
CMCC-ESM2	Fondazione Centro Euro-Mediterraneo sui Cambiamenti Climatici,Italy	1.25°×0.9375°
FGOALS-f3-L	Chinese Academy of Sciences, China	1.25°×1°
INM-CM4-8	Institute for Numerical Mathematics, Russia	2°×1.5°
INM-CM5-0	Institute for Numerical Mathematics, Russia	2°×1.5°
KACE-1-0-G	National Institute of Meteorological Sciences/Korea Meteorological Administration, Republic of Korea	1.875°×1.25°
MIROC6	The University of Tokyo, National Institute for Environmental Studies, and Japan Agency for Marine–Earth Science, Japan	1.4063°×1.4063°
MRI-ESM2-0	Meteorological Research Institute, Japan	1.125°×1.135°
NESM3	Nanjing University of Information Science and Technology, China	1.875°×1.875°
TaiESM1	Research Center for Environmental Changes, Taiwan	1.25°×0.9375°
MPI-ESM1-2-HR	Max Planck Institute for Meteorology, Germany	0.9375°×0.9375°
MPI-ESM1-2-LR	Max Planck Institute for Meteorology, Germany	0.9375°×0.9375°
FIO-ESM-2-0	FIO (First Institute of Oceanography, State Oceanic Administration, China), QNLM (Qingdao National Laboratory for Marine Science and Technology, China)	1.25°×0.9375°

WP4: Regional and global interactions

- Machine learning methods optimized global ensemble CMIP6 GCM dataset for climate change projection and its application

➢ **Multi-model ensemble methods**

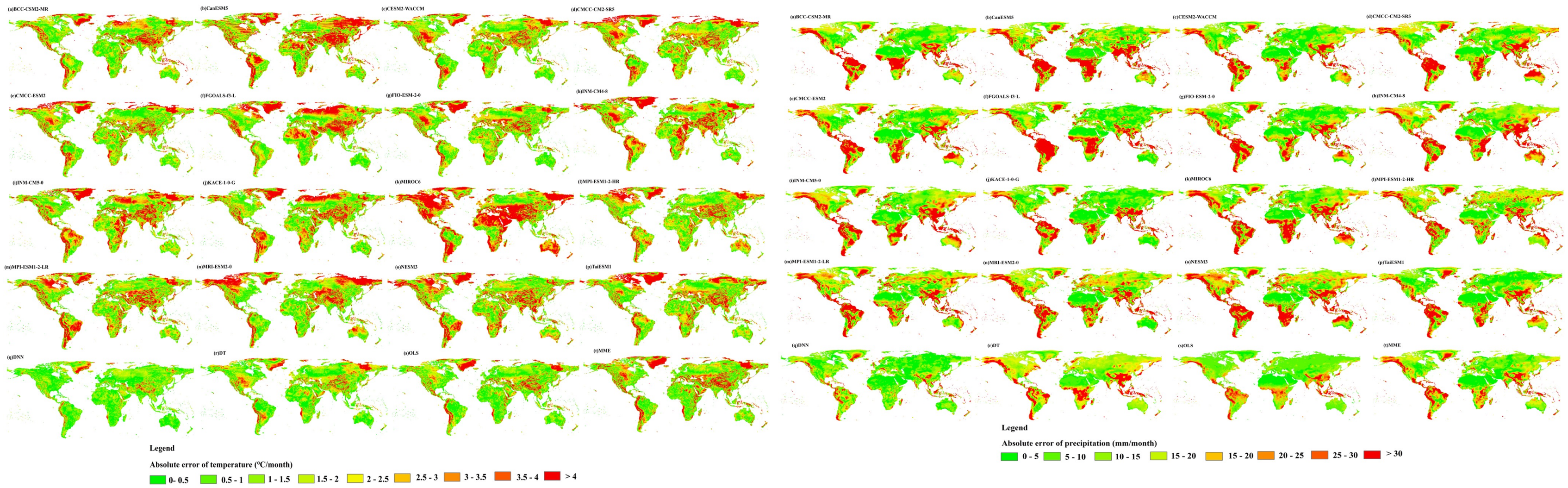

Global continental distribution of Absolute Error (AE) of temperature and precipitation produced by selected CMIP6 GCMs, DNN (Deep Neural Networks), DT (Decision Tree), OLS (Ordinary Least Squares regression) and MME (multi-model mean ensemble) relative to the mean value from CRU(1995-2014) which were applied as the baseline.

➢ **Years projection for temperature increasing under the 1.5°C (2°C / 3°C) global warming target**

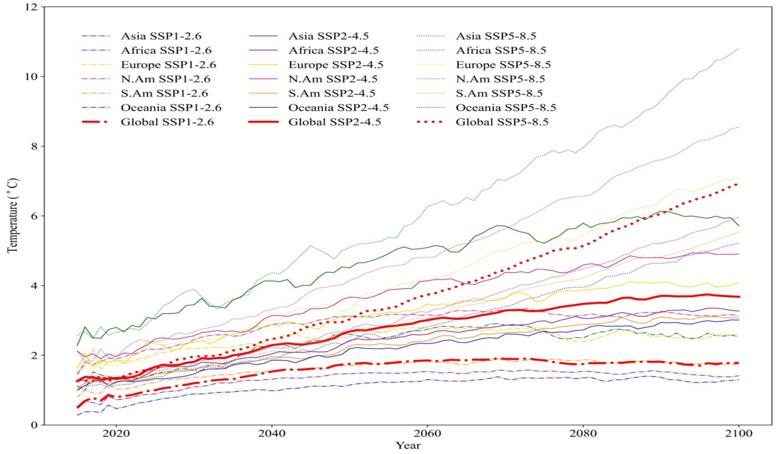

Temperature anomalies of global and continents under SSP1-2.6, SSP2-4.5 and SSP5-8.5 scenarios respect to pre-industrial temperature (1850-1900).

➢ **Under the SSP2-4.5 scenario, the years for Africa, South America and Oceania to break the 1.5 °C (2 °C) warming target are 2024 (2037), 2026 (2043) and 2029 (2038), respectively, and Europe will break the 2 ° C threshold in 2026.**

➢ **Under the SSP5-8.5 scenario, the polarization of drought and wetness of global land precipitation will become more severe.**

WP4: Regional and global interactions

- Based on the atmosphere-land coupling relationship, a method of quantifying the lag effect of soil moisture on meteorological elements (rainfall, temperature and evapotranspiration, etc.) is proposed.

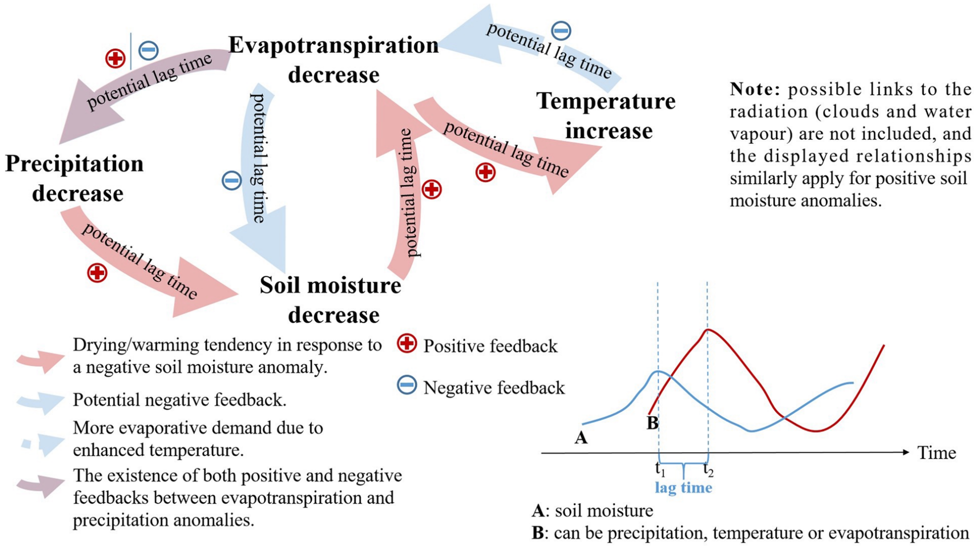

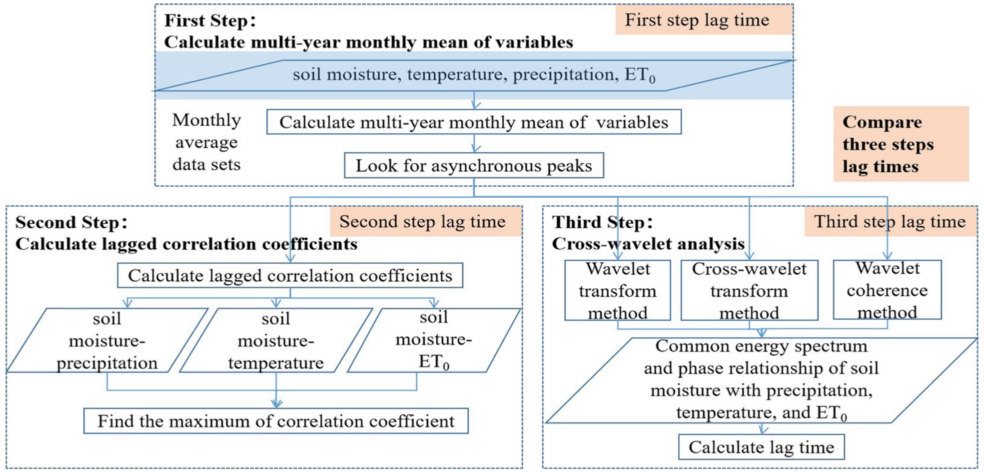

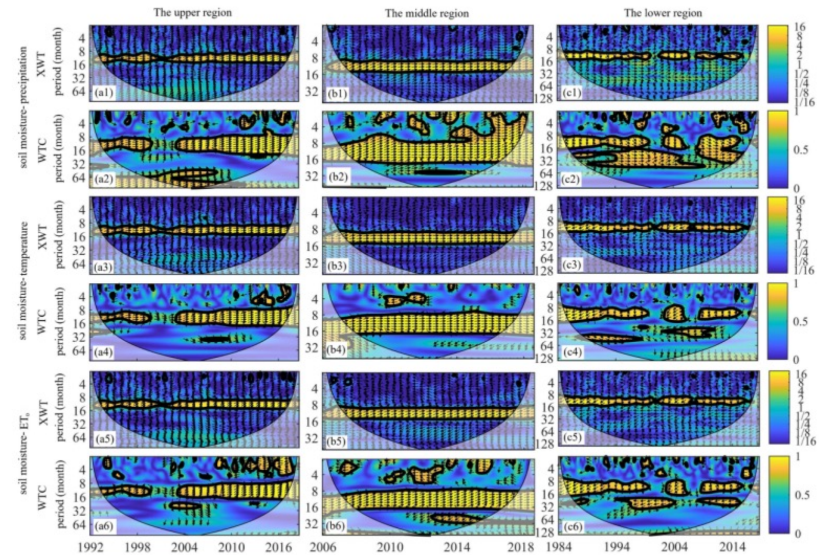

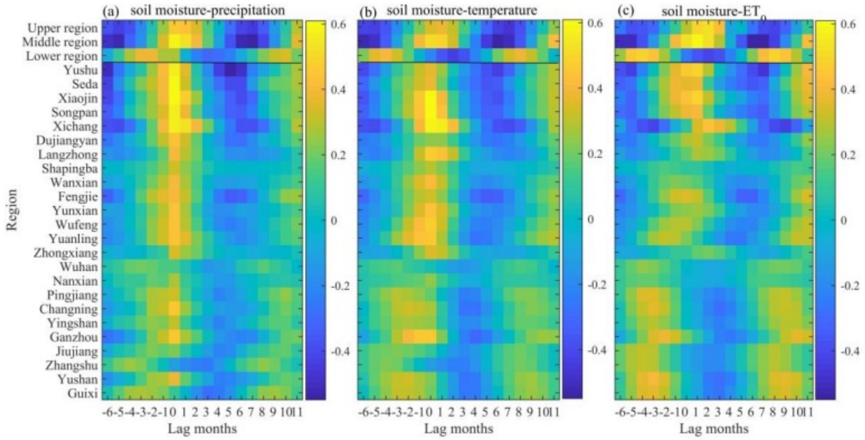

WP4: Regional and global interactions

- Based on the time-lag effect of soil moisture on meteorological factors, a comprehensive agricultural drought index (CDAI) was proposed, which can effectively monitor agricultural drought in the Yangtze River watershed during growing season.

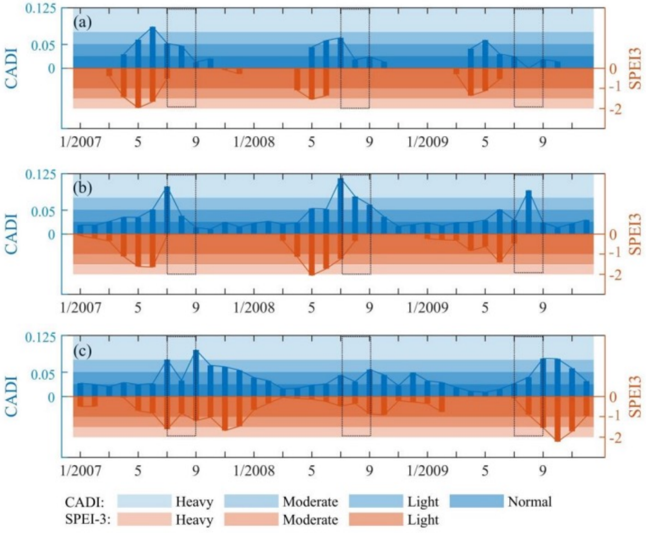

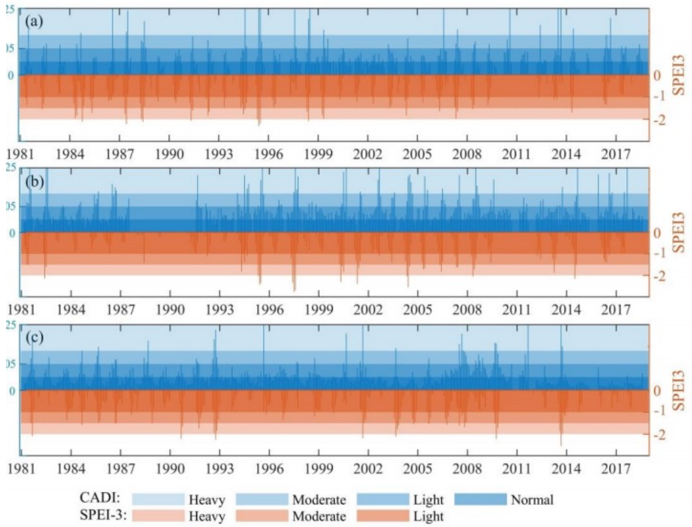

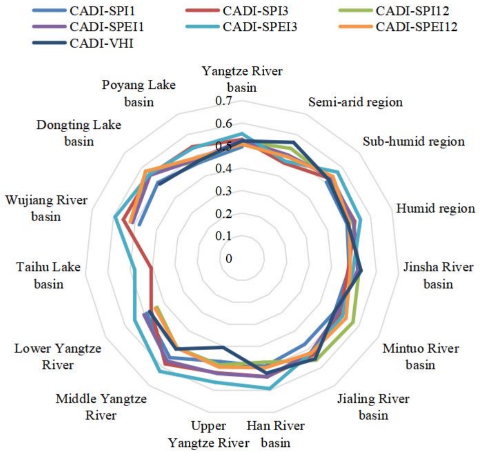

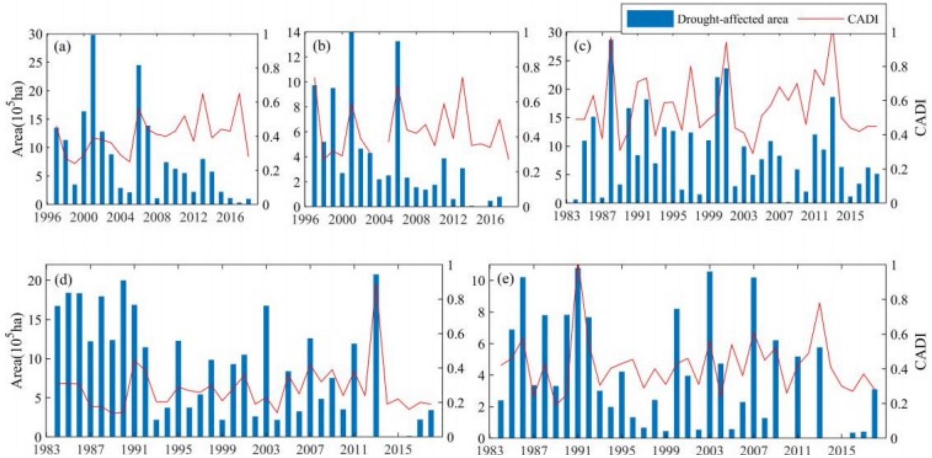

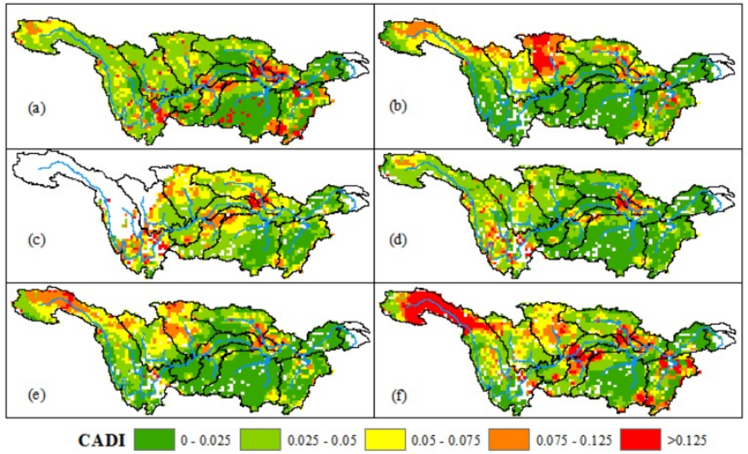

WP4: Regional and global interactions

- Estimation of critical soil moisture (CSM) based on surface energy partitioning characterizing land aridity

  - Energy constraint and water constraint regimes to define aridity:

$$\Delta \mathrm{Corr} = \mathrm{Corr}(\mathrm{EF}_{SFE}', \mathrm{Tair}') - \mathrm{Corr}(\mathrm{EF}_{SFE}', \mathrm{SM}')$$

  - Compared with the traditional drought index, the spatial pattern of surface drought in China defined by available energy and soil moisture is more spatially heterogeneous, which is better than that defined by only evapotranspiration.

(a)

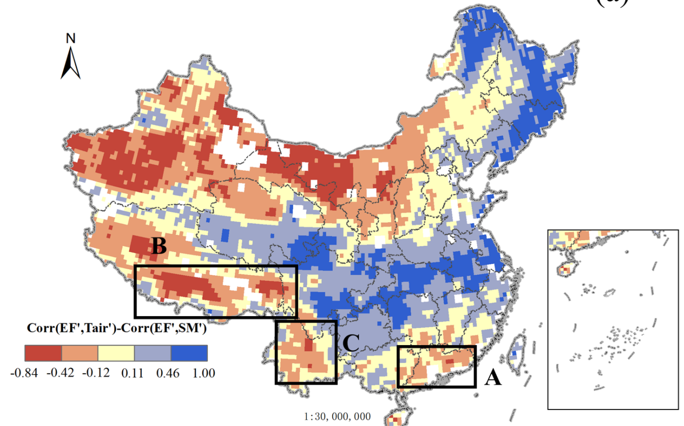

Land aridity classification map based on ΔCorr by 75% and 25% percentile

(c)

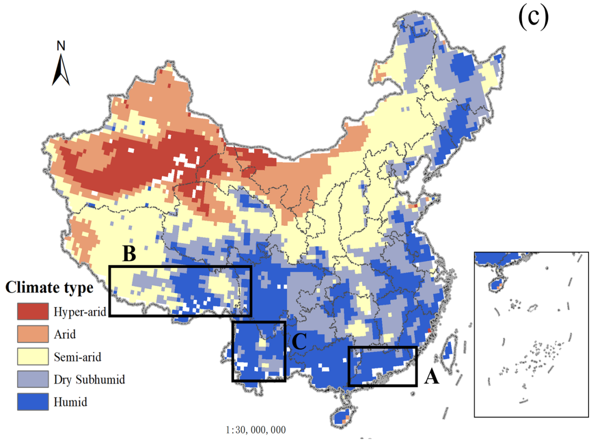

Spatial pattern of climate types based on Aridity Index classification

(d)

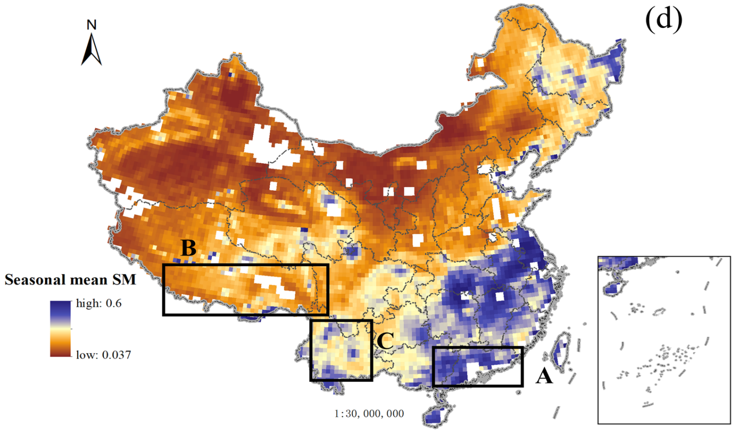

Summer mean soil moisture from 2002 to 2018

(b)

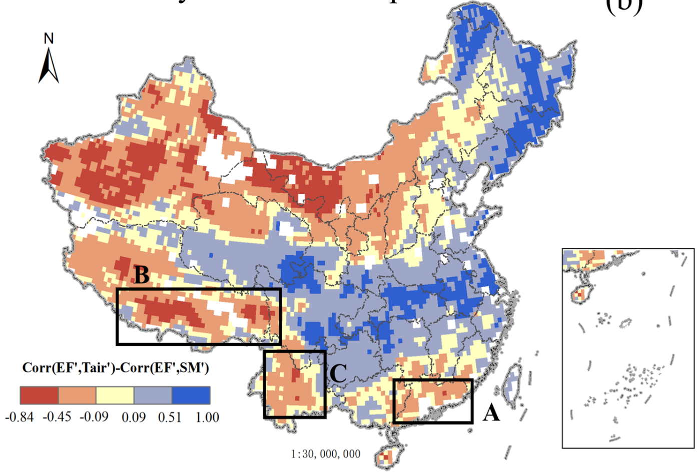

Land aridity classification map based on ΔCorr by 80% and 20% percentile

WP4: Regional and global interactions

- Estimation of critical soil moisture based on surface energy partitioning characterizing land aridity in China

➢ Estimation of the large-scale Critical Soil Moisture (CSM)

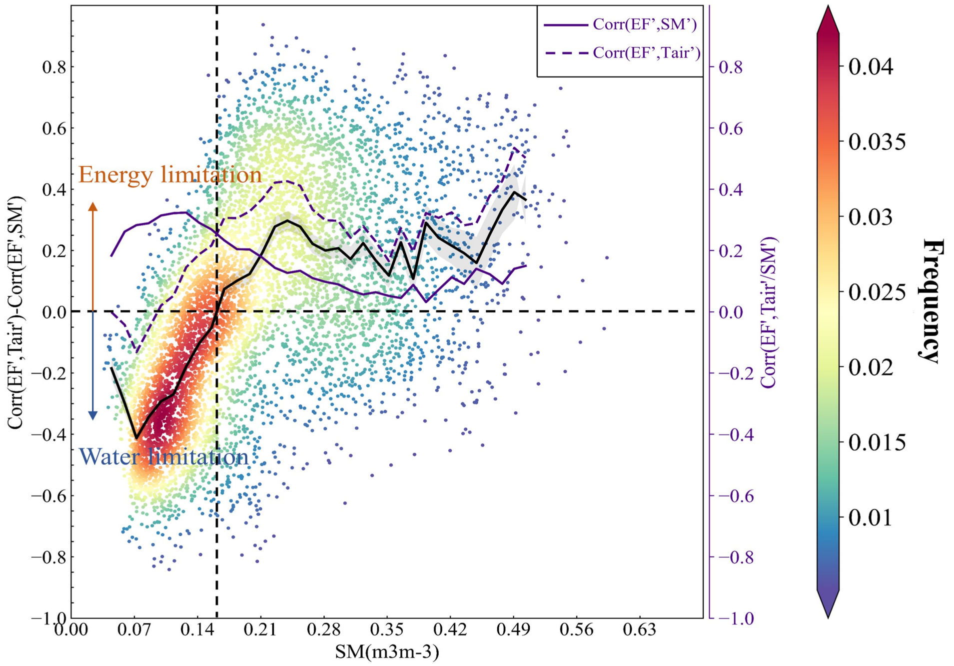

Sensitivity of ΔCorr to SM across all grid cells in China. Each dot represents a particular grid cell in JJA. The black line is a moving average through the points, while the gray ribbon indicates a 90% confidence interval. The color imposed on the data points reflects the density of the data points.

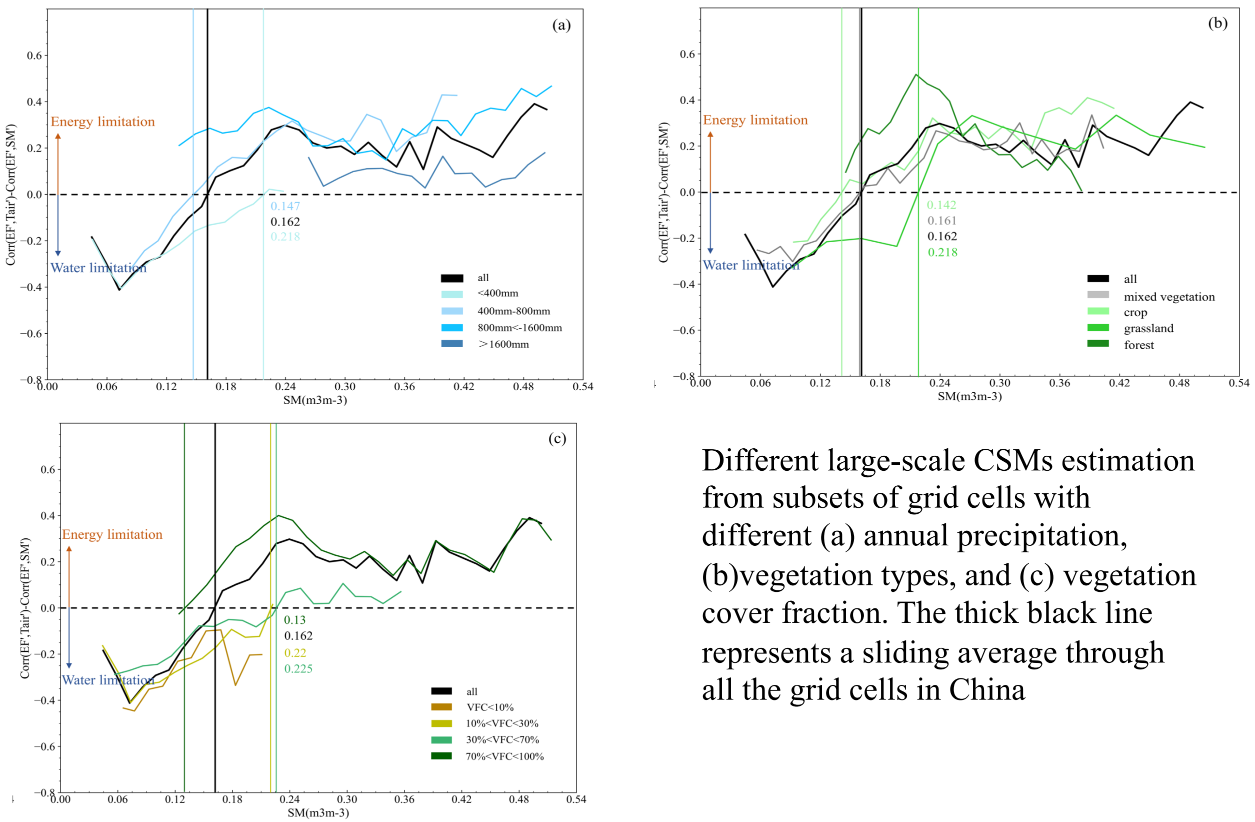

Different large-scale CSMs estimation from subsets of grid cells with different (a) annual precipitation, (b)vegetation types, and (c) vegetation cover fraction. The thick black line represents a sliding average through all the grid cells in China

➢ This study reveal the areas with water constraint and energy constraint in China and their dependence on average surface soil moisture. The CSM was identified over China for a large scale, which represents the drought transition between water constraint and energy constraint in China.

➢ The impact of precipitation and vegetation coverage on CSM were also investigated in a local grids scale over China.

WP4: Regional and global interactions

- Response of wetland vegetational type to hydrological regime

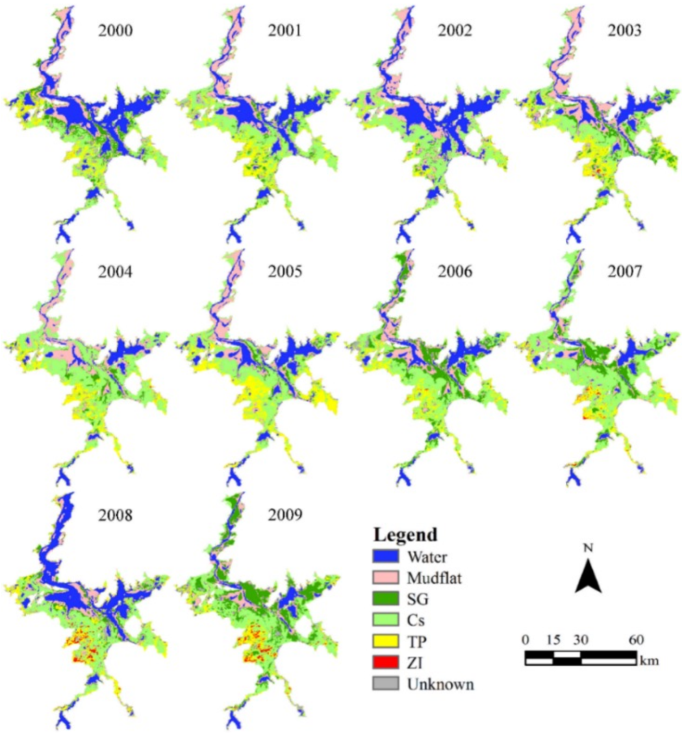

Phenology-based wetland vegetation classification from remote sensing observation

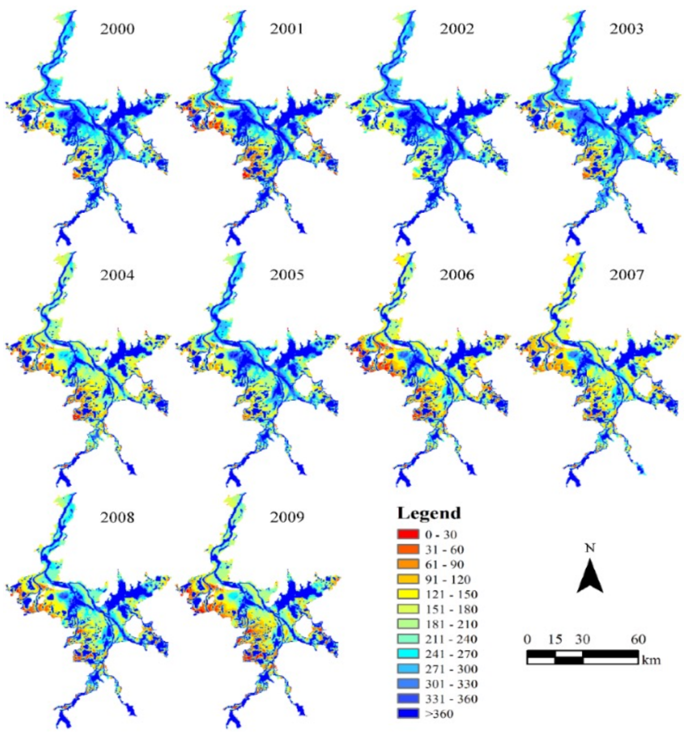

Inundation conditions of Poyang Lake during 2000-2009 by hydrodynamic model.

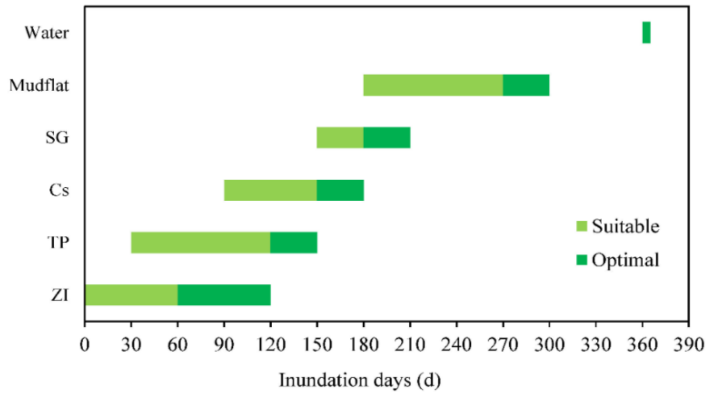

Optimal and suitable inundation conditions for different cover

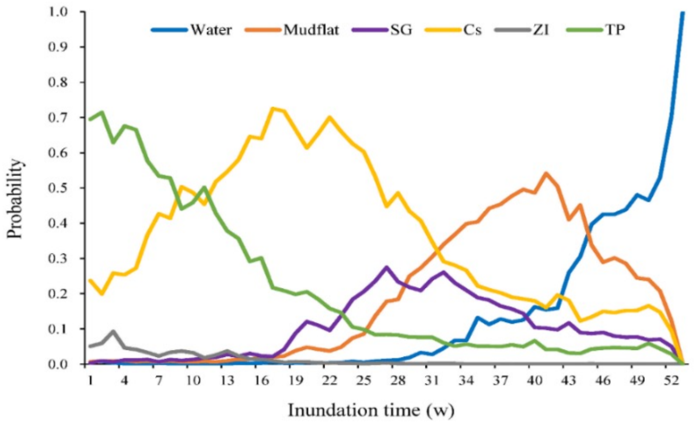

Occurrence probability of different cover types against inundation conditions

- Water and mudflats showed a decreasing trend, and all vegetation types showed an increasing trend in the Poyang Lake wetland.
- Inundation duration decreased significantly during 2000-2009.
- Hydrology is critical to wetland cover, but not the unique determined factor!

WP4: Regional and global interactions

- Impacts of Agricultural Topdressing Practices on Cyanobacterial Bloom Phenology

➢ Long-term cyanobacterial phycocyanin pigment (PC) concentration retrieval from RS based on PCI

$$PCI = R'_{rc}(620) - R_{rc}(620)$$

$$R'_{rc}(620) = R_{rc}(560) + \frac{620-560}{665-560} * (R_{rc}(665) - R_{rc}(560))$$

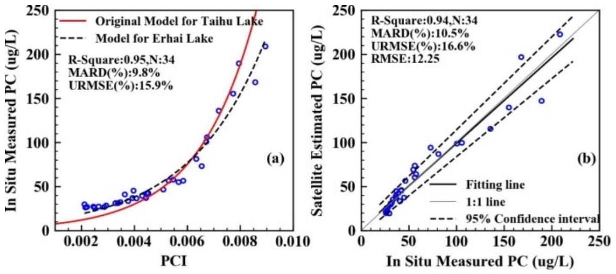

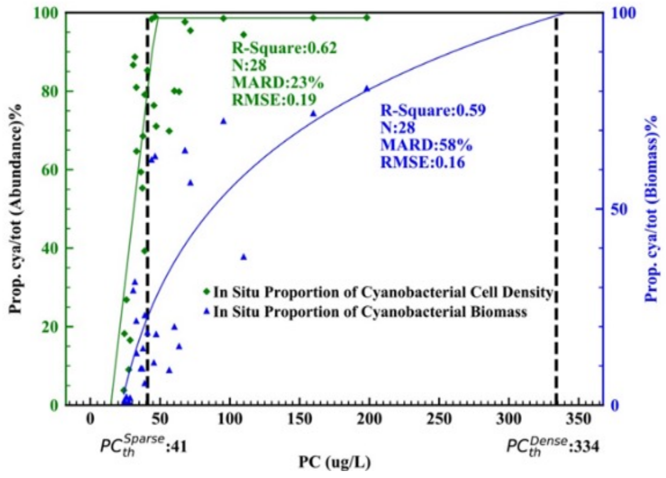

➢ Spatial-temporal pattern

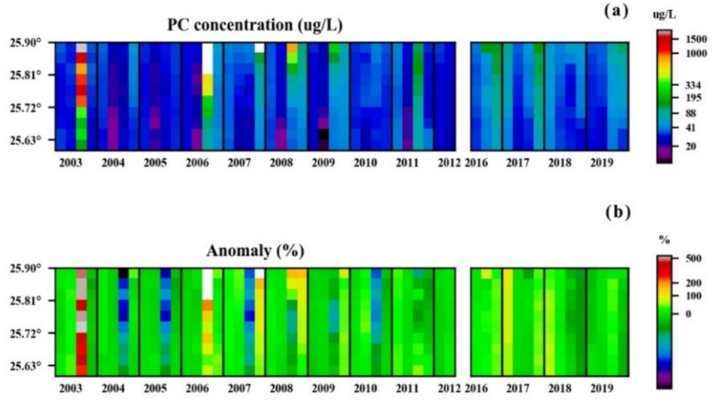

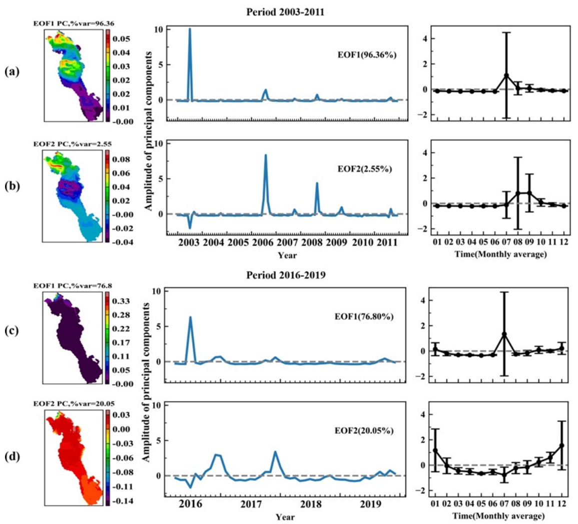

➢ Cyanobacterial bloom

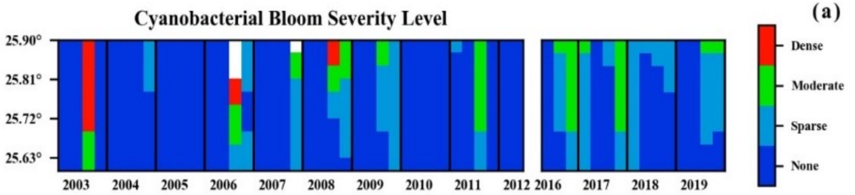

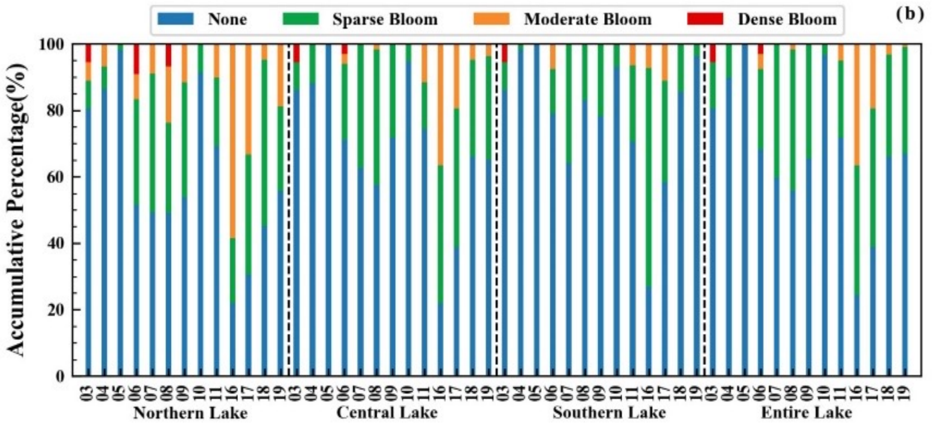

➢ Northern lake and middle in summer and autumn during 2003-2011（MERIS）

➢ Northeast of the lake in summer and winter during 2016-2019（OLCI）

WP4: Regional and global interactions

- Impacts of Agricultural Topdressing Practices on Cyanobacterial Bloom Phenology

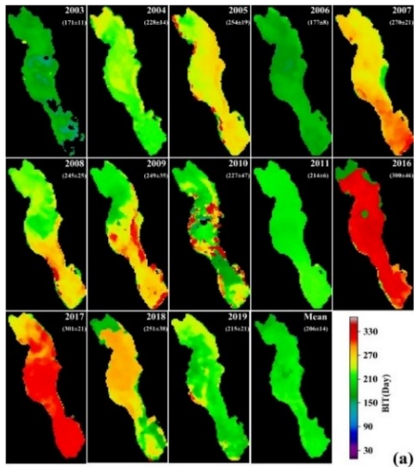

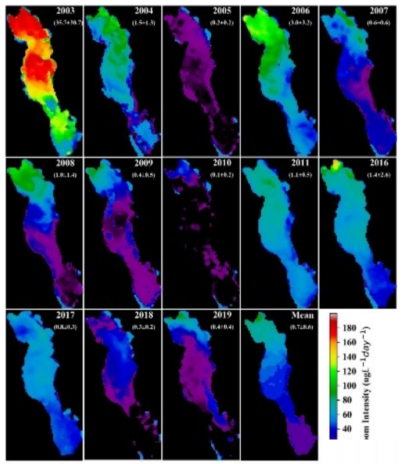

➢ The northern lake area is prone to cyanobacteria bloom, which has the characteristics of high intensity, early start date, and large coverage.

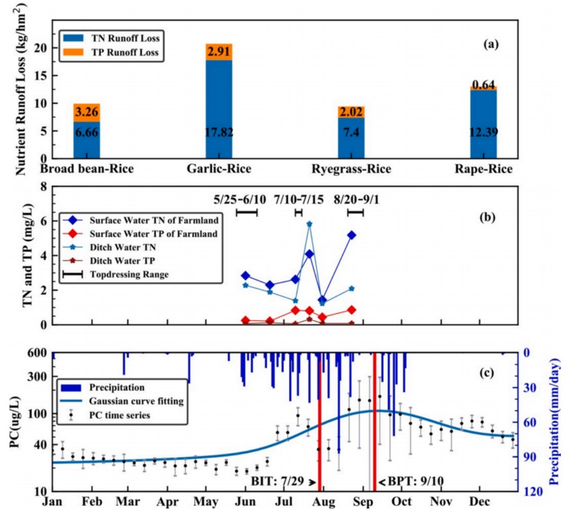

➢ The Bloom Initial Time (BIT) had great inter-annual variation.

➢ it was closely related to the increase in total nitrogen level and the decrease in wind speed.

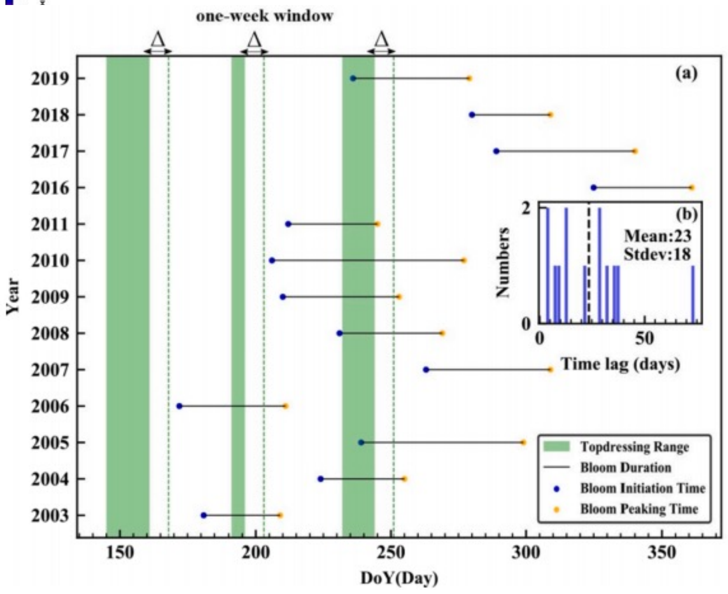

➢ We find that, after a week of topdressing, the BIT of bloom outbreak was delayed by about 23 days after nutrients entered the lake through river runoff with high-intensity rainfall,.

WP4: Regional and global interactions

- Long and short-term flood risk assessment using the multi-criteria analysis model

  - A multi-criteria method combining AHP-Entropy model was proposed to long-term and short term flood risk in Poyang Lake Watershed.

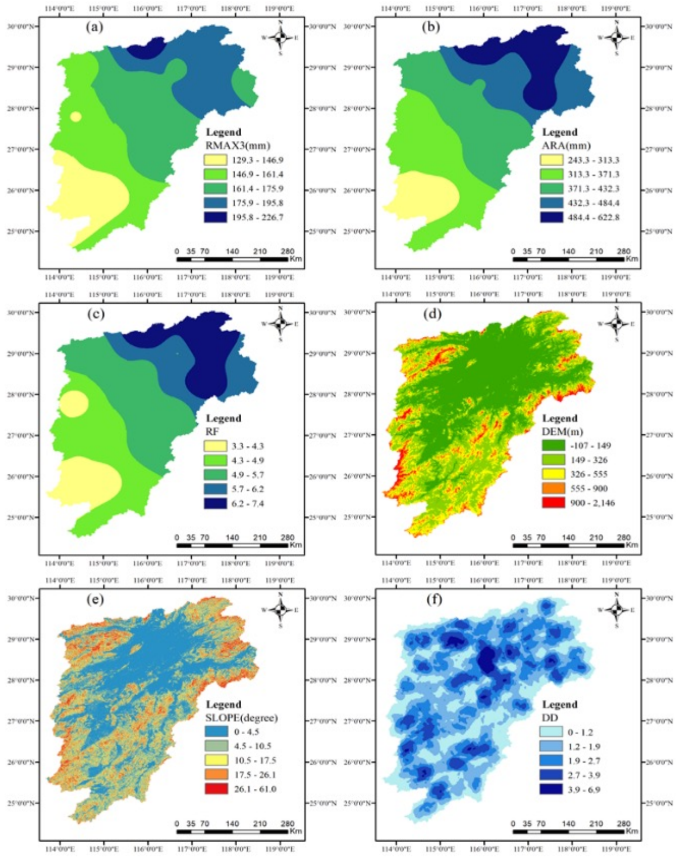

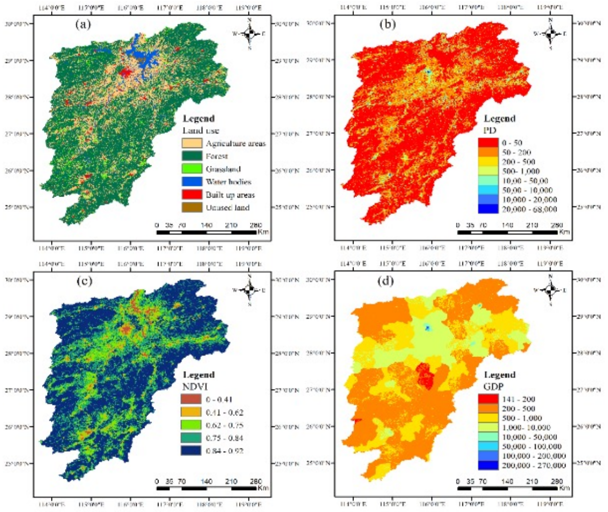

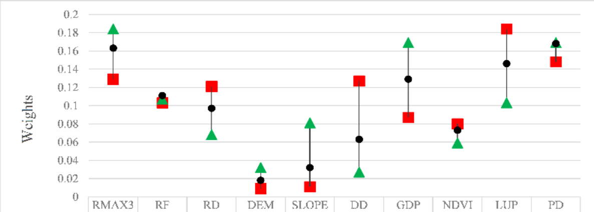

	RMAX3	RF	RD	DEM	SLOPE	DD	GDP	NDVI	LUP	PD
AHP	0.184	0.107	0.068	0.032	0.081	0.027	0.169	0.059	0.103	0.169
Entropy	0.129	0.103	0.121	0.009	0.011	0.127	0.087	0.08	0.184	0.148
Combined	0.163	0.111	0.097	0.018	0.032	0.063	0.129	0.073	0.146	0.168

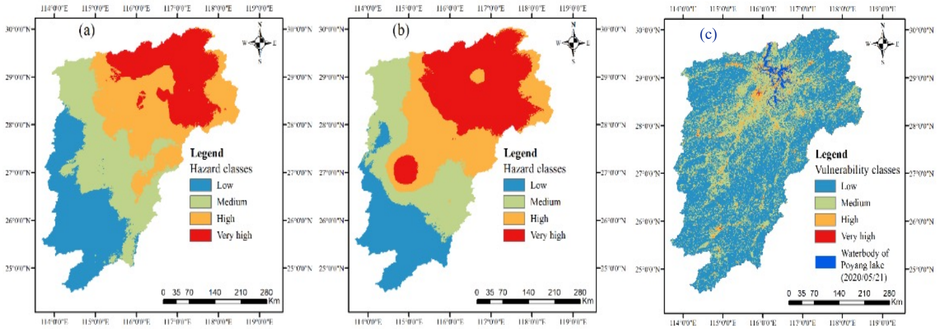

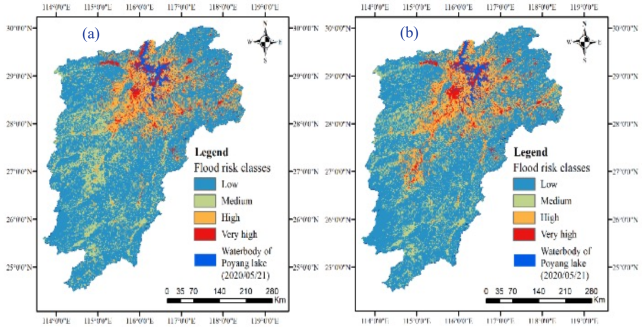

  - The long and short-term flood risk maps show a similar spatial pattern with a correlation coefficient of 0.90.

WP4: Regional and global interactions

- Long and short-term flood risk assessment using the multi-criteria analysis model

  - ➢ The short-term flood risk was validated using the catastrophic flood during the summer of 2020 in the Poyang Lake region. There was a high agreement between the flood risk assessment map and extracted flooding area from Sentinel-1 SAR images.
  - ➢ The flood risk assessment model has an accuracy of more than 50% in very high-risk zones for floods, and more than 90% for high and very high-risk floods.

Risk classes	**Area (km2) of flood risk classes**	**Percentage of each risk class**
Low	10.40	66.43%
Medium	1.78	11.37%
High	2.85	18.18%
Very high	0.63	4.02%

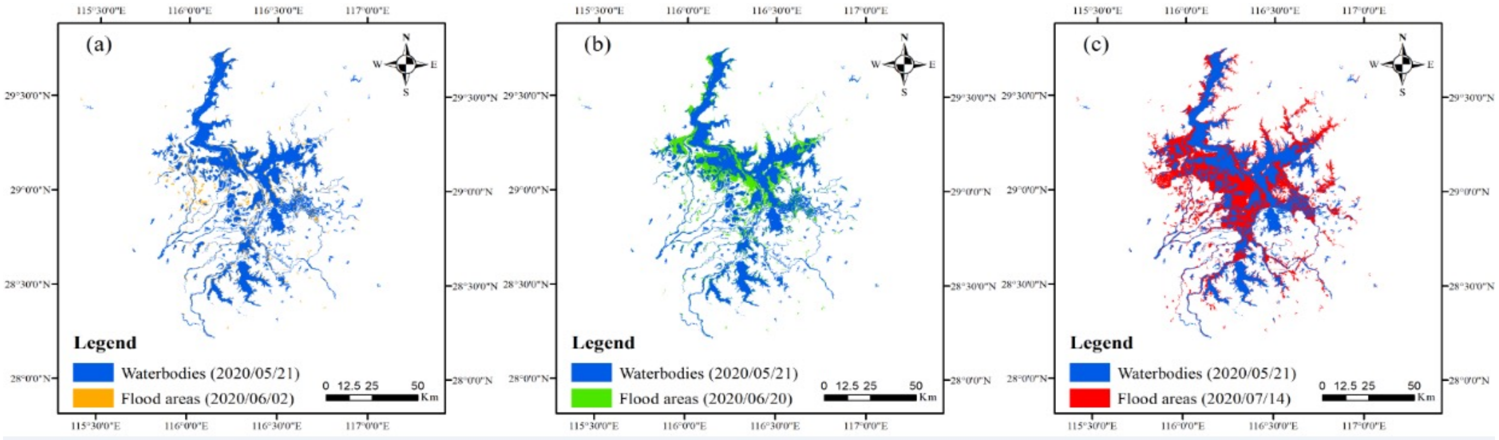

✓ On June 2, 2020, the area under very high flood risk assessed by the flood risk model accounted for 52.65%, followed by the area under high flood risk with 42.92%.

✓ On June 20, 2020, the presented flood risk model accurately predicted 77.66% of flood-prone areas with a very high-risk level, followed by the area under high flood risk with 14.99%.

✓ On July 14, 2020, the area under high and very high flood risk assessed by the flood risk model accounted for 91.39%, among which the area under very high flood risk with 51.19%.

- Full Lifecycle Monitoring on Drought-Converted Catastrophic Flood Using Sentinel-1 SAR

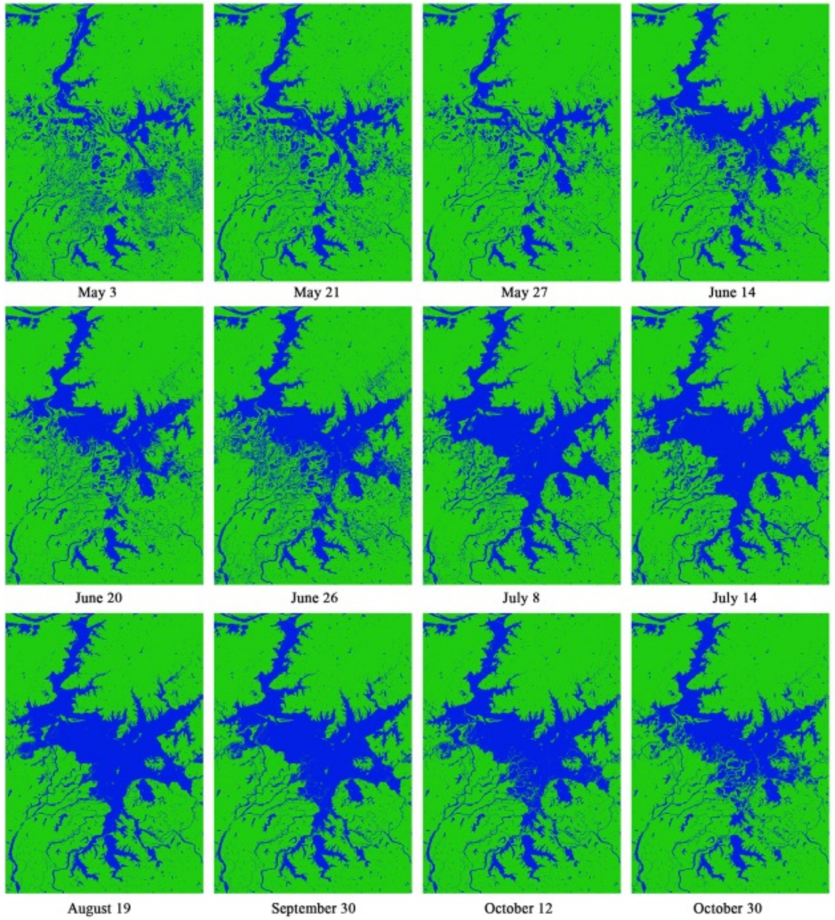

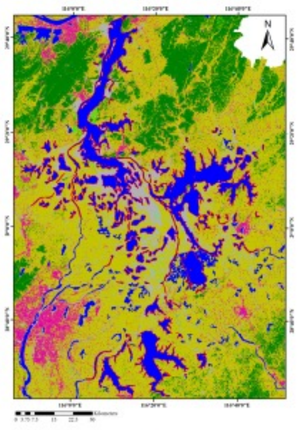

(a)

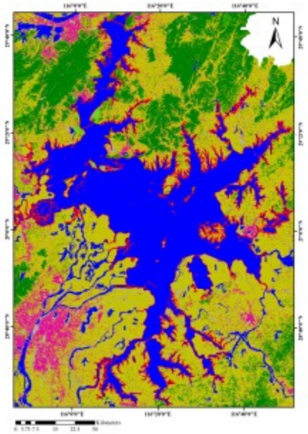

(b)

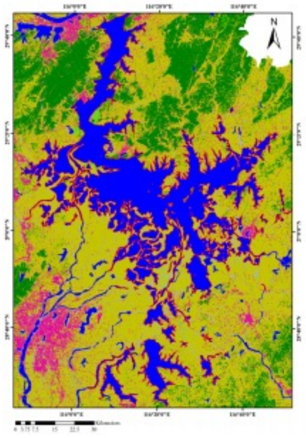

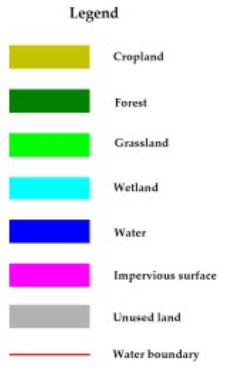

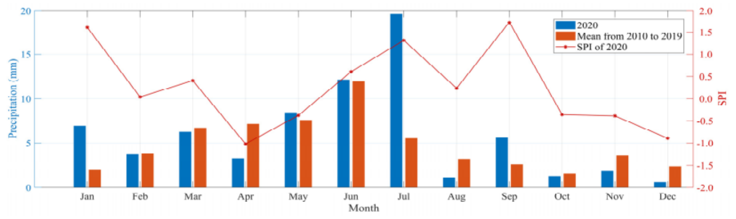

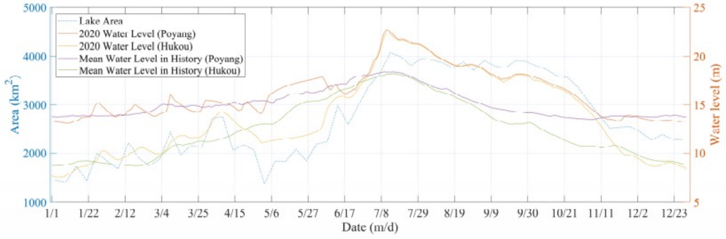

WP4: Regional and global interactions

- Flood mitigation effects of lake-reservoir group on the Poyang Lake watershed based on runoff-weighted model from multi-satellite weekly observation.

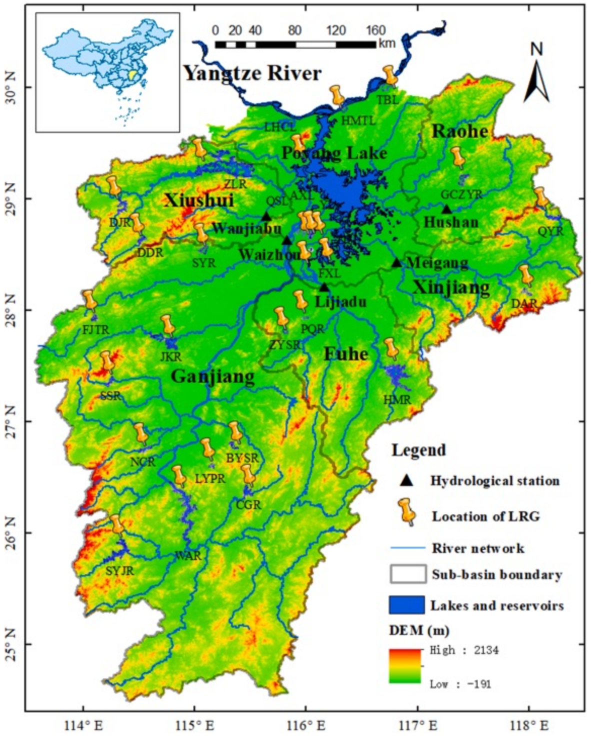

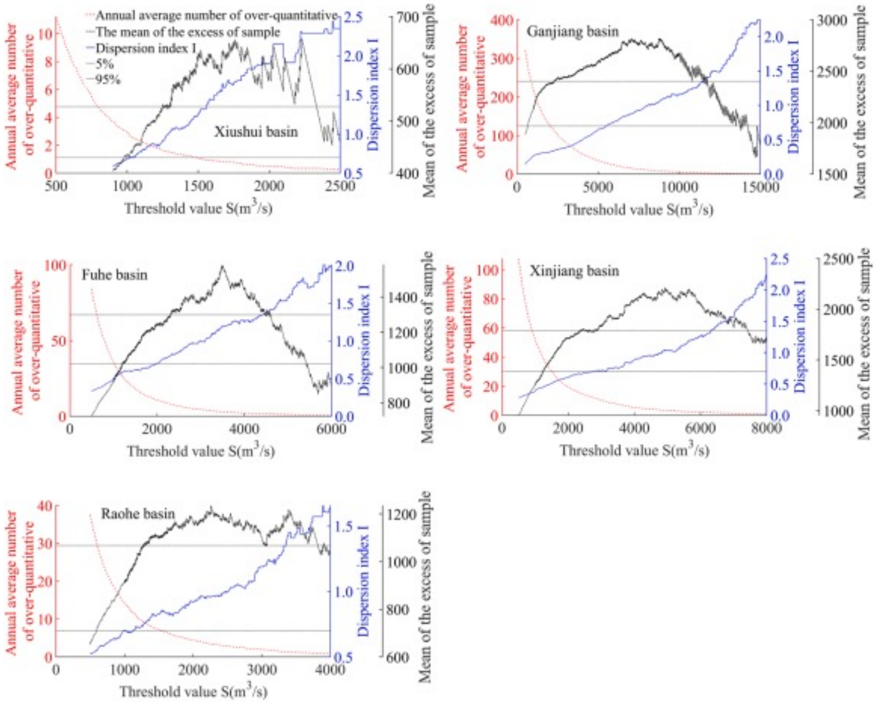

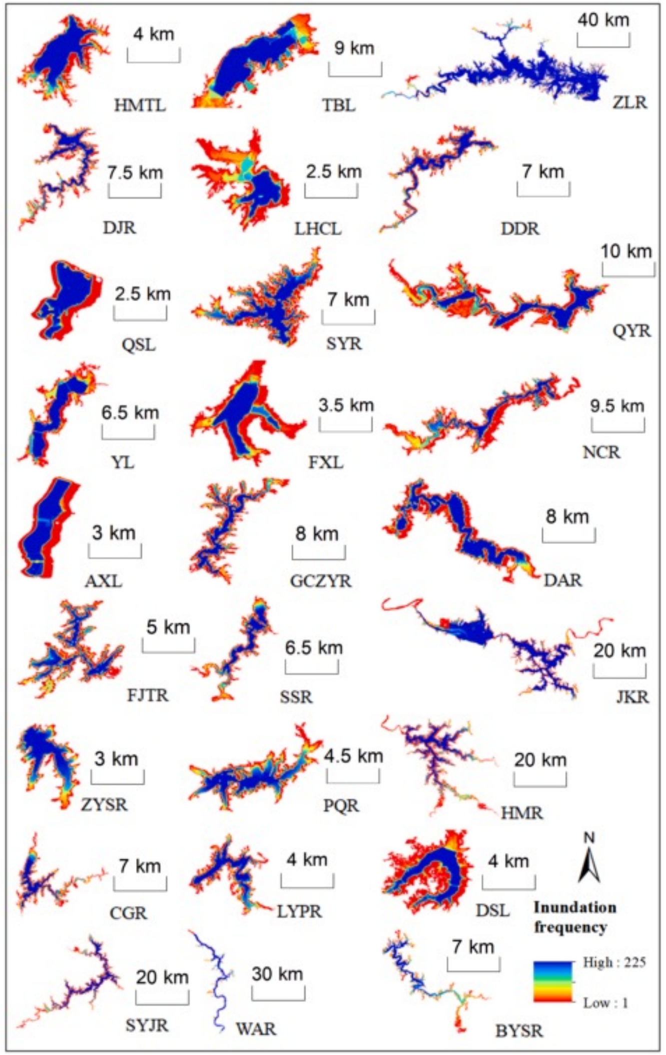

- ➢ Water boundaries of 27 lakes and reservoirs in the Poyang Lake watershed were extracted from 1300 GF-1 WFV images and 3500 Sentinel-1 SAR images during 2016-2020.
- ➢ Weekly water storage was calculated based on the capacity-area model.
- ➢ Flood events were determined based on Peaks-Over-Threshold (POT).

WP4: Regional and global interactions

- Flood mitigation effects of lake-reservoir group on the Poyang Lake watershed based on runoff-weighted model from multi-satellite weekly observation
  - ➢ The proposed runoff-weighted model was prior to the calculated detained flood volume and residence time of the retained flood, compared to the traditional precipitation-ET model.

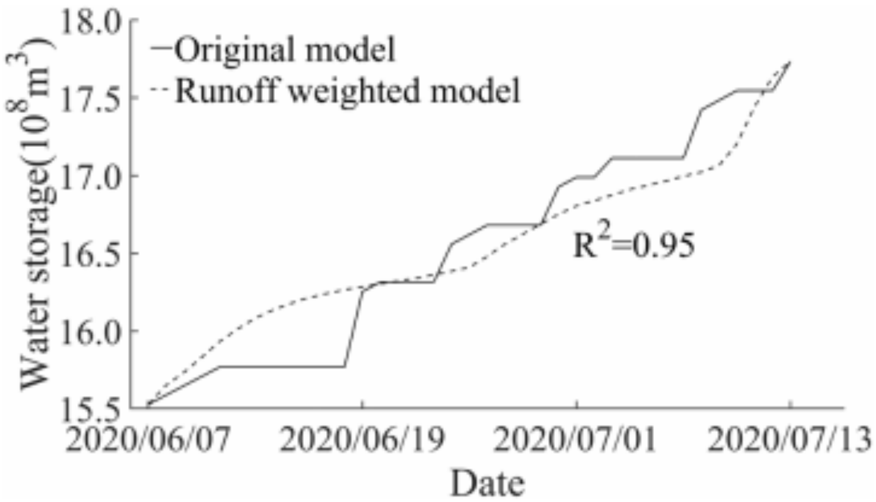

Flood detention and flood duration of the LRG in each basin of the Poyang Lake watershed from 2016 to 2020.

Basin	Start Date	Flood Peak Date	End Date	Flood Detention Capacity (10^8 m^3)	Annual Average Flood Detention Capacity (10^8 m^3)
Xiushui basin	2016/05/30	2016/07/05	2016/07/05	3.86	4.39
	2017/06/12	2017/06/24	2017/07/16	5.68	
	2020/05/27	2020/07/09	2020/08/01	3.65	
Ganjiang basin	2017/06/06	2017/06/30	2017/07/17	4.70	5.06
	2019/05/27	2019/07/11	2019/07/31	3.70	
	2020/05/21	2020/07/11	2020/07/31	6.78	
Fuhebasin	2016/05/06	2016/05/10	2016/05/18	2.14	1.64
	2017/05/19	2017/06/29	2017/07/20	1.97	
	2018/06/01	2018/07/07	2018/07/19	1.34	
	2019/05/27	2019/07/10	2019/08/07	1.47	
	2020/06/26	2020/07/10	2020/07/20	1.28	
Xinjiang basin	2016/04/07	2016/05/11	2016/05/11	0.69	0.54
	2017/06/01	2017/06/27	2017/07/24	0.67	
	2019/05/23	2019/07/10	2019/07/21	0.29	
	2020/05/16	2020/07/10	2020/08/01	0.49	
Raohe basin	2017/06/13	2017/06/25	2017/07/24	0.21	0.15
	2019/05/23	2019/07/13	2019/08/02	0.11	
	2020/04/28	2020/07/09	2020/07/15	0.12	

WP4: Regional and global interactions

- Analysis of vegetation greenness change and influencing factors

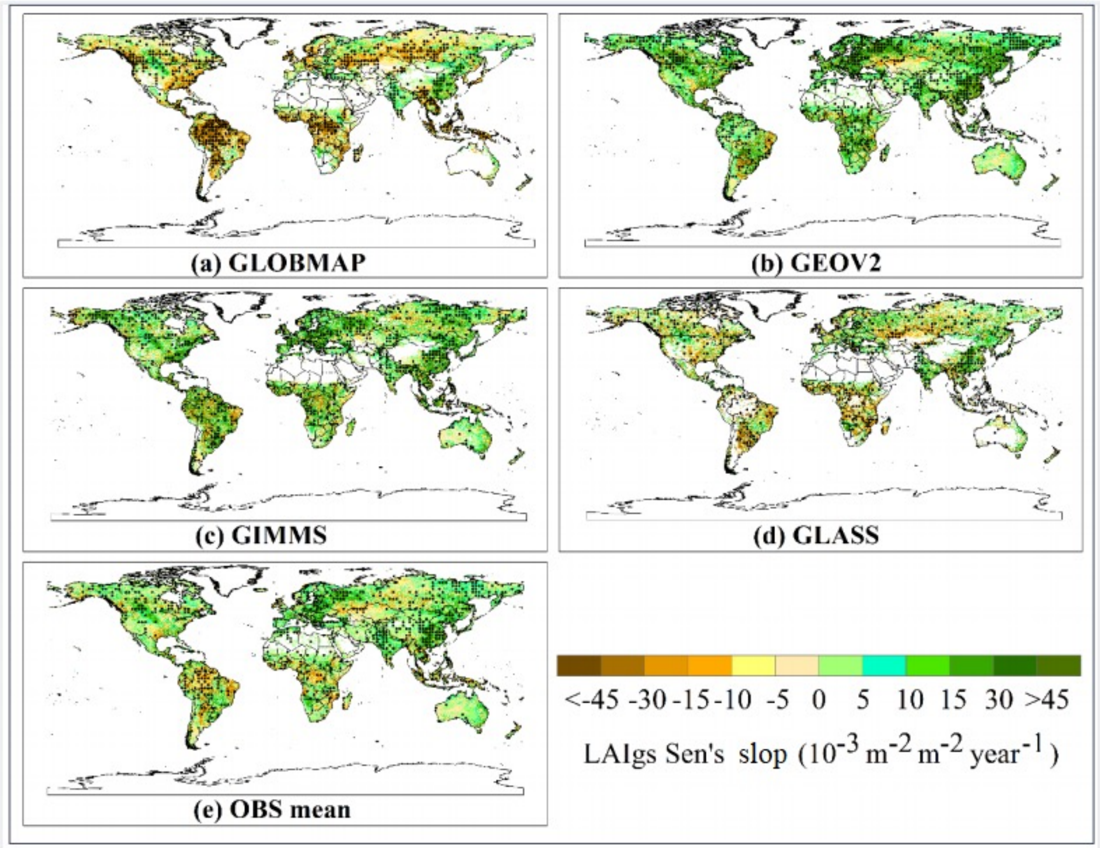

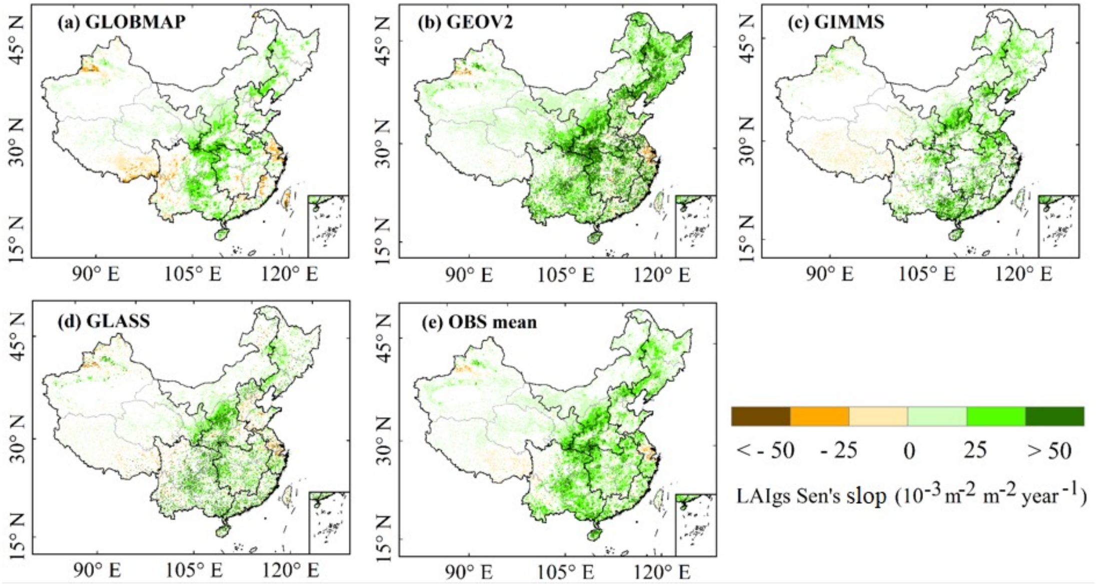

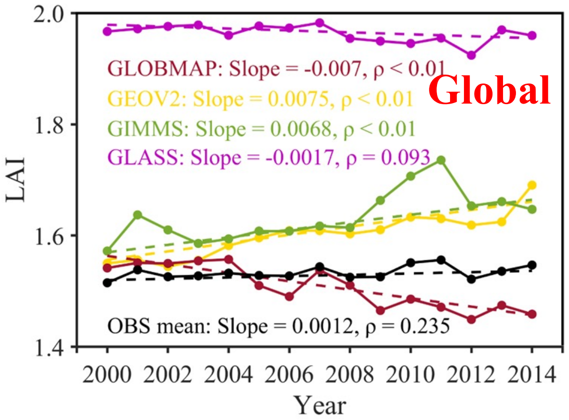

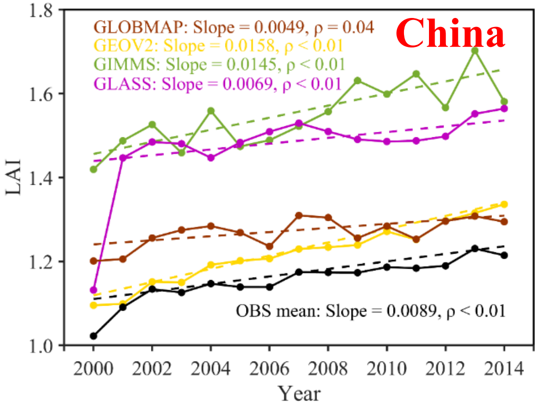

- Different satellite products showed significant greening in China, but different LAI products had great uncertainties

WP4: Regional and global interactions

- Analysis of vegetation greenness change and influencing factors

  - ➢ Forestry projects and climate change

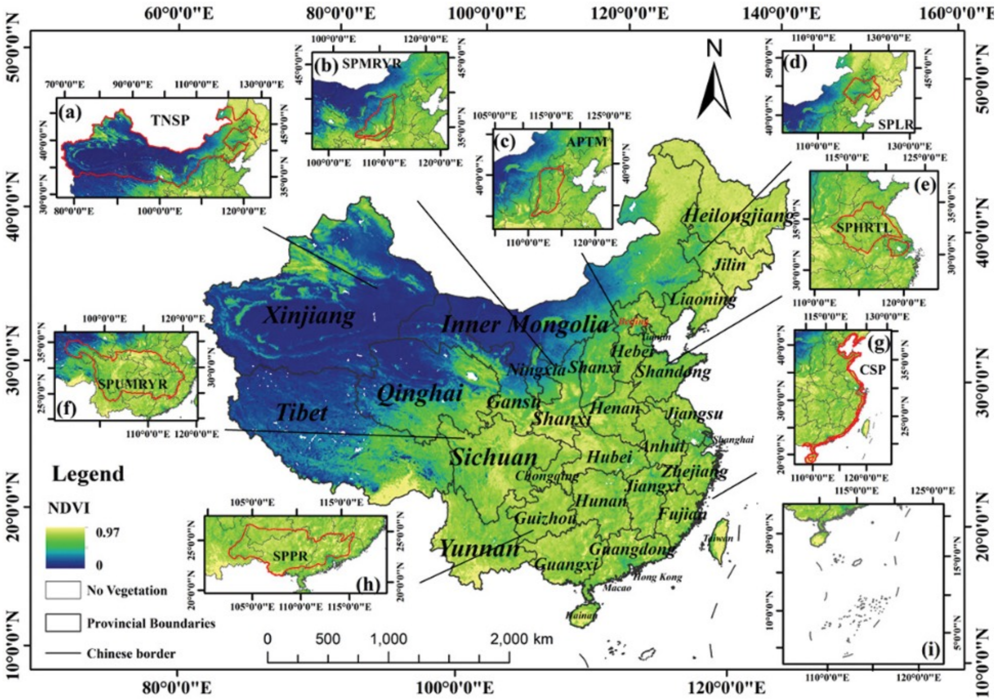

The vegetation greening in China and the eight forestry projects

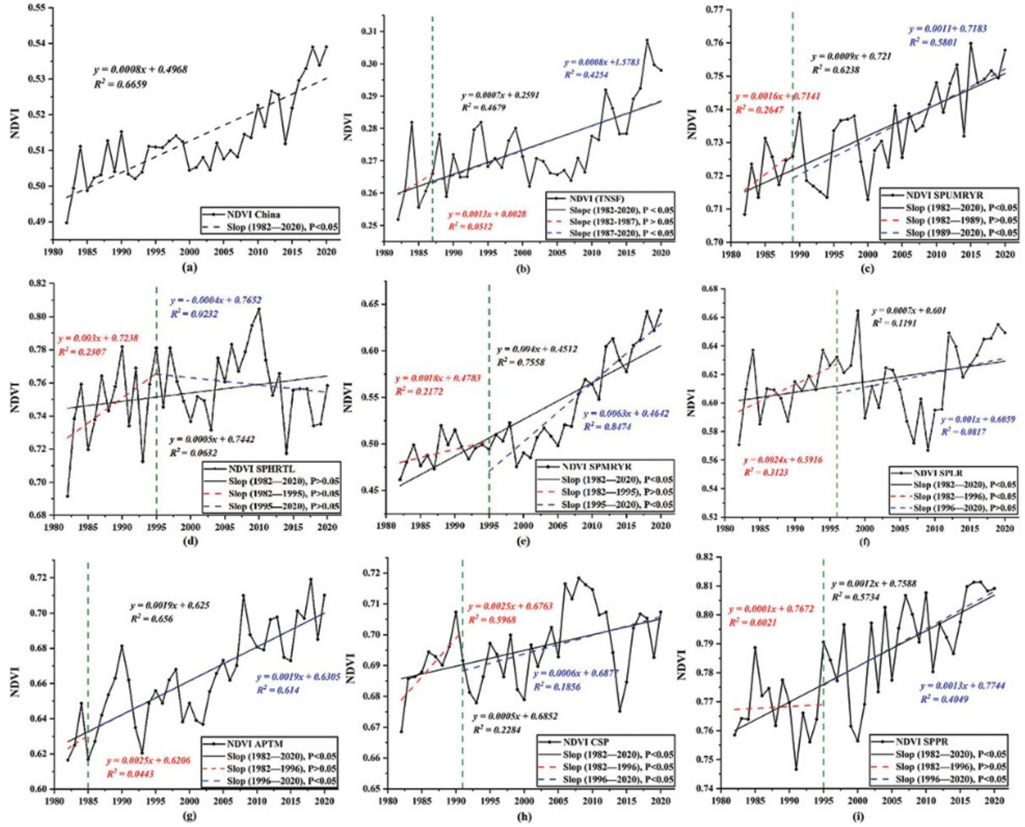

- ➢ We investigated the vegetation change in eight forestry projects in China, and the results showed that the vegetation in seven forestry projects improved significantly after the implementation of ecological engineering.

WP4: Regional and global interactions

- Analysis of vegetation greenness change and influencing factors
  - ➢ The relative contribution of forestry projects and climate change to vegetation restoration (degradation)

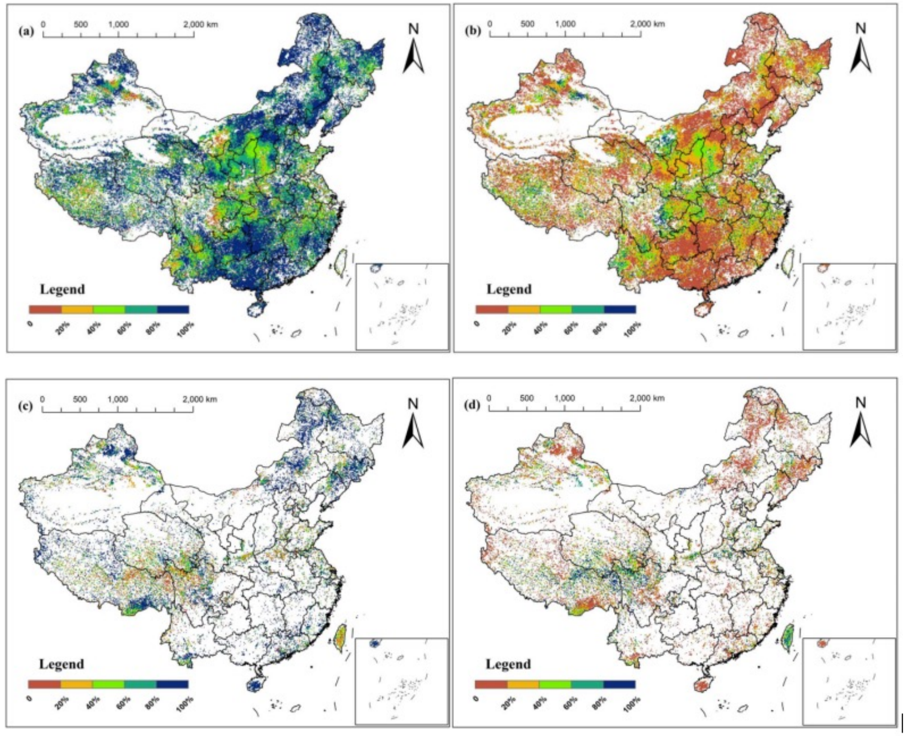

Relative contribution of climate change (a) and human activities (b) to vegetation improvement during 1982-2020; Relative contribution of climate change (c) and human activities (d) to vegetation degradation during 1982-2020.

Table 1. six scenarios were established to identify driving forces for forest dynamics.

Forest Status	Scenario	S_{ONDVI}	S_{PNDVI}	S_{RNDVI}	Dominant Driving Force	Relative contribution of climate change	Relative contribution of human activities
Forest restoration	1	>0	>0	<0	Climate-dominated vegetation restoration (CDR)	100	0
	2	>0	<0	>0	Human-dominated vegetation restoration (HDR)	0	100
	3	>0	>0	>0	Both dominated vegetation restoration (BDR)	$\frac{S_{PNDVI}}{S_{PNDVI}+S_{RNDVI}}$	$\frac{S_{RNDVI}}{S_{PNDVI}+S_{RNDVI}}$
Forest degradation	4	<0	>0	<0	Human-dominated vegetation degradation (HDD)	0	100
	5	<0	<0	>0	Climate-dominated vegetation degradation (CDD)	100	0
	6	<0	<0	<0	Both dominated the vegetation degradation (BDD)	$\frac{S_{PNDVI}}{S_{PNDVI}+S_{RNDVI}}$	$\frac{S_{RNDVI}}{S_{PNDVI}+S_{RNDVI}}$

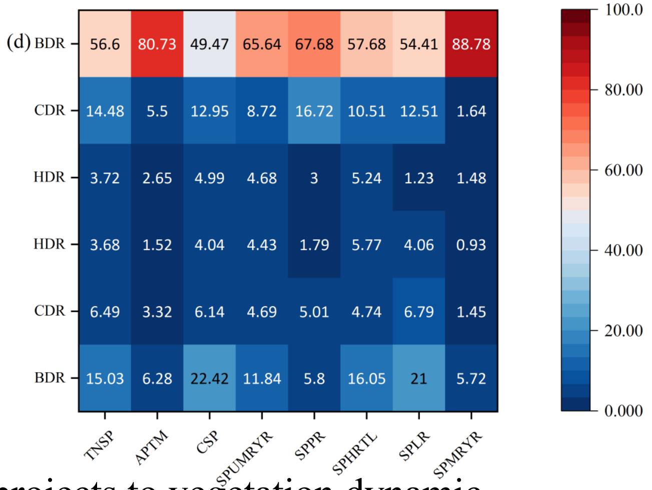

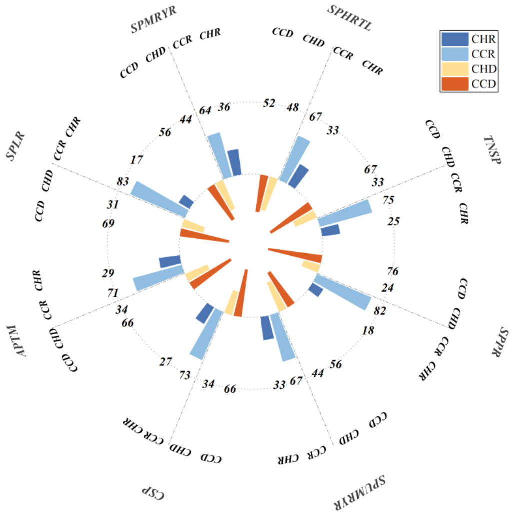

- ➢ We further quantified the the contribution of climate change and forestry projects to vegetation dynamic.
- ➢ The results show that the contribution of forestry projects to vegetation restoration has obvious spatial heterogeneity due to differences in topogra phy, climatic conditions and human management methods.
- ➢ At the national scale, the contribution of forestry projects to vegetation change was about 27%, while in the Loess Plateau it was more than 60%.

Visit & exchange Dragon 5

Name	Institution	Welcome place	Contribution including period of research
Wenchao Tang	Institute of Space Science and technology Nanchang University	TRIO ICUBE University of Strasbourg	April 2022 March 2023

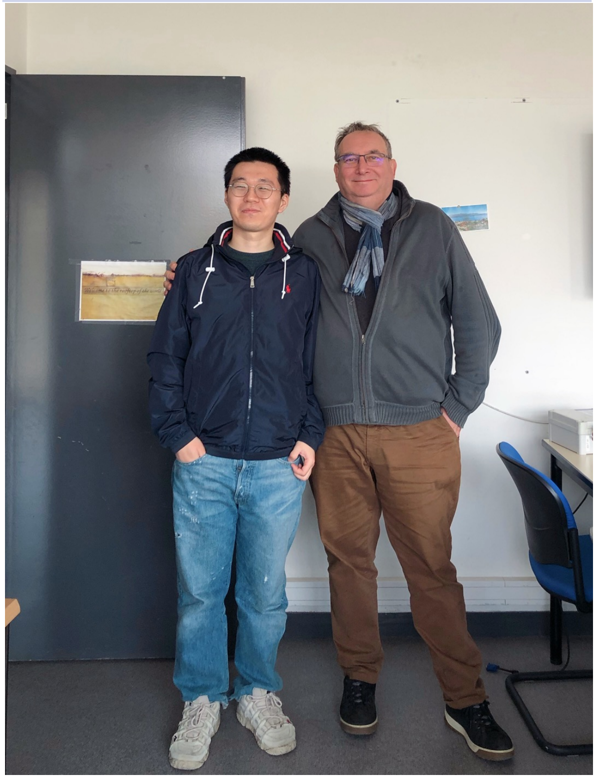

Poster Presentation

- Synergy of HR SAR and Optical Imagery with Altimetric Data to Monitor Sensitive Areas of Western Dongting and Anhui Province Lakes

Sabrine Amzil et al.

- "Impact of Extreme Drought Event on Seasonal Hydrological Patterns of Poyang Lake by Using Sentinel-1 SAR"

Wenchao Tang, Hervé YESOU & Jinbo Weil

- Dynamic Changes of Vegetation in China Under the Combined Effects of Forestry Projects and Climate Change

Liang Zheng, Jianzhong Lu, Xiaoling Chen

European Young scientists contributions in Dragon 5

Name	Institution	Poster title	Contribution including period of research
Sabrine AMZIL	ICUBE UNISTRA	Synergy of HR SAR and Optical Imagery with Altimetric Data to Monitor Sensitive Areas of Western Dongting and Anhui Province Lakes	July 202 to now

Chinese Young scientists contributions in Dragon 5

Name	Institution	Poster title	Contribution including period of research
Liang Zheng Dong Liang, Shangbo Yang, Jinru Wu	Wuhan University	Evidence of vegetation greening benefitting from the afforestation initiatives in China	PhD 8 months/year (Liang Zhen)
Yongchao Zheng, Qing Tian, Jiaqian Liu, Xin Wang, Ruixin Li, Jianshu Wang, Mengyuan Yang, Ning Zhu	Wuhan University		MSc
Yaobin Ma	Nanchang University	"Impact of Extreme Drought Event on Seasonal Hydrological Patterns of Poyang Lake by Using Sentinel-1 SAR"	PdD
Tao Guo, Qize Li, Huazn Yang	Nanchang University	"Impact of Extreme Drought Event on Seasonal Hydrological Patterns of Poyang Lake by Using Sentinel-1 SAR"	MSc
2 PhD students 6 Mcs	IWF		

Chinese Young scientists contributions in Dragon 5

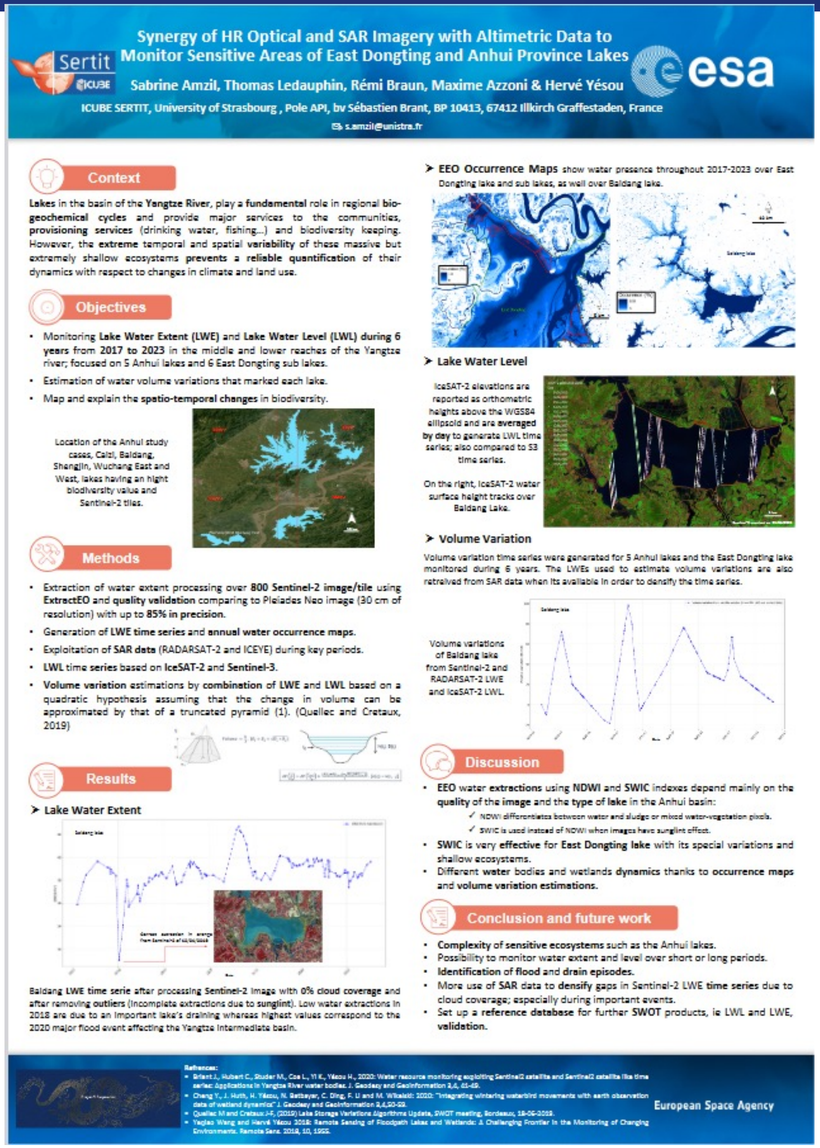

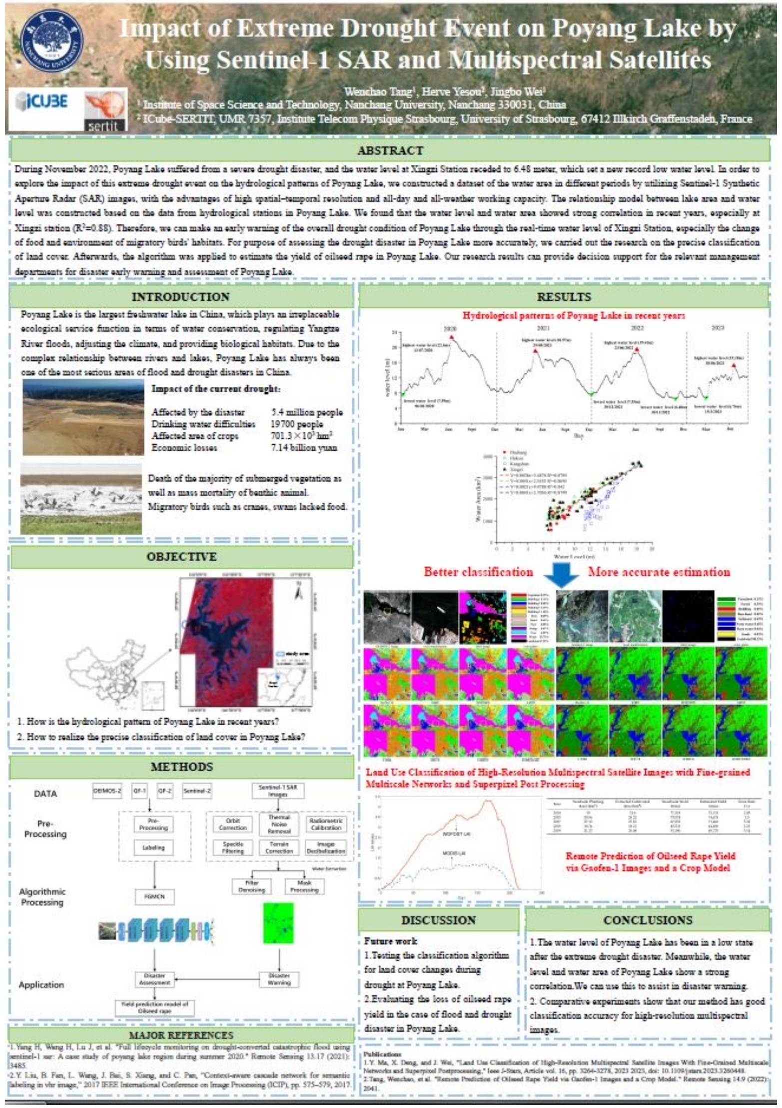

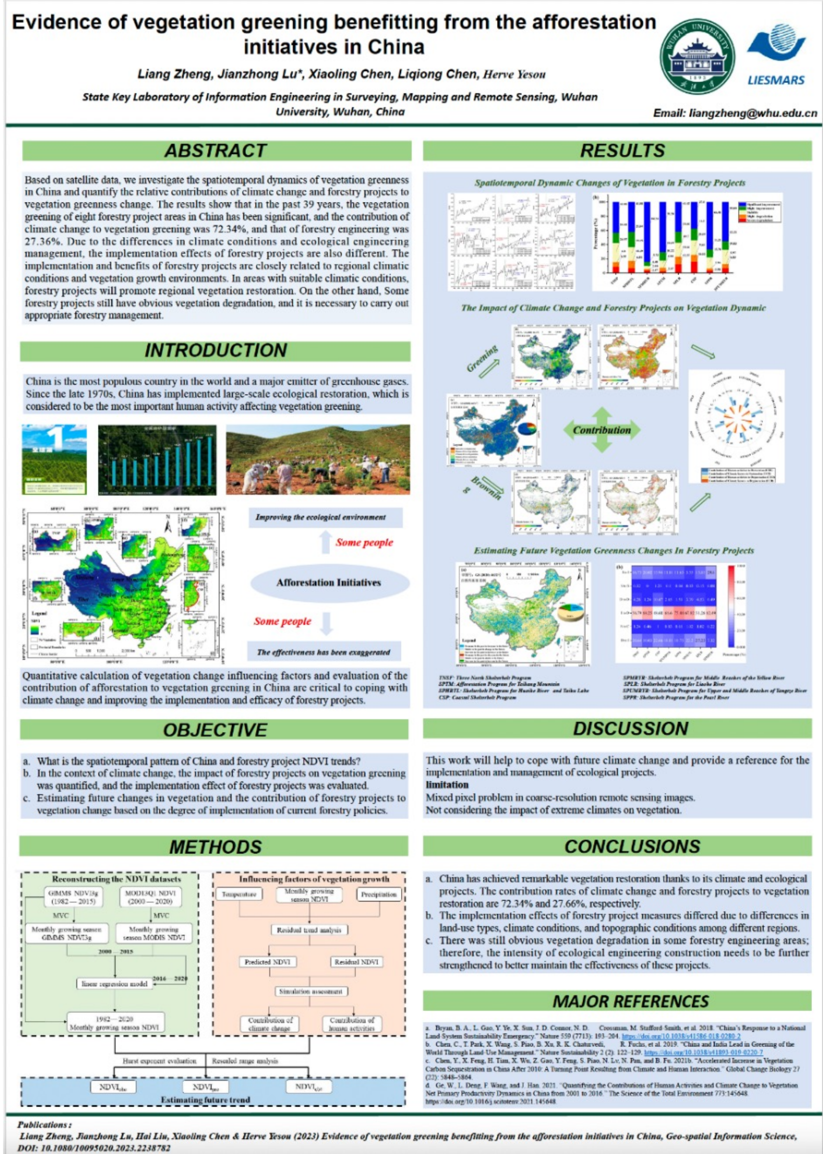

List of publications

- Huth, Juliane; Gessner, Ursula; Klein, Igor; Yesou, Herve; Lai, Xijun; Oppelt, Natascha and Kuenzer, Claudia (2020) *Analyzing Water Dynamics Based on Sentinel-1 Time Series - a Study for Dongting Lake Wetlands in China*. Remote Sensing, 12 (11), pp. 1-21. MDPI. *doi:10.3390/rs12111761.*
- Cheng, Yachang; Huth, Juliane; Yesou, Herve; Batbayar, Nyambayar; Ding, Changqing; Li, Fengshan and Wikelski, Martin (2020) *Integrating wintering waterbird movements with earth observation data of wetland dynamics*. Journal of Geodesy and Geoinformation Science, 3 (4), pp. 50-59. Surveying and Mapping Press. *doi:10.11947/j.JGGS.2020.0405.*
- *Publications*
- *Ghosh S, Lu J, Das P, et al. 2023. Machine learning algorithms for merging satellite-based precipitation products and their application on meteorological drought monitoring over Kenya. Climate Dynamics, 2023, doi:10.1007/s00382-023-06893-6.*
- *Zheng L, Lu J, Liu H, et al. 2023. Evidence of vegetation greening benefitting from the afforestation initiatives in China. Geo-Spatial Information Science, 2023.doi: 10.1080/10095020.2023.2238782*
- *Yang S, Lu J, Chen X, et al. 2023. Unraveling environmental influences on the spatial and temporal dynamics of cyanobacterial blooms in Lake Erhai during its early stage of eutrophication. Geo-Spatial Information Science, doi: 10.1080/10095020.2023.2217860*
- *Wu J, Lu J, Chen X, et al. 2023. Performance of the WRF model in simulating convective rainfall events in the humid subtropical monsoon climate region-Poyang Lake basin. Theoretical and Applied Climatology, 153: 889-911.*
- *Li Y, Cao S, Yu Y, Yao J, Lu J. 2023. Quantifying the impacts of a proposed hydraulic dam on groundwater flow behaviors and its eco-environmental implications in the large Poyang Lake-floodplain system. Journal of Environment Management, 336:117654.*
- *Das P, Zhang Z, Ghosh S, Lu J, et al. 2023. Historical and projected changes in extreme high temperature events over East Africa and associated with meteorological conditions using CIMP6 Models. Global and Planetary Change, 222:104068.*
- *Wang X, Lu J, Chen X, et al. 2022. Flood mitigation effects of lake-reservoir group on the Poyang Lake watershed based on runoff-weighted model from multi-satellite weekly observation. Journal of Hydrology: Regional Studies, 44:101265.*
- *Li Y, Lu J, Shu H, et al. 2022. Spatiotemporal estimation of model error to improve soil moisture analysis in ensemble Kalman filter data assimilation. Journal of Applied Remote Sensing, 2022, 16(3): 034531.*

List of publications

- Wang J, Yang M, Chen Z, **Lu J**, et al. 2022. An MLC and U-Net integrated method for Land Use/Land Cover Change detection based on time series NDVI-composed image from PlanetScope satellite. *Water*, 14(21):3363.
- Wu J, **Chen X**, **Lu J**. 2022. Assessment of long and short-term flood risk using the multi-criteria decision-making model with the A[illegible] in Poyang Lake basin. *International Journal of Disaster Risk Reduction*, 75: 102968.
- Yaseen A, **Lu J**, **Chen X**. 2022. Flood susceptibility mapping in arid region of Pakistan through ensemble machine learning [illegible] *Environmental Research and Risk Assessment*, 36(10):3041-3061.
- Wang J, **Lu J**, Zhang Z, et al. 2022. Agricultural non-point sources and their effects on chlorophyll-a in a eutrophic lake over three decades (1985-2020). *Environmental Science and Pollution Research*, 29(31): 46634-46648.
- Tian Q, **Lu J**, **Chen X**. 2022. A novel comprehensive agricultural drought index reflecting time lag of soil moisture to meteorology: A case study in the Yangtze River basin, China. *Catena*, 209, 105804.
- Sajjad A, **Lu J**, **Chen X**, et al., 2022. Riverine flood mapping and impact assessment using remote sensing technique: a case study of Chenab flood-2014 in Multan district, Punjab, Pakistan. *Natural Hazards*, 110, 2207-2226.
- Yang S, Chen X, **Lu J**, et al., 2021. Impacts of Agricultural Topdressing Practices on Cyanobacterial Bloom Phenology in an Early Eutrophic Plateau Lake, China. *Journal of Hydrology*, 594: 125952.
- Yang H, Wang H, **Lu J**, et al., 2021. Full lifecycle monitoring on drought-converted catastrophic flood using Sentinel-1 SAR: A case study of Poyang Lake Region during Summer 2020. *Remote Sensing*, 13(17), 3485.
- Tan Z, Li Y, Zhang Q, Liu X, Song Y, Xue C, **Lu J**. 2021. Assessing effective hydrological connectivity for floodplains with a framework integrating habitat suitability and sediment suspension behavior. *Water Research*, 201: 117253.
- Dao D M, **Lu J**, Chen X, et al., 2021. Predicting tropical monsoon hydrology using CFSR and CMADS data over the Cau River basin in Vietnam. *Water*, 13(9): 1314.
- Liu Z, **Lu J**, Huang J, et al., 2021. Projection of reference crop evapotranspiration under future climate change in Poyang Lake Watershed, China. *Journal of Hydrologic Engineering*, 26(1): 05020042.
- Jiang H, Liu Y, **Lu J**. 2021. A new algorithm for monitoring Backflow from Fiver to Lake (BRL) using satellite images: A case of Poyang Lake, China. *Water*, 13(9): 1166.
- Liang D, **Lu J**, Chen J, et al., 2020. An investigation of the hydrological influence on the distribution and transition of wetland cover in a complex lake-floodplain system using time-series remote sensing and hydrodynamic simulation. *Journal of Hydrology*, 587:125038.

List of publications

[1] J. Wei, L. Chen, Z. Chen, and Y. Huang, "An Experimental Study of the Accuracy and Change Detection Potential of Blending Time Series Remote Sensing Images with Spatiotemporal Fusion," Remote Sensing, vol. 15, no. 15, p. 3763, 2023. [Online]. Available: https://www.mdpi.com/2072-4292/15/15/3763
[2] Y. Ma, X. Deng, and J. Wei, "Land Use Classification of High-Resolution Multispectral Satellite Images With Fine-Grained Multiscale Networks and Superpixel Postprocessing," Ieee J-Stars, Article vol. 16, pp. 3264-3278, 2023 2023, doi: 10.1109/jstars.2023.3260448.
[3] J. Wei, H. Yang, W. Tang, and Q. Li, "Spatiotemporal-Spectral Fusion for Gaofen-1 Satellite Images," Ieee Geosci Remote S, vol. 19, pp. 1-5, 2022, Art no. 5002205, doi: 10.1109/LGRS.2021.3111961.
[4] W. Tang, R. Tang, T. Guo, and J. Wei, "Remote Prediction of Oilseed Rape Yield via Gaofen-1 Images and a Crop Model," Remote Sensing, vol. 14, no. 9, May 2022, Art no. 2041, doi: 10.3390/rs14092041.
[5] Y. Ma, J. Wei, and X. Huang, "Balancing Colors of Non-overlapping Mosaicking Images with Generative Adversarial Networks," Ieee Geosci Remote S, vol. 19, pp. 1-5, 2022, Art no. 8024405, doi: 10.1109/LGRS.2021.3126261.
[6] J. Wei, W. Tang, and C. He, "Enblending Mosaicked Remote Sensing Images With Spatiotemporal Fusion of Convolutional Neural Networks," Ieee J-Stars, vol. 14, pp. 5891-5902, 21 May 2021 2021, doi: 10.1109/JSTARS.2021.3082619.
[7] Y. Ma, J. Wei, W. Tang, and R. Tang, "Explicit and stepwise models for spatiotemporal fusion of remote sensing images with deep neural networks," Int J Appl Earth Obs, vol. 105, p. 102611, 2021/12/25/ 2021, doi: https://doi.org/10.1016/j.jag.2021.102611.
[8] Y. Ma, J. Wei, and X. Huang, "Integration of One-Pair Spatiotemporal Fusion With Moment Decomposition for Better Stability," (in English), Frontiers in Environmental Science, Original Research vol. 9, no. 401, 2021-October-11 2021, doi: 10.3389/fenvs.2021.731452.

List of publications

- 1. A surface water mapping framework combining optical and radar remote sensing and its application in China， GEOCARTO INTERNATIONAL， 2022.10
- 2. Research on retrieval of chlorophyll-a concentration in Danjiangkou Fancheng reach of Han River based on Sentinel-2 satellite data， The Thirteenth International Conference on Digital Image Processing (ICDIP 2021)， 2021.5
- 4. Estimation of Soil Moisture with SAR Data in Large Area Based on Support Vector Regression， 13th International Conference on Digital Image Processing, ICDIP 2021， 2021.5
- 5. A comparative study of different deep learning models for land use and land cover mapping of flood detention basin， IOP Conference Series Earth and Environmental Science， 2022.10
- 6. Study on Regional Drought Monitoring Based on Multi-Sources Data in China， IGARSS 2020 - 2020 IEEE International Geoscience and Remote Sensing Symposium， 2020.0
- 7. Situation and prospect of flood disaster monitoring by remote sensing in China, China Water Resources, 2021(15):15-17. DOI:10.3969/j.issn.1000-1123.2021.15.017.
- 8. Application of space-air-ground integrated monitoring technology in river and lake supervision and future prospect,China Water Resources, 2021(23):41-44. DOI:10.3969/j.issn.1000-1123.2021.23.031.
- 9. Study on simulation of scale effect of hydrological processes in karst area by SVAT model, Journal of China Institute of Water Resources and Hydropower Research, 2022,20(4):352-361
- 10.Application and prospect of satellite remote sensing technology in river and lake supervision. Satellite Application,2021(6):27-32. DOI:10.3969/j.issn.1674-9030.2021.06.007